The study of U^* index Theory for Load Transfer Analysis and its Application in Design Evaluation of Vehicle Components

by

Khashayar Pejhan

A Thesis submitted to the Faculty of Graduate Studies of

The University of Manitoba

in partial fulfillment of the requirements of the degree of

Doctor of Philosophy

Department of Mechanical Engineering

University of Manitoba

Winnipeg

Thesis Advisors   Author

Christine Q. Wu, Igor Telichev   **Khashayar Pejhan**

The study of U* index Theory for Load Transfer Analysis and its Application in Design Evaluation of Vehicle Components

Abstract

Load transfer analysis deals with one of the most important functions of any engineering structure, which is the ability of structure in transferring imposed loads to the supporting points. A thorough load transfer analysis is now considered to be one of the most significant elements of structural analysis in Mechanical Engineering. Although stress value has proved to be an efficient index for performing the failure analysis, the necessity of defining an index for evaluation of structure stiffness has led to the introduction of the U* index theory. The load transfer index (U*), is a new concept in structural analysis compared to conventional stress analysis. The U* index characterizes the internal stiffness distributions, which is an indicator of the load transfer in the analyzed structure. Although the U* index theory have been proved to be useful in design, it is missing necessary steps toward becoming a mature theory for structural analysis.

Firstly, as any new theory, U* index theory needs to be examined and validated by experimental testing. Therefore, an experimental setup is proposed and tested, and the validation of the theory is performed by comparing the results to the U* index theory. This experimental validation plays a significant role as a benchmark for any further application of this theory in structural analysis.

Secondly, a systematic comparison between the conventional stress analysis and the load transfer analysis (based on U* index) is lacking. To show the potentials and unique capacities of the U*

index theory a detailed comparison is made between the results of U^* index and stress analyses of a vehicle component. The results are also compared to observations of experimental testing on the identical structural element. In many aspects, there is an agreement between the results of U^* index analysis and the conventional stress analysis. However, it was shown in this study, that in some cases, application of conventional stress analysis might be limited, less precise or even useless.

Thirdly, design modification capabilities are one of the most important features of the U^* index theory and therefore it is necessary to demonstrate that real life problems can benefit from this factor. In this study, sample structures representing the components of multiple passengers carrying vehicles are selected and analyzed by U^* index theory. Based on the results of this analyses design modifications are proposed and implemented on the structure. The results of these modifications are shown to have better structural performance.

Lastly, as any well-developed structural analysis method, the U^* index theory should be applied to different types of problems, including nonlinear domain. Hence, to remove the limitations of linear analysis that is a part of the original theory, an extension of U^* index theory to the nonlinear domain is proposed and tested. This extension is viewed as the first step toward achieving a general U^* index theory.

In summary, U^* index theory provides an understandable explanation of load transfer in the structure, which in turn, provides designers with a general awareness regarding structural performance and a better vision for improvement opportunities. Based on the results of the current study it can be claimed that the existing methods of structural analysis have limitations in certain aspects that can be overcome by combining the perspective of U^* index analysis to the existing structural analysis paradigm. The further development of the U^* index theory and

expanding its application in industrial problems can provide a new, useful and well-matured tool for achieving engineerign designs with efficient structural performance.

Acknowledgement

I wish to thank my thesis advisors, Dr. Christine Wu and Dr. Igor Telichev for their invaluable advice, support, guidance and patience during my research at mechanical engineering department of the University of Manitoba. I have been blessed with their positive and encouraging attitude that helped me to face the challenges of the Ph.D. research with more confidence.

I would also like to sincerely appreciate the comments I got from my committee members, Dr. Nan Wu and Dr. Young-Jin Cha. Their insights helped me to orient my way of thinking and contributed to improving the quality of my research.

This research was possible because of the generous cooperation of Motor Coach Industries and NSERC who truly understand the importance of research and development at this level.

I would like to acknowledge the help of my friends in the heavy ground vehicles laboratory: Mr. Qingguo Wang, Mr. Anton Kuznetcov, Mr. Hamid Giahi and Mr. Wei Zhou. It was a great experience as we researched, learned and innovated together. Moreover, during my four years of study at U of M I was lucky to get academic and moral help from two of my great friends, Ms. Ida Khosravipour and Dr. Yun-Hsiang Sun.

This thesis is dedicated to my parents, Ali and Mehri and my sisters Shervin and

Shabnam for their continuous love and unconditional support and encouragement.

Table of Contents

List of Tables

List of Figures

Nomenclature

U Total strain energy of the system

U' Total strain energy of the modified system

P_A Applied load to the system

P'_A Applied load to the modified system

d_i Displacement at the point i

K_{ij} Internal stiffness between points i and j

U^* Load transfer index

U_{NL}^* Load transfer index of nonlinear domain

λ Gradient of load transfer index

U_1^* Load transfer index for the applied loads

U_2^* Load transfer index for the reaction forces

U_{sum}^* Combination of load transfer indices for the applied loads and reaction forces

Chapter 1: Introduction

1-1)   Background and Motivation

In the twenty-first century, the automotive industry is challenged by major environmental and economic concerns. From an environmental perspective, the global warming has become a real threat to the environment. According to statistics almost 30 percent of all U.S. global warming emission is produced via transportation devices and 18% of this amount is made by buses and similar heavy vehicle [1]. As a result, vehicle industry in general, and heavy vehicle manufacturers specifically are obliged morally and legally to produce vehicles with lower emission rates. Moreover, economic problems in last decade have urged customers to buy vehicles with lower fuel consumption. Therefore, manufacturers have no other choice but to modify their designs to shrink the fuel consumption. Lower fuel consumption and lower emission can be achieved mainly by two approaches. The first way is to design hybrid vehicles that will provide an acceptable amount of power while producing less toxic fumes. Some examples of studies focusing on this approach are studies on modifying hybrid engine performance and application of modern braking systems in vehicles by Fazeli et al. [2, 3]. The second way is to reduce the overall weight of the vehicle, which will accordingly reduce the fuel consumption and emissions significantly. Effect of vehicle weight reduction on fuel consumption

of different vehicles have been studied and presented in [4]. Many of previous studies about weight reduction in vehicles were mainly about the effect of using lighter materials to lower the weight [5, 6]. Although modern light weighted materials have shown to be very effective in achieving low fuel consumption, there has always been a challenge to use these materials and keep the integrity of the structure in the vehicle within the acceptable safe zone. Another criterion coupled with the vehicle weight reduction is the passive safety of vehicles. Designers are supposed to design vehicles such that passengers in accidents remain as safe as possible. There are strict standards and regulations for different types of accident that a vehicle should meet before it gets the permission to enter the market. For example, in the case of a rollover impact of buses, there are different regulations like ECE-R66 [7] and FMVSS 220 [8]. The requirements of these regulations have sometimes led designers to add excessive material to the structure to ensure adequate overall stiffness and integrity. Thus, in some cases, designs are affected by regulation limitations and more fuel is consumed because of higher weight.

Therefore, it seems that industry can benefit a lot from a new design evaluation approach that can provide a new paradigm of structural analysis. Such an approach should probe the global behavior of the structure. Also, it should be capable of finding a meaningful relation between the performance of different segments of the structure and the overall stiffness of the structure. Such relationship can help designers to distribute the mass in the structure more efficiently. In this study load transfer analysis is studied deeply as a candidate theory that can provide the new approach for designers to get a global understanding of the performance of the structure along with a numerical tool for stiffness evaluation of the structure.

Load transfer is one of the fundamental objectives of designing and manufacturing engineering structure. However, the study of load transfer in the engineering structures has achieved less

attention compared to other types of structural analysis, especially stress-strain analysis. As a result, more research seems to be necessary on the subject of load transfer analysis to provide engineers with a new and reliable tool for design evaluation and modification.

1-2) Objective of dissertation

In this research, the main purpose was to investigate the load transfer analysis as an emerging branch of structural analysis. The basis of this research was the existing industrial problems of a motor coach manufacturer. Several components of the multiple passengers carrying vehicles were chosen based on the real-life problems presented by the manufacturer and structural analysis with a focus on load transfer was performed on them.

The U^* index theory is the chosen methodology for load transfer analysis. This theory was first studied thoroughly, and it was shown that this method provides valid and reliable results for design evaluation. Real life problems of vehicle industry were addressed by the U^* index theory for load transfer analysis, and the capabilities of this theory were shown and compared systematically, for the first time, with the existing structural analyses methods. Moreover, two major contributions were made to the existing U^* index theory for load transfer analysis.

Firstly, the U^* index theory was validated through experimental testing. This validation was done for the first time in the literature and can provide a reliable reference point for further application of this theory in industrial problems. Secondly, the U^* index theory was extended to the nonlinear case of analysis. The original U^* index theory is limited to linear analysis. However, the presented extension of the theory showed that not only the concept of load transfer analysis with the U^* index applies to the nonlinear case of analysis, but also it is necessary to use the

presented nonlinear extension of U^* index in some cases. In summary, the objectives of this dissertation can be categorized as:

- Investigation of the load transfer analysis with U^* index method;

- Experimental validation of U^* Index theory;

- Theoretical extension of U^* index theory to nonlinear criteria;

- Application of the U^* index theory in the structural analysis of components of the multiple passenger vehicles.

1-3)   Organization of Dissertation

In this section, different chapters of this dissertation are presented with a short description about each of them.

Chapter 1

The first chapter of this dissertation is an introductory part. It explains where the work performed under this research fits. It brings up industry needs regarding a new approach in structural analysis that can provide designers with information about the global behavior of structure in transferring the imposed loads to the constraints. Also, the first chapter defines research objectives and tasks leading to their achievement. This description of the dissertation organization closes up the chapter one.

Chapter 2

Chapter two contains a literature review. In the beginning, it describes the necessity of load transfer studies in the modern structural analysis. Then, the two major approached to load transfer analysis are presented and compared. The next section shortly presents published work on the load transfer analysis using the U^* index theory. It brings up shortcomings and overly

simplifications in some of these research studies. It also explains the need for further study of the U^* index theory and its application in the vehicle industry. Finally, a conclusion is made upon the literature review that highlights the motivation and objectives of the presented work.

Chapter 3

Chapter three describes the theoretical preliminaries of the U^* index theory. This theory is the main theory used in this dissertation for load transfer analysis, and this chapter summarizes the fundamentals of this theory and the design criteria defined based on this theory.

Chapter 4

Chapter four introduces a procedure for the very first experimental validation of the U^* index theory. The motivation for this experiment is described in chapter 4, followed by the testing procedure. Finally, the results of the experiment are presented and compared with simulation results to validate the U^* index theory.

Chapter 5

Chapter five contains a thorough description of three cases of application of U^* index theory for load transfer in real industrial structures. A multiple passengers carrying vehicle is chosen for this research and three load carrying components of this vehicle are studied from load transferring perspective. The first part to focus on is the strut of the parcel rack. The load transfer study on the strut is accompanied by an experimental testing that can clearly show some of the exceptional capacities of the U^* index theory. In the next section of this chapter, the window pillar, which is one of the main load carrying parts of the coach is studied using the U^* index theory and also experimental testing. In the last section of this chapter, a bay section of the coach

is modeled and analyzed by U^* index theory. This analysis shows the potentials of U^* index theory for design modifications.

Chapter 6

In chapter six a theoretical extension is proposed for U^* index theory. The basic U^* index is limited to linear elastic problems, and in this research, a mathematical extension to nonlinear elastic problems is proposed. Two sample case studies are presented in the next sections of this chapter to show the difference between the original U^* index and the proposed U^*_{NL} index.

Chapter 7

This chapter includes the summary of the dissertation and the conclusions resulting from the research.

Chapter 8

Chapter eight contains a list of references used in this dissertation.

Chapter 2: Literature Review

2-1)   Introduction

In the last 50 years, Finite Element Analysis (FEA) has been developed and widely applied to study the response of engineering structures to different loading conditions. These studies have covered diverse aspects of mechanical engineering, from the static and dynamic analysis, to vibration and fatigue studies [9, 10]. The stress analysis provides quantitative, and localized information about the structure response to the loadings and the stresses are the direct indication of potential structure failure. However, one of the main functions of any engineering structure is to transfer the load efficiently to the supporting points. Some studies (e.g. [11] and [12]) in civil structure design have considered the load transferring in the structure. However, machine components are subjected to different loading and boundary conditions and have specific requirements for their structural design. Consequently, the conventional load transfer analysis used in civil engineering cannot be applied to mechanical systems.

Load transfer analysis will provide information regarding internal stiffness of the structure, and it can be used to evaluate different parts of a complicated structure. Such evaluation can determine if the structure is performing, as expected by designers, in the load carrying process. There have

been some studies targeting different aspects of load transfer and load path through the structure, but this concept still needs to be investigated more as it evolves to become a well-matured tool in structural analysis. The two main approaches for load transfer analysis are reviewed in the following sections to show the capacities and limitations of each one. Then, a conclusion is made based on the presented literature to clarify the direction of this research study.

2-2) Stress Trajectory Method

Kelly et al. [13] proposed this method in 1995, as one of the first efforts to introduce load transfer analysis in mechanical engineering. In that study, Kelly and Elsley presented the first rigorous definition of the load path as the course taken by a unit of applied load within a structure, beginning at the point of application and ending at the equilibrating boundary constraint [13]. This definition became a stepping stone for the further development of this method in different research studies [14], [15] and [16]. In 2001 Kelly et al. [16] provided a more clear description of their method based on FEM results. They defined the load flow for components of the applied loads lying in an arbitrary set of orthogonal axes. They claim that there is always a state of equilibrium between the loads applied to the system in the structure and the according reaction forces. Thus the separation of the applied load into a set of orthogonal components can help designers to find a load path by a simple equilibrium. To show how this works a small review on the original paper by Kelly et al. [16] can be helpful.

Unlike a fluid flow in which continuity law governs, the normal force on a surface in conventional stress analysis will not follow the continuity. Instead, by assuming a set of arbitrary orthogonal direction equilibrium guarantees that the components of the force will follow continuity. Figure 1 shows an example from [16]. In Figure 1a the continuity of flow in a fluid flow is shown while a normal force is applied on the left surface of the structure in Figure

1b. A combination of shear and normal stress react the applied load and resulting moments. For each component of the force, a passage can be mapped throughout the structure in which that component remains constant.

(a)   **(b)**
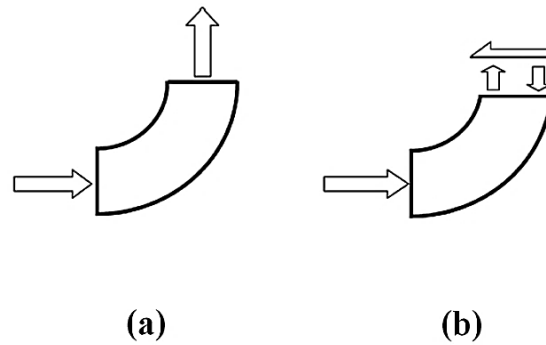
Figure 1) a: Continuity of a flow field and b: Equilibrium of forces in the structure [16] © Emerald Group Publishing

In simple words, the load path for a force in a given direction is a region in which the force in that direction remains constant [17]. By assuming that the structure of interest is the one shown in Figure 2 [16], definition of the load path means: $F_a = F_b$

$$F_b = \iint \sigma_{xx} \, dA$$
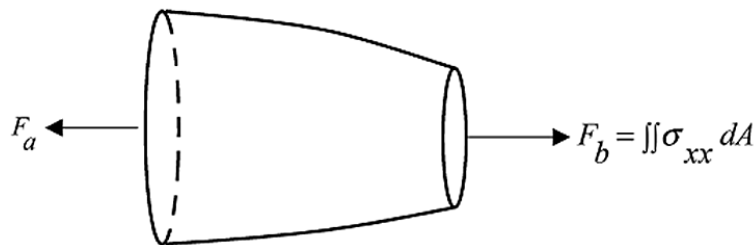
Figure 2) Sample structure and horizontal component of applied load [16] © Emerald Group Publishing

If Figure 3 [16] illustrates a small section of the side surface of this structure with a unit area, then a normal vector for this surface can be imagined as vector $\hat{n}$.
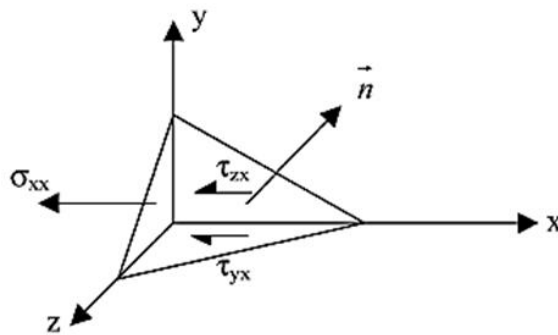
Figure 3) a unit area of surface of the side wall along with the normal vector, and horizontal components

of the total stress [16] © Emerald Group Publishing

Following the approach presented in [16] the force components acting on the area shown in Figure 3 can be found using the total stress vectors and the components of the normal vector ($\hat{n}$) and it can be shown that the tangent vector of the load path is defined by components of the total stress vector. Appendix A of this dissertation reviews the details of this approach along with an example. In summary, the total stress vectors define the local direction of transfer of a component of the applied load. After developing the theory an algorithm was proposed by Kelly et al., [17] to detect load paths in real world problem; using total stress components and Runge-Kutta method [17]. Appendix A of this report reviews basic steps of this algorithm based on [17].

Using this algorithm some application case studies for detecting load paths can be found in the literature. One of the best examples is the investigation of the load path in impact response of a helicopter fuselage frame [18]. Although this study applied the concept of load path detection with stress trajectory method in a dynamic analysis, it lacks providing meaningful results that cannot be achieved by conventional FE stress analysis. Complicated stress distribution of structure forced authors to combine deformation results to evaluate the load path in the structure. Therefore, it seems that there are shortcomings in using this method for load path detection.

Kelly, Reidsema and Lee [17] showed another example of the application of this approach for detecting the load paths in the structure. They studied the load path topology for a yacht hull using stress trajectories [17]. However, the structure chosen for this study had a simple geometry that implies the inefficiency of following total stress vectors in a more complicated mechanical structure. Nevertheless, this theory has shown capacities in dealing with composite materials too. Load path trajectories predicted by this method were used in [19] to improve the efficiency of the fiber steeled composite joints and in another study [20] similar concept was used to improve the strength of fiber steering around a pin loaded hole. However, in [20] the stress path term was used, which clearly shows the direct relation between the stress distribution and the load path detected by this methods. So it can be concluded that although stress trajectory method for load path detection has shown some potential in simple mechanical structures it has major limitations due to four main reasons:

- Following total stress pointing vectors can be very difficult or impossible in some cases. Therefore, additional set of information, like displacement field, will be necessary to follow the load path;

- The predicted load path directly illustrates the stress trajectory, thus the information provided by this method is very close to outcomes of a conventional stress analysis

- Stress concentration, which is a common feature of mechanical structures, can have a misleading influence on the predicted load paths. Next section covers this aspect in details, as the next method of the load path detection is introduced.

- This method merely predicts load paths in the structure and thus, provides limited information for design modifications.

Therefore, there was a necessity for an alternative approach for load path detection. This method had to apply to complicated machines, provide additional information compared to the conventional stress analysis and be immune to local features as stress concentration. Moreover, it would be very beneficial to designers if the alternative approach was able to provide unique information about the design of the structure that other methods of analyses cannot find. This alternative is the Load Transfer Index (U*) theory that is covered in the next section.

2-3) The U* index Method

The U* index method for load transfer analysis provides a numerical index that can quantify the load transfer in the structure and predict the load paths. A group of Japanese scientists introduced the foundation of the U* index theory in 1995 [21]. A study on relative rigidity, done by Kunihiro Takahashi in 1986 [22] was the main inspiration for the idea of an index for internal stiffness. In that study, the term "relative rigidity" was introduced and became the stepping stone toward a better-defined theory for load transfer in 1995 [21], in which U* index is introduced and derived.

Mathematical details of this theory are presented in chapter 3 but in summary, the U* index is a parameter that shows the degree of connectivity between the loading point and any given point in the structure. This theory provides a general picture of load transfer in the structure and evaluates the overall internal stiffness of the structure

In one of the earliest applications of this theory in the vehicle industry, Hoshino et al. [23] used the theory of load transfer paths to reduce the vibration of the cabin in a heavy duty truck. According to them [23] one simple approach to reduce vibration in the structure is stiffening the rigidity of the body. However, it is essential to use a systematic approach for choosing locations

for stiffeners to avoid adding unnecessary mass in random places. Therefore, U^* index theory can be helpful in locating the best places for adding stiffeners. To perform such analysis, Hoshino et al. [23] had to correlate the vibration reduction study, which usually involves the vibration modes, to the static analysis of load paths with U^* index theory. Therefore, they used a simple mass- spring model to define the relationship between the values of the spring constants for the connecting components and the characteristics of the cab floor vibration. Thus, with some simplifying assumptions they discussed the vibration reduction as a static problem [23]. To be precise, the U^* index theory was used to study the load transfer from the cab mounts to the cab structure, and the role of each component in this process was evaluated. Finally, Hoshino et al. [23] were able to find out discontinuities of load transfer in the frontal cross member of the cabin, which is directly effective on the noise and vibration of the structure.

Although substituting the conventional modal analysis of vibrating structures with a static analysis can be a questionable assumption, there are two important aspects of this study that make it be a significant research in the field of load transfer. Firstly, it was one of the very first times that U^* index theory was applied to solve a real life problem in vehicle industry and secondly, three design criteria were introduced and used in this study based on the U^* index analysis. These criteria that will be discussed in Chapter 3 can be employed for design improvements. Moreover, they can provide quantitative data as new goal functions for optimization. In other words, using U^* index theory will open a new window for structural optimization.

In less than a decade from the first introduction, the U^* index theory was developed to such an extent that various variations of the theory along with different calculation methods were introduced by 2007. For instance in 2007, Sakurai et al. [24] proposed a method for reducing the

calculation time of U^* index. The significance of this modification will be much clearer in the bigger structures with their massive FEA calculations. For a sample model with around 350 nodes, the modified method needs about 2000 seconds to calculate the U^* index for all nodes while the basic method requires 10,000 seconds for a model with just over 100 nodes [24]. Chapter 3 presents the details of this time efficient approach.

In another extension of the U^* index theory, Sakurai et al. [25] extended the theory of U^* index calculation for multiple loading points and in a more significant research on U^* index, Wang et al. [26] introduced the new U^{**} index. This new index can be summarized as a theory to follow the load transfer in a structure with distributed loading, while the original U^* index theory is more efficient in cases with concentrated loading condition. Later in 2009, this extension was applied [27] to study the load paths in a vehicle body structure under eigenmodes deformation of bending vibration. Initially, a natural frequency analysis was performed on a passenger vehicle structure. Then, the obtained vibration modes were imposed as forced displacements to all nodes in the structure and the reaction forces were measured at the designated supporting points. Finally, these reaction forces were imposed to the system to regenerate the bending mode in the structure. Due to the nature of the structure and selected loading points, a distributed loading condition was necessary, and thus, the newly introduced U^{**} index was used to follow the load transfer in this structure.

In a more recent study, Wang et al. [28] used both U^* and U^{**} indices to evaluate the load transfer in the truck cab structure in the initial phase of a frontal collision. This study showed that the distribution of U^* and U^{**} indices for the assumed loading and boundary condition are very similar while the exact values of the indices were significantly different. The most important feature of this study was to apply U^* index analysis, which is fundamentally applicable to linear

problems, to a frontal collision case, which is clearly nonlinear. Wang et al. [28] proposed two approaches to overcome the conflict between the nonlinearity of the problem and the limitation of linear U^* index theory. The first method was the so-called "Substitution- Stress Method," in which the structure is assumed to have two distinct areas: one in nonlinear and the other one in the linear domain. In this method, before the U^* analysis, the stresses are applied on the border between the linear and nonlinear regions and thus it can be stated that the nonlinear effects are reproduced on the linear region [28]. However, due to the computational difficulties, this method was not used by Wang et al. [28]. Instead, they used a hypothetical linear modulus for the nonlinear region. In this approach, which is called the "Substitution Modulus Method" the initial linear modulus (E_i) will be modified by a parameter (m), and the modified modulus ($E_s=E_i/m$) will be considered for the nonlinear zone [28]. Clearly, this will lead to having less precise results because of the approximate approach that was used to tackle nonlinearities in the structure. Although Wang et al. [28] opened up a new approach for applying U^* index theory in the nonlinear domain, their method had significant simplifying assumptions, such as considering a safety cage in the cab that remains in the linear zone during the impact and also an approximate method to cover the nonlinearities.

Research studies of the literature have demonstrated that U^* index analysis helps designers to achieve a better design, regarding more efficient load transferring and lower structure weight. Along with the previously mentioned, U^* index based design criteria, which were introduced in [23], there are other variations of U^* index theory that help engineers to get a general understanding regarding the structural behavior of the design. One of them is the U^*_{sum} index that will be covered in Chapter 3. This index combines the load transfer indices for both applied loads and the reaction forces and provides a global tool to quantify the effectiveness of each

component of the structure in the load transfer process. Koboyashi et al. [29] applied the U^* index theory to a vehicle structure in 2011 in a study done by Honda Research and Development Centre. They used the U^*_{sum} index to perform a comprehensive study to compare the results of load transfer analysis under different loading conditions. According to [29], there is a tendency that U^* indices go higher in parts with higher coupling rigidity, irrespective of the loading condition. Therefore, [29] predicted that there should be similarities in load transfer and U^* index distribution under different loading conditions. Four loading conditions were considered to be applied to the vehicle structure from the suspension: torsional loading, lateral loading, longitudinal loading and bending loading. Then, the U^*_{sum} distribution for each case was calculated and compared. It was shown, by a comprehensive comparison of the results, that the torsional loading condition displays a high level of similarity to the other loading conditions from load transferring perspective [29]. These results were used to evaluate the ability of the structure to transfer different kinds of loading efficiently. Moreover, the similarity analysis proved that the structure was designed to carry the torsional loadings in the most efficient way in comparison to the other types of loading. This research is important because it highlights another important application of U^* index theory. Following the same idea as Koboyashi et al. [29], designers can evaluate their design to find out the most dangerous loading conditions that can harm their structure or they can select loading and boundary condition in a way that an existing structure can provide most efficient load transfer.

Since U^* theory quantifies the internal stiffness of structure, it can be used efficiently to modify the design of a structure to achieve desirable overall stiffness without adding excessive weight to the structure. Naito et al. [30] used the U^* index theory to evaluate weight efficient structures. The significance of this research is the application of histogram of U^*_{sum} values to study the

distribution frequency of U^*_{sum} values and provide a macroscopic understanding of the body structure. Naito et al. [30] extended the research that was done on the vehicle under for load condition [29] and used the results of U^*_{sum} to locate areas with low stiffness. Then, thickness optimization was conducted for different parts of the vehicle to achieve an efficient design with improved stiffness. Although the optimization was done based on the stress values and not based on the U^* index distribution - an obvious drawback - it can be stated that authors [30] were capable of stiffening the structure using the U^* index theory.

Following the same line of thinking, it can be concluded that the results of the U^* index analysis can potentially help designers to choose best locations for material removal without lowering the internal stiffness in an extreme manner that might put the integrity of the structure in danger.

In another application, U^* index theory has also been used in the evaluation of welded structures. Naito et al. [31] used the U^* index theory to study the sheet steel joints with spot welds in 2012. They used the U^* indices values as an expression of the strength of connections between the load points and support points. Such expression for strength is an aid in the design of welded structures that will be highly effective in increasing stiffness. Naito et al. [31] selected simple but widely used structures of vehicle industry to study the capacities of U^* index theory in the evaluation of spot weld locations. They studied hat-shaped section beams and selected three different spots for adding welds, at the center of the top face of the beam, near the edge of the top face and the side faces of the beam and compared the U^* index distributions. Then using a consistency analysis they chose the best location for spot welds for efficient load transfer using the results of a U^* index analysis [31].

In 2013, Nambu et al. [32] approached the U^* index theory from a statistical point of view. Using the histogram of U^*_{sum}, they defined a new statistical concept, called U^* variance [32]. Nambu et

al. [32] suggest that it is desirable to have low U^* variance values in the structure. The U^* index variance shows the distribution of the stiffness throughout the structure, and since a desirable design should distribute the load almost equally in all components of the structure, a low U^* variance value represents a relatively equal contribution of all parts of the structure in the load transfer process. Nambu et al. [32] studied a vehicle body under 18 loading conditions to provide a database for statistical comparison. Using different loading conditions they managed to create a relationship between the stiffness and the U^* variance. These results can be employed by other researchers who work in vehicle field, as a benchmark, to compare the U^* variance of different parts with the existing data for body parts.

In recent years there has been more research to extend the application of U^* index. One of the most important one of them is the study presented by Takahashi et al. [33] in 2013. They proposed a method to consider the effect of inertia in the calculation of U^* index. Satoshi et al. [34] described this approach in English in a more recent study in which they opened a new window for application of U^* index theory for impact problems. The details of this study are presented in [34] in which, the new index was applied to side impact of the vehicle, and the effect of design variations to the load transfer was studied, considering the effect of inertia.

2-4) Conclusion

Based on the presented literature it can be concluded the load transfer analysis is getting more and more attention from engineers to study the structural behavior of mechanical machines. However, from the two major existing approaches, the U^* index theory has shown more potential, fewer drawbacks and has been applied to more industrial problems. Therefore, in the presented work, the U^* index theory is selected for performing load transfer analysis.

There have been several studies in literature trying to extend and complete the U^* index theory to make it a well-stablished theory as the conventional stress analysis is. However, certain steps should be taken toward achieving such goal, which seems to be missing in the literature. Firstly, as conventional stress analysis has been in application for more than half a century, it is essential to have a comprehensive and detailed comparison of U^* index theory with the stress analysis. This way, all the unique capacities of the U^* index theory can be highlighted, and agreements between outcomes of the U^* index and stress analyses can verify the accuracy of U^* index results. Therefore, in the presented study after going through fundamentals of the U^* index theory a comprehensive comparison to the convention stress analysis is performed on real life vehicle components under working loading conditions. Moreover, although U^* index has shown exceptional capacities in literature, it is missing a rigorous experimental validation. Thus, an experimental validation testing procedure is proposed and conducted in this study to create a solid referral point for future computational studies.

Another aspect that put limitations on the application of this theory is its linear foundation. Consequently, to extend the concept of load transfer to the nonlinear domain, a theoretical extension is proposed and tested computationally for a load transfer index for structures with geometrical nonlinearities (U^*_{NL}[1]). Although the newly proposed index will not cover all types of nonlinearities, it can open up space for further extensions of the theory.

Finally, almost all of the application of the U^* index in literature are limited to the floor and frontal panels of passenger vehicles. Therefore, in this study, several components of a multiple passengers vehicle were selected and analyzed for load transferring using U^* index theory. These components vary from a parcel rack holder structure (also named as the strut) of a motor coach

---

[1] To be discussed in chapter 6

in working loading condition, to the window pillars of the frame of the coach in most severe loading conditions and the roof and emergency exit of the superstructure in a rollover impact scenario. Moreover, some of these components were tested physically under same loading condition to evaluate the results of the U^* index analysis in comparison with real testing.

The outcome of this research will be beneficial to automotive industry, especially for structural analysis of heavy or multiple passenger vehicles. This study can help designers to modify their design based on the results of load transfer analysis, while the structure still meets the requirements based on the failure criteria on one side, and safety requirements on the other side. Achieving a general awareness regarding the structure will lead to designs with an optimum mass-stiffness relation. Such goal can be accomplished by considering the load transfer and stress analysis, like two wings for designers in their journey toward a perfect design.

Chapter 3: U* index Theory

3-1) Introduction

The U* index theory [21] presents a numerical indicator for the internal stiffness of the structure. The theory claims that the imposed load to the structure will be carried through parts with highest U* value; i.e., a load path will be the path on the structure that connects the points with the highest U* index values. This theory is based upon a mathematical foundation presented in [21], which is reviewed in the "*Theoretical Preliminaries*" section. Using U* values, three new design criteria for structural analysis were introduced that will be discussed in the "*Design Criteria*" section. These parameters were then used to evaluate the structures, selected as the case studies in this dissertation.

3-2) Theoretical Preliminaries

In this study, the methodology introduced by Shinobu in 1995 [21] is used to define and calculate the U* index. This index quantifies the internal stiffness between any points in the structure and the loading point, which is the first and probably the most important aspect of the U* index theory. As Shinobu et al. [21] clarified, "Internal stiffness" used in the load transfer index (U*) theory is not the same as the conventional stiffness matrix calculated by summing up

the local stiffness matrices defined in Finite Element Analysis. The internal stiffness of any point in the structure is the degree of connectivity between that point and the loading point.

The U* index theory is based upon total strain energy of the system under different boundary conditions. Consider the structure shown in Figure 4a which is loaded at point A and is constrained at point B. This structure can be illustrated with three linear springs, as shown in Figure 4b. In this figure, point A, the loading point, is connected to the supporting point (point B) and an arbitrary point (point C) with two linear springs.
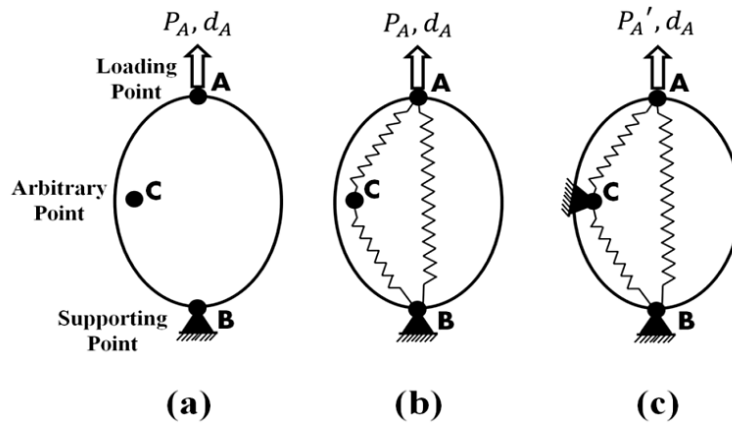
Figure 4) Sample structure for U* analysis: (a) Original structure, (b) Spring model and (c) Modified constraints

The total strain energy of the structure shown in Figure 4b can be calculated using Equation 1:

$$U = \frac{1}{2} P_A d_A \tag{1}$$

where U is the total strain energy that stored in system and P_A and d_A are respectively the applied load and resulting displacement at the loading point (point A).Since the springs were assumed to be linear, they follow the linear elasticity equations. As a result, the force-displacement of the springs will follow Equation 2:

$$\begin{bmatrix} P_A \\ P_B \\ P_C \end{bmatrix} = \begin{bmatrix} K_{AA} & K_{AB} & K_{AC} \\ K_{BA} & K_{BB} & K_{BC} \\ K_{CA} & K_{CB} & K_{CC} \end{bmatrix} \begin{bmatrix} d_A \\ d_B \\ d_C \end{bmatrix} \qquad (2)$$

In this equation P_i (i=A,B,C) represents the applied loads at each end of springs, d_i (i=A,B,C) is the according displacement and K_{ij} (i,j=A,B,C) represents the internal stiffness of each spring. It is important to note that the K_{ij} matrix is not the conventional FEM global stiffness matrix, and it represents the actual stiffness of each illustrative spring; i.e. K_{ij} shows the actual internal stiffness between any two points of i and j (i,j=A, B, C,…) in the structure. Considering the boundary condition, shown in Figure 4b, the only loading point in the selected sample structure is point A, and the force-displacement for this structure will be as Equation 3:

$$P_A = K_{AA}d_A + K_{AC}d_C \qquad (3)$$

where, P_A is the applied load on the structure and d_A and d_C are displacements at point A and C. The term K_{AC} in this equation is the stiffness of the illustrative spring between points A and C. K_{AA} is not an independent parameter, it can be shown that for rigid translation of the structure, K_{AA} have the same magnitude as summation of the stiffness of the springs between point A and the other two points; i.e. $K_{AA} = -(K_{AB} + K_{AC})$. By substituting the P_A from Equation 2 into Equation 1, the strain energy of the system will be as:

$$U = \frac{1}{2}(K_{AA}d_A + K_{AC}d_C)d_A \qquad (4)$$

All terms of this equation have already been defined in Equations 1 to 3. In the next step, a modification should be made on the loading and boundary condition of the system. As Figure 4c shows, the arbitrary point C is constrained, while the same displacement (d_A) is supposed to be kept at the loading point. Therefore, the necessary load for creating same displacement (d_A) will

change from P_A to P'_A. For this system, d_B and d_C are equal to zero and using the similar procedure shown in Equation 4; the strain energy can be written as:

$$U' = \frac{1}{2} P_A' d_A = \frac{1}{2} (K_{AA} d_A) d_A \tag{5}$$

where, U' is the stored strain energy in the modified system and P'_A is the required load that should be applied to the modified system, for achieving the same displacement(d_A) at point A (loading point). Here the load transfer index (U^* Index) can be defined based on the proposed equation in [21]:

$$U^* = 1 - \frac{U}{U'} = \left(1 - \frac{2U}{(K_{AC} d_c).d_A}\right)^{-1} \tag{6}$$

In this equation is U^* is the load transfer index and it is shown this index is proportional to K_{AC}^2. In other words, the U^* index is an indicator for the internal stiffness between the loading point (point A) and any arbitrary point (point C) in the structure. By calculating the U^* index for every point in the structure, the U^* distribution can be found. As shown in the schematic demonstration of the U^* distribution in Figure 5, the U^* index will be equal to 1 at the loading point, and it will be equal to 0 at the supporting point.

The U^* index quantifies the internal stiffness of the structure, and the applied load tends to pass through parts with highest internal stiffness. Therefore, based on the definition of the U^* index theory, the main load path is the path that connects the loading point to the supporting point passing over the point with highest U^* index (highest degree of connectivity to the loading point). So, if a vector λ is introduced as:

---

[2] Appendix B provides a simplified explanatory example to show the proportionality of U^* to K_{AC}

$$\lambda = -grad\ U^* \tag{7}$$

Then, the successively traced line along the smallest λ value is the load path [28]. In a simple case like the structure shown in Figure 5, the main load path is simply the ridge line of the contour curves of U^* distribution.
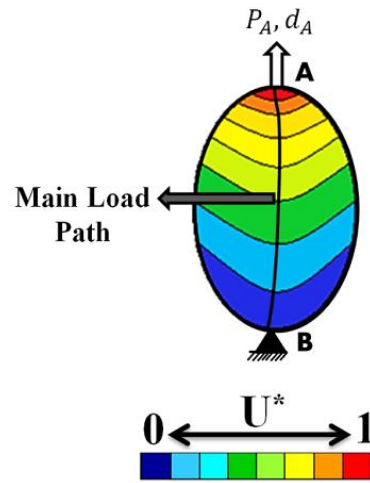
Figure 5) The U^* Distribution and the main load path for the sample structure

The calculated load transfer index predicts the transfer of applied load in the structure, which can be named as U^*_1 index. By implementing the same concept, it is possible to follow the reaction forces that go back through the structure from the supporting point. The resulting index for load transfer of the reaction forces can be named as U^*_2. Then, to achieve an index that can represent a complete picture of load transfer in the structure U^*_{sum} [29] can be defined as:

$$U^*_{sum} = U^*_1 + U^*_2 \tag{8}$$

The higher U^*_{sum} in a part of the structure represents more significant role in load transfer and vice versa. Moreover, since U^*_{sum} value of any point in the structure represents its significance in the load transfer, creating a histogram of all U^*_{sum} values can depict how balanced the load transfer in the structure is.

The concept of U^*_{sum} variance of the U^*_{sum} histogram was introduced more recently [32]. The U^*_{sum} variance can be used to find out how cooperative are all parts of the structure in the load transfer process. A low variance of U^*_{sum} histogram implies that all parts of the structure contribute to the load transfer, relatively in the same manner. Therefore, achieving a design with low U^*_{sum} variance can be considered as a new goal in the design process.

3-3)   Design Criteria

It was shown in the previous section, that the U^* index is an indicator for internal stiffness and consequently the load transfer in the structure. However, unlike the stress trajectory-based methods for load transfer analysis [13], which can only predict the load path; the U^* index method can be used for both load path detection and design evaluation. The design evaluation capacity of U^* index theory is an excellent feature of this theory for structural analysis that can give a general awareness regarding the global behavior of the structures. Based on U^* theory, three main criteria are introduced for design evaluation [23], which have been applied to several case studies in the literature [31, 35].

These design criteria, shown in Figure 6 and Figure 7, are as follows [23]:

1) Uniformity: Uniform decay of U^* along a load path (Figure 6a);

2) Continuity: Smoothness of the curvature of U^* along a path (Figure 6b);

3) Consistency: Coincidence between the main load paths from the loading point and from supporting points (Figure 7).

Since U^* theory is based upon modeling the structures using illustrative springs, the ideal case (dashed lines in Figure 6) represents the variation of U^* index (or its curvature) in a linear spring. Clearly, in a linear spring, the U^* index value varies linearly from 1 at the loading point to 0 at the supporting point. Accordingly, the curvature of U^* variations will remain constant zero along

the spring. However, in the engineering structures, it is probable that the U^* variation (or its curvature) does not follow the same behavior as in the spring. Therefore, there will be deviations between the curves for real case scenarios (dotted curves in Figure 6) and the ideal ones (dashed curves in Figure 6) which can be seen in Figure 6 as shaded areas. Engineers can improve the structure behavior by design modifications that can lead to reducing these shaded areas. Optimizing the design can also be achieved by considering a minimum shaded area as one of the goal functions of the optimization process.
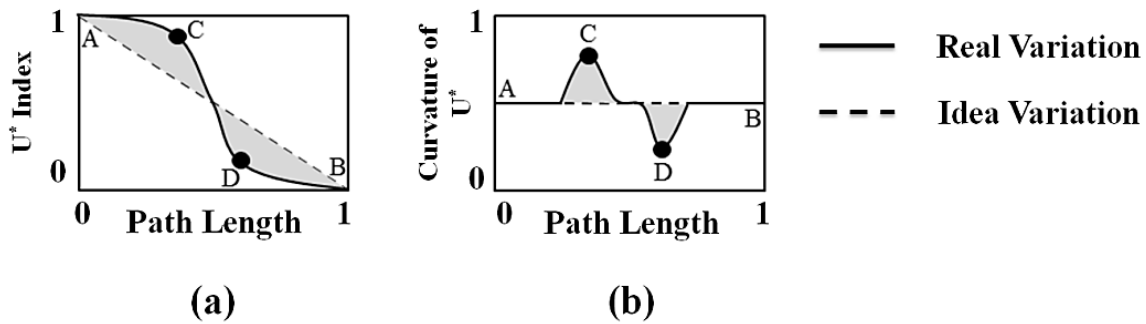
Figure 6) U^* based design criteria a: Uniformity, b: Continuity

The other useful design criterion, based on U^* index, is the consistency of the main load paths. In the ideal case of a linear spring, the load paths of both U^*_1 (index for applied load) and U^*_2 (index for reaction forces) are consistent. Figure 7a shows a schematic picture of desirable consistency of load paths. However, in the engineering structures, the load paths of applied load and reaction forces might probably pass through separate courses. Such deviation between load paths is shown In Figure 7b. Designers can modify their design to achieve a more desirable load transfer in the structure by making changes that lead to a smaller (or a minimum) deviation area between the two load paths.
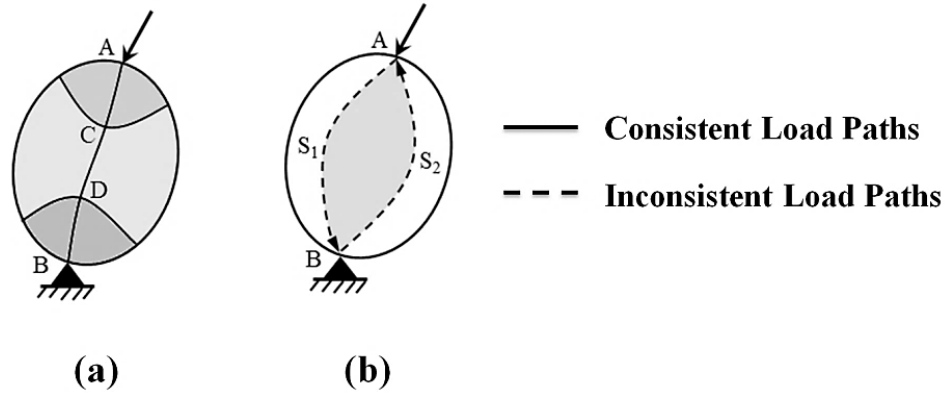
Figure 7) Load path consistency criteria, a: Ideal Consistency, b: Undesirable consistency

3-4) Development of the Algorithm for Calculation of U*

Since U^* is a relatively new concept, it is not available in conventional commercial FEA software[3]. In this study, a program is developed for calculating U^* following the framework proposed by Shinobu et al. [21].

Based on Equation 6, to find the U^* value at each point, the total strain energy of the system should be calculated for two different boundary conditions (free and fixed) at that point (like point C in Figure 4). Consequently, the boundary condition should be changed by fixing one node at a time (point C), while keeping the rest of the nodes free in all directions. Therefore, calculation of strain energy shall be performed by the number of nodes.

A computer program, written in Matlab (2012b, The MathWorks, Inc. Natick, Massachusetts, United States), is developed for the repetitive task. This computer code will automatically generate models with different boundary conditions and send them for FEM analyses. The in-house developed program will then use the results of these FEM analyses to calculate the U^* value on each node of the structure. MSC NASTRAN and ANSYS Mechanical APDL were

---

[3] MSC Nastran in Japan is developing an additional, optional, toolbox for U^* index calculation

employed in this study to perform the required FEM analyses. Figure 8 is a schematic illustration of the explained algorithm.

```
┌─────────────────────────────┐
│   Total strain energy (U)   │
│        calculation          │
└─────────────────────────────┘
              │
              ▼
┌─────────────────────────────┐
│  Fixing node i and imposing │◄──────┐
│   d_A at loading point      │       │
└─────────────────────────────┘       │
              │                        │
              ▼                        │
┌─────────────────────────────┐       │
│    Total strain energy      │       │
│   calculation for modified  │       │
│       system (U′)           │       │
└─────────────────────────────┘       │
              │                        │
              ▼                        │
┌─────────────────────────────┐       │
│     U*_i = 1 − U/U'_i        │       │
│        i = i + 1            │       │
└─────────────────────────────┘       │
              │                        │
              ▼                        │
      No   ╱─────────╲                 │
   ┌──────<  Is i > number  >──────────┘
   │       ╲ of nodes? ╱
   │         ╲───────╱
                 │ Yes
                 ▼
        ┌─────────────┐
        │   Finish    │
        └─────────────┘
```

$$U_i^* = 1 - \frac{U}{U_i'}$$

$$i = i + 1$$
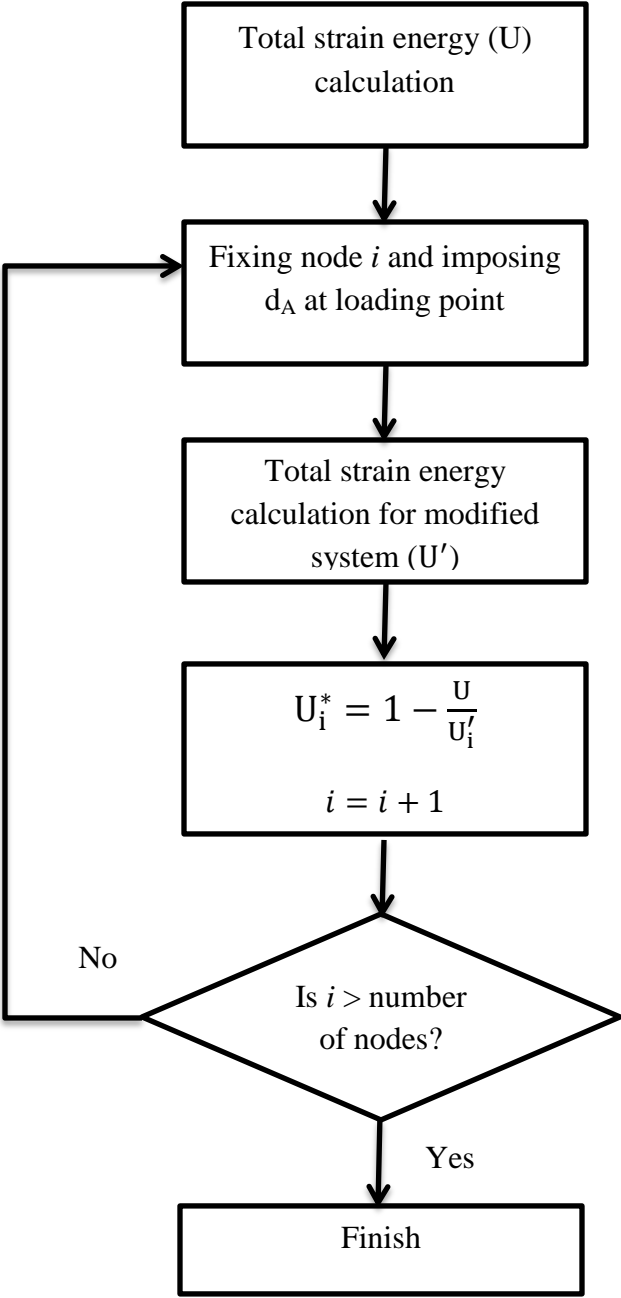
Figure 8) U*calculation algorithm of current study

3-5)   Time efficient approach for U* index calculation

The proposed method of Shinobu et al. [21] for the U*index calculation is justified and the proposed algorithm in this study for implementing the discussed method of calculation has been proved to be valid (to be discussed in Section 3-6). Nevertheless, there is a limitation in this approach that makes it tough to apply it for analyzing large structures like multiple passenger vehicles. For measuring U* at any sole point on the structure, the boundary conditions should be modified, and the FEM analysis should be done for the new boundary condition. This procedure is very time-consuming. Some basics of FEM analysis are pointed out here to prove a better picture.

Finite Element Method can be divided into two main methods [36]: the displacement method (Stiffness method) and the force method (Flexibility method). MSC Nastran, as most of the commercial software, is designed based on the displacement method, and in displacement method, whenever the geometrical boundary condition changes, structural stiffness matrix should be calculated again. As a result, in the current algorithm, each time the Matlab code send the new input file to the MSC Nastran, much time will be consumed on generating new stiffness matrix. Therefore U* calculation is a time-consuming process.

3-5-1- New U* calculation method

Sakurai et al. [24] proposed the solution to this problem in 2007. As Sakurai et al. claim, replacing the multiple geometrical boundary conditions into multiple mechanical boundary conditions will lead to significant reduction of the calculation time. Their main idea for performing this task is to fix the loading point and impose a set of independently linear

inspection loads on the arbitrary point C. In this way, for each point C, the following information can be easily derived:

- Reaction forces on the previously loaded point A (R_A)

- Displacement of point C, due to the imposed inspection load (d'_c).

Based on these data, one can easily calculate the stiffness (internal stiffness K_{AC}) between point A (loading point) and any arbitrary point C. Then, by inserting the calculated K_{AC} in equation 6, U^* values for each point can be derived. As Sakurai et al. [24] has shown, this method decreases the calculation time significantly. It should be mentioned that this time difference is more noticeable as the number of nodes in the structure exceeds 500 nodes (Figure 9).
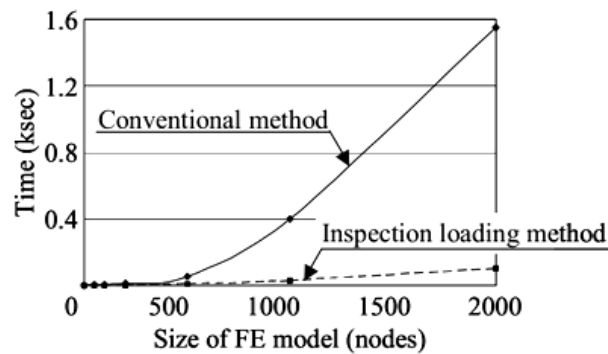
Figure 9) Difference in calculation times by ordinary and new method of U^* calculation **[24]**

3-5-2- Development of an algorithm for implementing new method

Similar to the regular method of U^* calculation, it was necessary to develop an algorithm for applying the proposed method of Sakurai et al. [24]. A Matlab program was written which generates models with three linearly independent loads on each node (one node and one load at a time). These models were then sent for FEM analysis by MSC Nastran. The results obtained in FEM analysis were used in the Matlab program to calculate the internal stiffness between the loading point and each node. Consequently, the program can calculate the U^* at each node. A

schematic demonstration of this algorithm is depicted in Figure 10. It is important to notice that in Figure 10, d_C represents the actual displacement of the arbitrary point C under actual loading while D_c is the displacement of this point under inspection loading while both points A and B are fixed.

```
┌─────────────────────────┐
│  Total strain energy (U) │
│       calculation        │
└─────────────────────────┘
             │
             ▼
┌─────────────────────────┐
│   Fixing the loading and │
│ supporting points & applying │
│ inspection loading on node i │
└─────────────────────────┘
             │
             ▼
┌─────────────────────────┐
│  Measuring displacement at │
│ node i (Dc) and reaction forces │
│  at loading point (RA)   │
└─────────────────────────┘
             │
             ▼
┌─────────────────────────┐
│   KAC = RA DC⁻¹          │
│                          │
│   Ui* = (1 - 2U/((KACdc)·dA))⁻¹ │
└─────────────────────────┘
             │  i = i + 1
             ▼
        ◇ Is i > number of nodes? ◇
             │
```

$$K_{AC} = R_A D_C^{-1}$$

$$U_i^* = \left(1 - \frac{2U}{(K_{AC}d_C)\cdot d_A}\right)^{-1}$$

$i = i + 1$

Is $i >$ number of nodes?

No

Yes

Finish
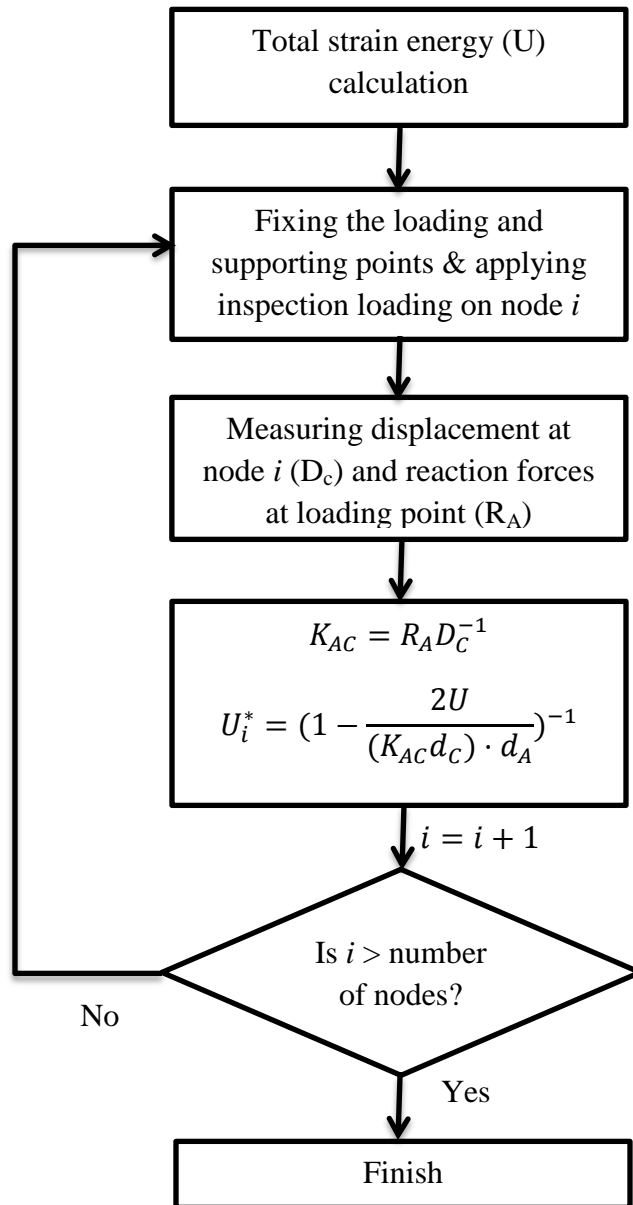
Figure 10) Schematic flow chart of proposed algorithm

3-6)   Verification of proposed algorithms

Since U^* is not a default variable in this software, the calculated U^* values for all of the nodes were assigned to them as the values of the temperature variable. The U^* distribution on the plate with a circular hole in the middle, which has been already studied by Koboyashi et al. [29] (Figure 11a), can be considered as the perfect benchmark to validate the developed programs in this study. Figures 11b and 11c show the results of the current study for deriving the U^* distribution on the similar plate with the two proposed algorithms. Obviously, the results are in complete agreement with results of [29], and the proposed algorithms can be used for the structure in the case studies.

(a)   (b)   (c)
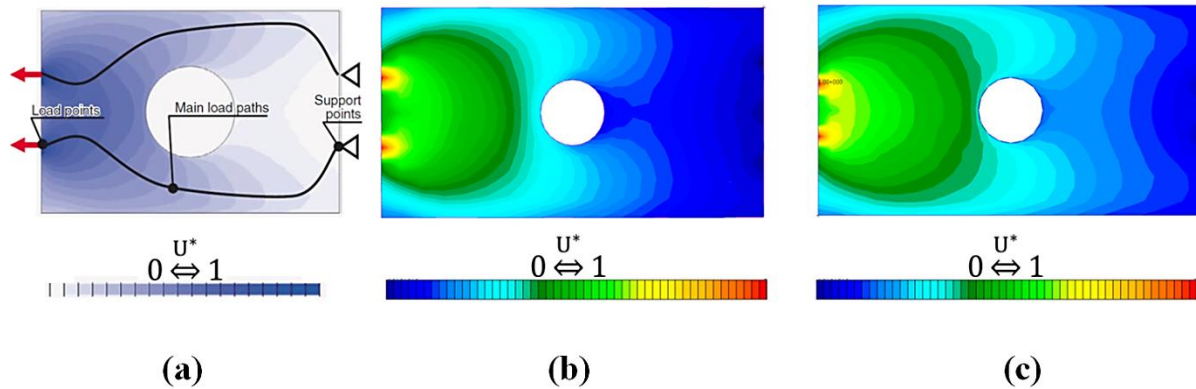
Figure 11) U^* distribution on a plate loaded on left face a: Results from literature, Reprinted with Permission from SAE International [30], b: Results from initial algorithm (changing geometrical boundary condition) and c: Results from secondary algorithm (changing mechanical boundary condition)

It is also beneficial to point out a significant advantage of U^* index theory for load path detection to stress based methods using the provided example of Figure 11. For the given structure with the marked loading and boundary condition, the load paths are predicted to diverge from the edge of the circular hole in the middle of the plate. However, if stress trajectory method were

used to detect the load paths, the load path would have converged to the circular hole due to stress concentration effects. Such prediction is clearly false, as the hole cannot be a load transferring part of the structure as it has no material. Although a full comparison of U* index theory is presented in chapter 5, this example can provide some preliminary information regarding the advantages of U* index theory for load path detection.

Chapter 4: Experimental Validation of U* index Theory

4-1)   Introduction

As the literature review section showed, several researchers have used the U* index theory for different studies in the mechanical engineering field. However, most of these studies focus on the application side of the U* index theory. Therefore, in this section of the dissertation, the main objective was to present a stepping stone for further theoretical expansion of the theory by providing the first experimental validation of the U* index theory. This experimental validation proves that U* index is a true measure of load transfer in the structure. This section will show that a load path which includes points with higher U* index values in the simulation, indeed carries more load in the physical testing; i.e. is the main load path in the structure.

4-2)   U* index theory validation

Based on the definition, the U* index theory is supposed to be able to predict the significance of different parts of the structure in the load carrying process. In other words, this theory suggests that a path consisted of points with higher U* index value, carry more load in the structure. A structure with different possible load paths under one loading condition was considered to validate the U* index theory. First, the main load path was identified physically through an

experiment. Then, the results of U* index simulation of the same structure were compared to the experimental results to validate the accuracy of the load transfer index theory, (i.e. to validate that the path connecting the points with high U* values carries the majority of the load).

4-2-1) Experimental testing

The test setup of the proposed experiment contained a table-shaped main part and two loading bars. The table-shaped structure was made of Aluminum and is marked as "Part A" in Figure 12, while the two loading bars, marked as Part B, were made of steel. Part A has two circular stands, marked as the "Thick" and "Thin" shafts in Figure 12. These shafts carry the applied loads to the structure toward the supporting points. The stands are both 8" (20.32 cm) long, and their centroids are 5" (12.7 cm) apart from each other. Figure 12 includes all other dimensions of the structure.
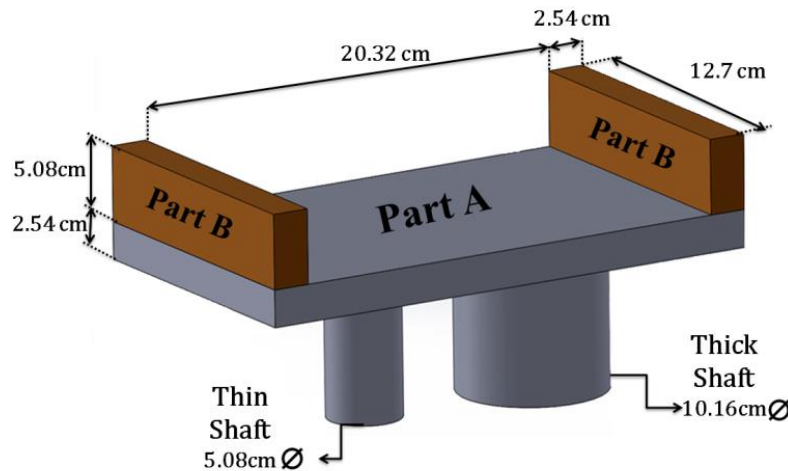
Figure 12) Test structure of the experiment

The test procedure initiated by placing the main structure (Part A) on the two force plates shown in Figure 13, such that each shaft was located on one force plate. These force plates were built in the BERTEC instrumented treadmill [37], which can measure 6-components of loading with an

accuracy of 0.1 N. However, in this test only the vertical loading was of interest. Then, the external non-body force was applied to the system by placing steel bars (Part B) on the two edges of Part A. The cylindrical shafts carried this load to the foceplate. This loading process was repeated three times with the same setup to verify the repeatability of the experiment. Moreover, to make sure that force plates were behaving identically, the whole experiment was repeated completely after rotating the structure on the force plates such that each shaft stood on the other force plate.

The primary measurement during this experiment was the vertical component of load on the force plates using the built-in, 16-bit digital data acquisition system of the force plates. The measured digital data was then amplified with an external amplifier and recorded on a computer. Figure 13 depicts a schematic picture of the whole experiment setup.
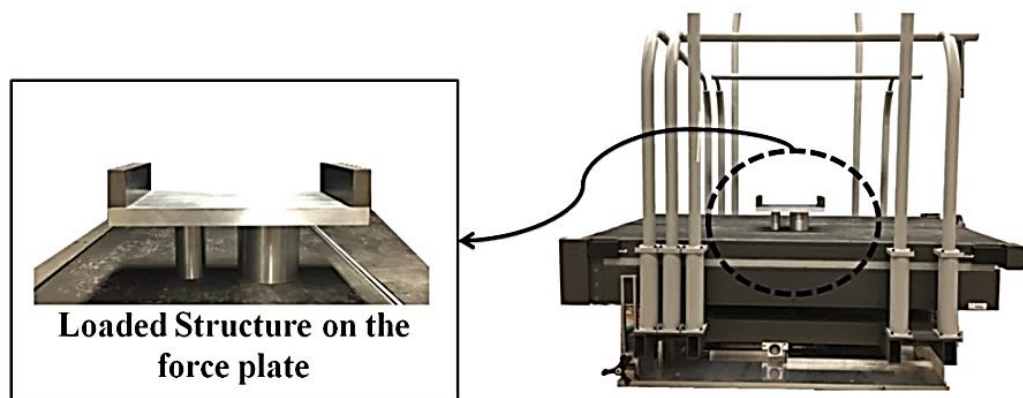
Figure 13) Testing specimen on the force plate

The data acquisition in this experiment was performed in two stages. In the first stage, only Part A was placed on the force plates. Consequently, the gathered data in this step showed the distribution of the structure's weight (body force) between the two shafts. Then, in the second phase, to solely measure the added external (non-body) force to Part A, the readings of the

software were set to zero, and then the external loading (non-body force) was applied to Part A by placing Part B on top of it (Figure 12). In other words, in this stage, the force plates were ignoring the initial weight of Part A, and the measured data on each force plate showed the portion of the external load that was carried by the shaft standing on that force plate. This information was representing the ending point of load paths in the structure and was used to detect the amount of load that was carried through each path. Finally using the U^* index theory, the main load path for the externally applied non-body force in the structure was determined, and the result was then compared to the experimentally detected load path.

4-2-2) Computer modeling

After the experiments, the U^* index distribution was calculated computationally for the model. Then, the computationally detected load path was compared to the experimental results to validate the theory. The FE modeling was performed using ANSYS Mechanical APDL software. Solid 185 (Tetrahedral) elements were used to mesh the structure. The model contained 2072 nodes, and it was constrained by fixing the nodes on the lower surface of the shafts. The results of the computer modeling are presented in the next section along with a comparison to the experimental testing results.

4-3)   Results and Discussion

By performing this test and simulations it was shown that the U^* index theory is a valid measure of load transfer in the structure, and thus, can be applied for predicting the load paths in the structure. The experiment was designed to show if the theoretically detected load path using U^* indices is accurate. The physical test results are presented in the next section to show the real load path in the structure. Then, the load path predicted by the U^* theory is presented in the

Simulation Results section to provide an opportunity for comparison of the results and validation of the theory.

4-3-1) Physical test results

As stated in the test setup description, the measured data in the experiment was the vertical load applied on each force plate through the supporting shafts of the testing specimen. Figure 14 demonstrates the readings of the two force plates as the percentage of the load that was carried by each shaft with or without external loading. During the initial phase of the experiment, the test specimen (Part A) imposed 77.27 N of body weight load on the force plates, out of which 59% was carried through the thicker shaft and 41% through the thinner shaft. Therefore, the structural stiffness of the systems dictated the amount of body weight that passed to each force plate.

	Unloaded Structure (Body Weight)	External Loading (Non-body loading)
▨ Total Measured Load	77.27	40.7
□ Load Carried by Thick Shaft	44.89	17.22
⊞ Load Carried by Thin Shaft	31.54	23.48
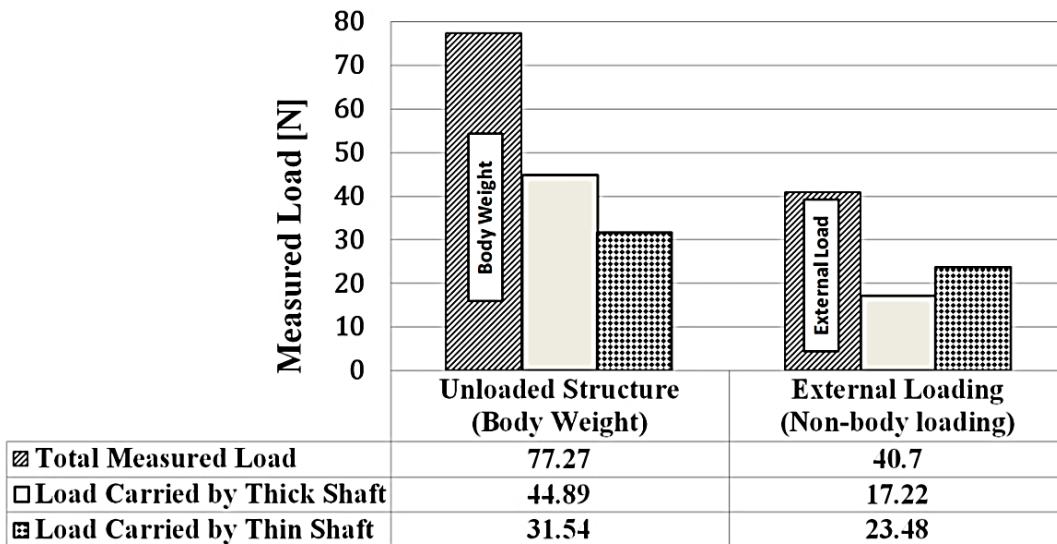
Figure 14) Results of Experiment

In the second step of the experiment, corresponding to the external loading applied by Part B on Part A, the data measurement setup was set only to read the added external loading. As shown in Figure 14, steel bars (Part B) applied a load of 40.7 N on Part A. The thicker shaft carried only

42% of this external loading, while the thinner shaft found to be the main carrier of the external load with 58% load carrying capacity. These measurements mean that in the presented case, the shaft with higher structural stiffness was carrying a lower amount of load.

4-3-2) Simulation results

An computational load transfer analysis with U^* index can prove whether the U^* index theory is capable of predicting the correct load path. Figure 15a shows the U^* index distribution in Part A due to the external loading applied on the system by placing the Part B on it. Starting from 1 at the loading point, the U^* index goes to zero at the supports at the end of the shafts.
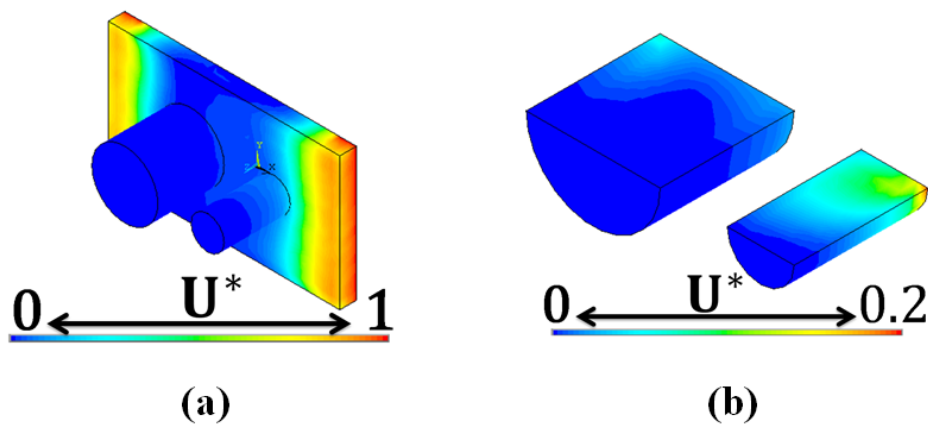
Figure 15) U^* index distribution: (a) throughout the whole Structure (b) through the shafts

Figure 15b shows the U^* distribution in the cross-sections of the shafts. Clearly, the thinner shaft shows higher values of U^*, starting from 0.204, while the U^* values in the thick shaft are much smaller. Different paths were considered on the shafts, and the U^* values were followed along those paths to compare the U^* index variation on them.

Figure 16 shows the U^* index variation along the edges of circular shafts. As it can be seen in this figure, the thinner shaft exhibits higher U^* values along the edges. Also, the main load paths

on each shaft were determined, and the U^* variation along these paths was calculated. The results are shown in Figure 17.
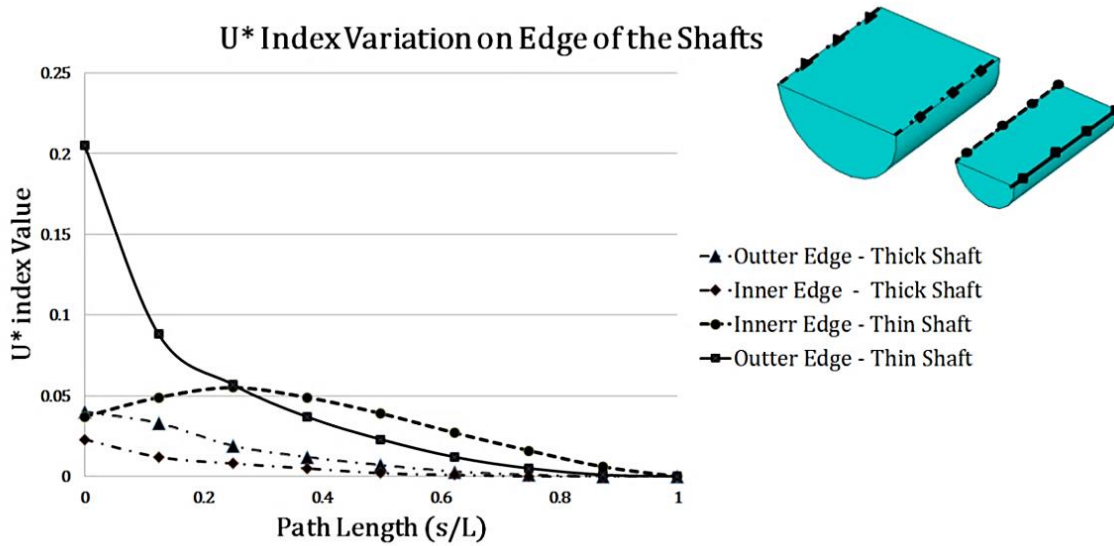
Figure 16) U^* index variation along the edges of the shafts

Based on the U^* index theory, these results reveal that for this loading condition, the internal stiffness of the thinner shaft is higher than that of the thicker one, and thus the thinner shaft is the main carrier of non-body external forces in this model.
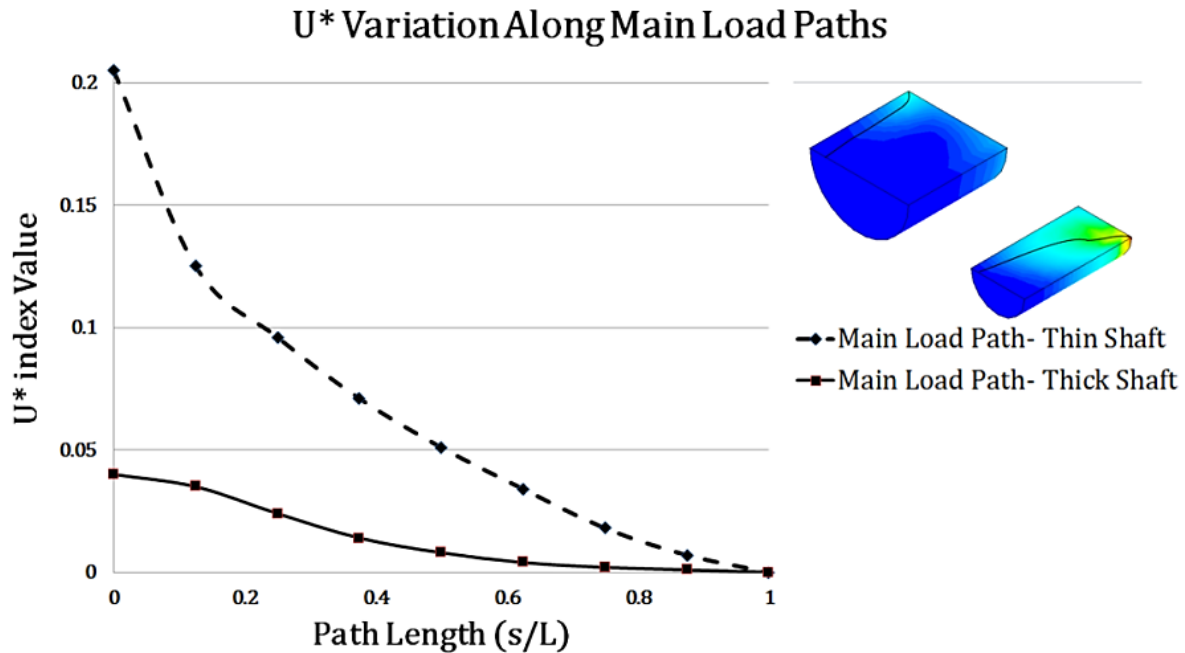
Figure 17) U* index variation along the main load paths of each shaft

4-3-3) Discussion on the results

The experiment suggests that the thicker shaft carries a greater portion of Part A's weight in the first stage of the experiment (only body weight); however, the thick shaft had a less significant role in carrying the external (non-body) load applied to Part A by placing Part B on it. So, based on the experimental results, the main load path for carrying this type of loading in the testing specimen passes through the thin shaft. On the other side, the computational load transfer analysis with the U* index shows that the thinner shaft has higher U* index values compared to the thicker one and according to the U* index theory, it carries a greater portion of the applied external load. This conclusion is in complete agreement with the experimental results and validates the U* index theory for the load transfer analysis. An additional conclusion that can be made based on the results of this experiment is the clarification of the significance of the internal

stiffness in determining the load transfer pattern in the structure. It was shown in this experiment that the thicker shaft carried, the lower amount of external (non-body) load to the supports. Instead, the thinner shaft, which had the higher U^* index carried the main part of the load. Consequently, it can be concluded that the internal stiffness, which is quantified with U^* index, is an adequate measure for identifying the load path and load transfer in the structure.

4-4)   Conclusion

In the presented section, the first physical validation for the U^* index theory was proposed and tested successfully. This theory has achieved a growing attention in the automotive engineering and by using the suggested test setup, it was shown that the U^* index is an adequate measure for load transfer in a structure. In this test, it was pointed out for the first time in a physical experiment, that the U^* index is representing the degree of connectivity of different points in the structure and the loading point. From a different perspective, this test also proved that conventional stiffness of an elastic body is inadequate when used for following the load path in the structure. Instead, the degree of connectivity between the loading point and a certain point in the structure (i.e. the internal stiffness), governs the amount of load that passes through that point in the structure which can be quantified with U^* index.

Finally, to prove that U^* index theory is capable of following changes in the internal stiffness, the loading condition, which is one of the two governing factors[4] in defining the internal stiffness, was modified in the experiment and simulation. A detailed explanation of this modified study and results are presented in Appendix C.

---

[4] Loading condition and Geometry are proved to be the two parameters that control the load paths

Chapter 5: Application of U* index Theory in Vehicle Industry Problems

5-1)   Introduction

This chapter covers three case studies in which U* index theory was used to perform structural analysis on the load carrying components of multiple passengers carrying vehicles. All of these case studies, as any other similar application-oriented research, are necessary steps toward getting a more mature theory of load transfer. However, in each case different features of U* index theory are highlighted to show the considerable distinct significances of them.

The first component to study was the strut of a parcel rack. The strut is the structure that carries the baggage load of the parcel rack into the vehicle frame, and it is essential to evaluate its design due to safety and weight efficiency requirements. Using the example of the strut, the first rigorous comparison of U* index theory to conventional stress analysis was performed, and capacities of U* index theory were shown clearly. The second case was a window pillar of a multiple passengers carrying vehicle. This structure undergoes several different loading in the vehicle and in the presented study a detailed analysis was done to select the most severe one. Then, the load transfer analysis with U* index was performed on the structure, and the results

were compared to experimental testing. In this case study, the U* analysis results were later used

to perform design modifications, and the modified structure was as well analyzed to show the

efficiency of the U* index theory for design improvements. Finally, the superstructure of the roof

of the multiple passenger vehicles was analyzed to study the load transfer in it. In this study, the

initial moment of a rollover impact was selected for analysis based on a proposed industrial

problem. In such impacts, there are strict regulations for different parts of the structure. Based on

the standards and the structural behavior, some design modifications were suggested that can

potentially improve the behavior of the structure under rollover impact loading. In the next

sections, these three sample studies are described in details.

5-2)   Load transfer analysis of the strut of a parcel rack

A strut of a parcel rack from a multiple passengers vehicle is the selected case study in this stage

of research. Figure 18 shows the parcel rack and the strut. The strut is connected to the pultrusion

component of the parcel rack and the roof frame, using five sets of bolted connections on the

marked locations of Figure 18a.

(a)   **(b)**
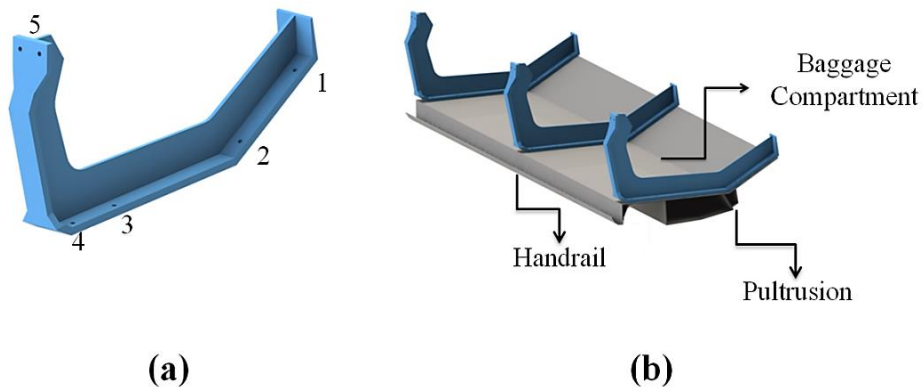
Figure 18) a: strut and boltholes, b: strut and parcel rack in a multi-passengers vehicle

First, a set of experimental tests was performed on the structure to provide benchmark data for evaluation of computer modeling and verifying the predictions of U* index theory. Then, using the U* index theory, load transfer analysis was performed on the structure, and the results were compared to conventional stress analysis results and experimental data.

5-2-1- Experimental testing of the strut

To provide a reliable comparison platform for the FEM results and to compare the results of U* analysis with the experiment, a set of failure tests was performed on the structure. These experiments focused on certain loading conditions and for each loading condition, three samples were used to assure that experiment is fulfilling the repeatability conditions and the results are not under the influence of some exceptional characteristics or flaws of a single specimen.

During the first stage of the experiment, the strut of a parcel rack was mounted on the test machine table bed, using the aluminum mounting plates (Figure 19a). Then the strut was loaded in the middle of its horizontal portion, while the loading condition was pulling at a crosshead rate of 10 mm/min. The experiment showed that the peak load at the failure was about 17800 N. In the next step, the side loading profile was considered for the test. This loading condition represents the imposed load on the strut at the very initial stage of a frontal impact of the vehicle. Figure 19b shows the strut under side loading. By imposing a constant displacement of 10 mm/min, failure occurred in the strut at approximately 3114 N. Common failure locations in both setups are marked and named in Figure 19 and details of the test outcome will be discussed later in the results section.
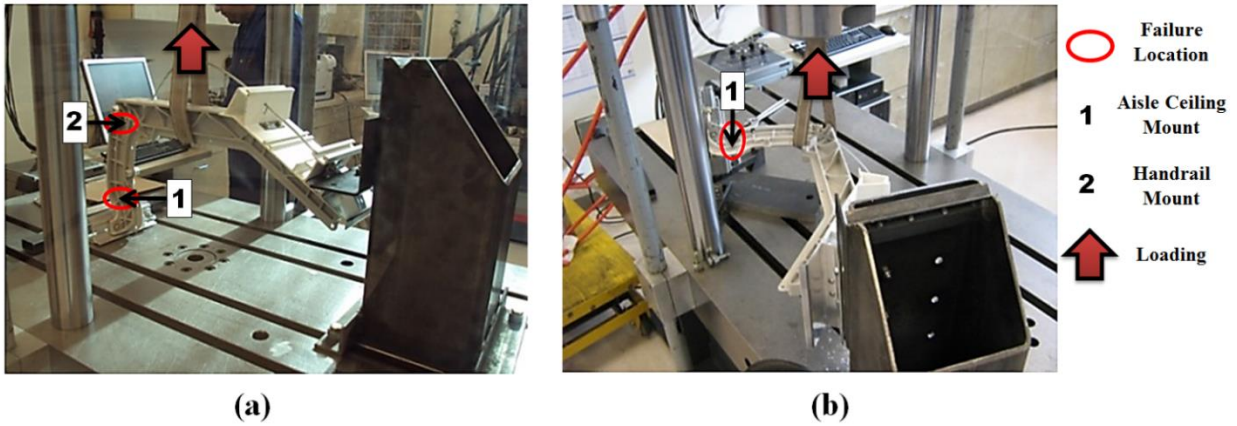
Figure 19) Failure test configuration and failure locations- a: Vertical loading b: Side loading

5-2-2- Computer Modeling

After producing the CAD model based on the actual structure, a FEM analysis was performed on the model with MSC Patran/Nastran. The material used for manufacturing the strut is Nylon, and Table 1 summarizes the Nylon properties.

Table 1) Material Properties of Nylon [38]

Material Name	Nylon
Young Modulus (GPa)	2.5
Ultimate Tensile Strength (MPa)	79
Poisson Ratio	0.4
Density (g/cm^3)	1.15

Two major loading profiles were chosen for the simulation. Based on the requirements of the manufacturer, the parcel rack should be able to carry 1000 N in the baggage compartment and

tolerate a handrail loading of 667 N per foot. Baggage compartment and hand rail were shown in Figure 18b. This loading condition was taken into account as one candidate for computer modeling. However, due to experiment configuration, it was also necessary to consider computer simulations with a loading profile similar to the test. Therefore, the computer modeling included vertical loading and side loading as in the experiment and an additional "working loading" condition. The "working loading" configuration was chosen based on the requirements of the manufacturer, in which the loading application regions were selected to be the frontal bolt holes of the strut. The loading was divided between them (1294 N on bolt-hole number 4 and 627 N on bolt-hole number 3 – Figure 20). The bolt holes connecting the strut to the vehicle frame were fixed as the constraints of the model.
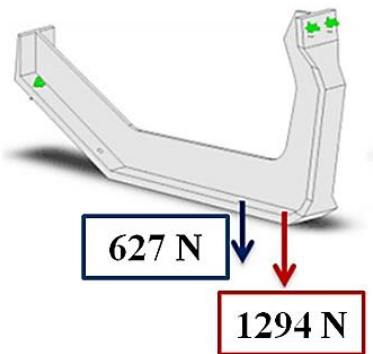
Figure 20) Isolated strut and one of the selected loading scenarios

The model was meshed in MSC Patran using Tet Elements with Tet10 topology. The MSC Nastran was then used to calculate von Mises stress distribution along with the total strain energy of the system in a linear static analysis. These data were used later for U^* index calculation and load transfer analysis.

5-2-3- Results and Discussion

The results are divided into two sections. In the first one, the experimental results, which includes vertical and side loading conditions, are reported, followed by the corresponding computational stress and U* analyses. This part will compare the capacities of stress analysis with U* analysis. Then, in the second section, the unique capabilities of the U* index in design evaluation are presented and discussed based on the loading condition of Figure 20.

5-2-3-1- Comparison of U* analysis with stress analysis and experimental results

a) Vertical Loading

In the vertical loading test, the failure occurred at 17800 N. Therefore, to simulate the load transfer at the moment of failure, the same loading magnitude was imposed to the middle of the strut. Figure 19 shows the most common locations of failure in the experiment, named as the aisle ceiling mount and handrail mount of the strut. The stress analysis result for this loading condition is illustrated in Figure 21a. Based on the distribution of von Mises stress on the structure, the stress magnitude in some locations (Area 1 and Area 3 in Figure 21a) exceed the ultimate strength of Nylon (79 MPa), which implies that the strut could experience failure at these locations. The upper neck of the strut is one of the places that the strut failed in all of the attempts in the real testing, and as the simulation shows, this segment of the strut is experiencing high stress (around 87 MPa). Thus, as expected, stress analysis results can predict failure in the structure. However, it does not give a precise explanation regarding the reason for the higher or lower stress values in different parts of the structure, or any information on how the performance of the structure can be improved.

In the next step, the load transfer analysis with U^* index theory was performed on the strut. Figure 21b shows the U^* distribution on the strut. As expected from the theory, the U^* value starts from 1 at the loading point and decreases as it gets closer to the geometric constraints, on which the U^* index is equal to zero.
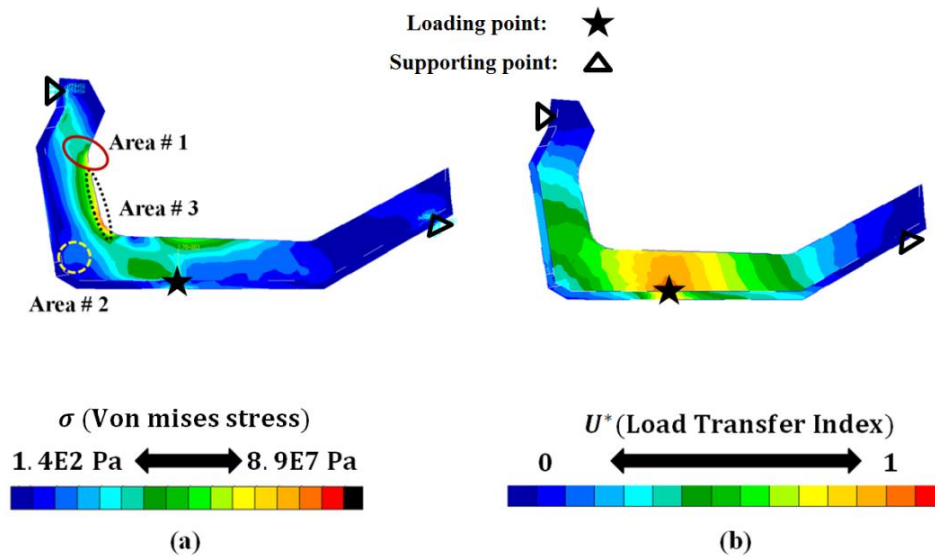
Figure 21) a: Stress distribution (von Mises), b: U^* index distribution

It is more beneficial to focus on the front and rear part of the strut separately to provide a more clear evaluation of the structural behavior of the stut using the U^* index distribution. Each of these selected segments contains a supporting point, and different load transfer behavior can be expected in them. Following the concept of uniformity of U^* index variation, introduced in Chapter 3, and by starting with the front member, (Figure 22a), a rapid drop and increase in U^* index values can be observed near the lower bent flange which is a clear sign of undesirable load transfer.

(a) (b)
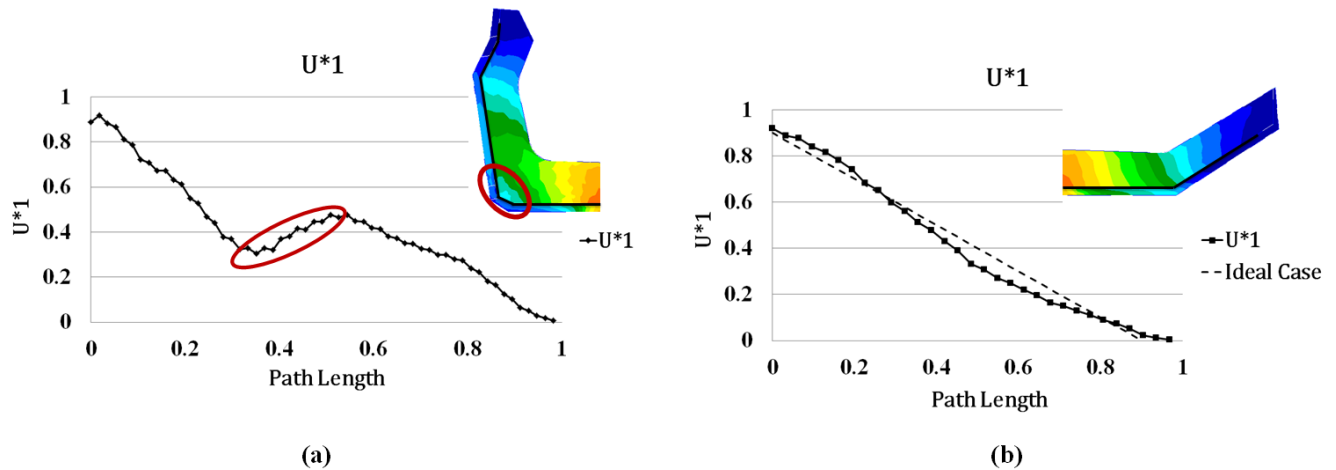
Figure 22) a: Undesirable load transfer near the actual failure point in experiment (compared to ideal case

for a linear spring; b: U* variation along the main load course of rear part vs. the ideal U* variation

Such load transfer behavior indicates an inappropriate stiffness variation in this area which can lead to failure under severe loading conditions. As experiment showed, one of the failure locations for U* is the so-called wire clamp hole (Area 2 in Figure 21a). However, surprisingly enough, the stress analysis did not show high stresses as a significant threat in that location (Figure 21a). On the contrary, U* index analysis reveals there is a major problem in the course of transferred load in comparison with the ideal expected behavior shown in Figure 6a. In other words, it was shown by U* analysis that there is complicated and rapid stiffness variation in the structure near the Area 2 of Figure 21a. Therefore, it can be stated that poor load transfer in this area, due to the bent flange in the structure, increases the risk of failure. This conclusion is an excellent example of the cases that the combination of the stress and U* index analyses provide a tool for a comprehensive judgment about structural behavior in failure.

Moving to the rear part of the strut, variation of U* index along the main load path is depicted in Figure 22b. Results show that although there is a slight drop in U* values near the rear bent

flange, the overall behavior of the rear part in transferring the load to the supporting point is close to the ideal case.

In another interesting application, U^* index analysis can be used to interpret the stress distribution on a structure. For instance, an area with high-stress value has been shown on the Figure 21a, as Area 3. There are no sharp corners or holes on this area. Nevertheless, stress magnitudes are higher in Area 3 compared to its neighboring areas. The reason for such high-stress values can be found using the U^* index distribution. As it can be interpreted from the thickness of colored segments on Figure 22a, the right edge of the vertical section has thinner colored contours, or in other words, the rate of U^* index variation on the right edge is much higher than the rest of structure. Such a sharp change in U^* index value implies rapid decay in stiffness of this segment, which in turn will lead to higher strain and stress values. In contrary, the gradual reduction of U^* index value on the left flange of the vertical segment suggests a desirable load transfer, and as shown in Figure 21a, that area is not tolerating high-stress values. So it can be concluded that U^* index is a powerful tool which in combination with stress analysis provides a better approach for locating the failure locations and interpret the reason for the existence of weak points in the structure.

b) *Side Loading*

Next set of simulations was performed to examine the load transfer during the side loading. Figure 19b showed the experimental setup for this test. After three sets of experiments the strut showed failure at multiple points but one common failure point in all sets of the experiment was the aisle ceiling mount, which was marked in Figure 19b. The von Mises stress distribution is shown in Figure 23a, while the U^* distribution from loading point is illustrated in Figure 23b.
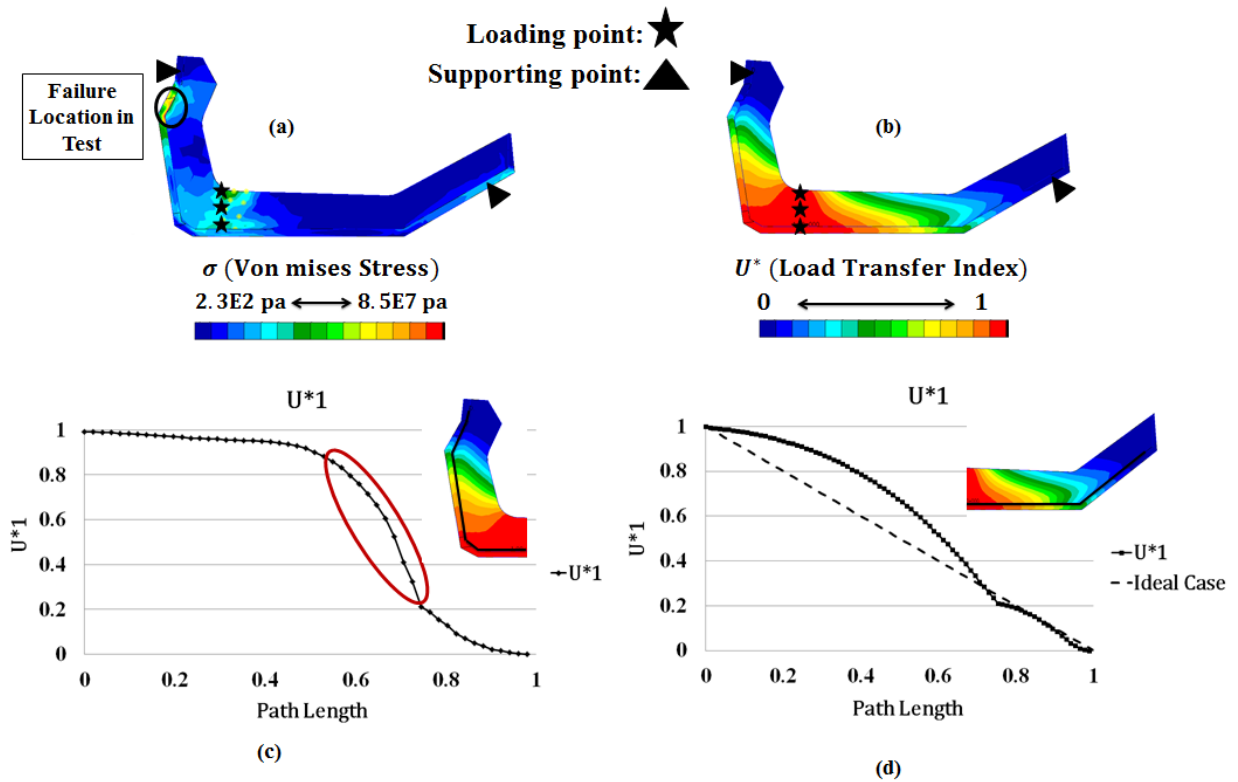
Figure 23) Results for side Loading Analysis; a: Stress Distribution, b: U* Distribution, c: U* variation along the path on frontal segment and d: U* variation along the rear segment of strut

The results show that the maximum stress occurs near the upper of the strut neck (close to the bent flange on the top section), and at a loading of 3600 N, stress value reaches 85 MPa, which is more than the ultimate strength of the Nylon and will lead to failure. The experiment showed the same failure location at the similar loading value. Based on the experimental results and by comparing the peak load value of 3336 N in the side loading with the 17792 N peak load of the vertical loading, it can be concluded that the load transfer in the structure in case of side loading is not desirable. Now the U* index theory can be tested to see if it is capable of providing the same conclusion and additional information on structural behavior.

The less than perfect performance of the structure in transferring the loads to supports can be detected in Figure 23c and 23d, where the U^* variations for front and rear parts are illustrated respectively. As shown in the results, not only the bent flanges impose sudden changes to the decay rate of stiffness, but also in segments with no geometric irregularity, U^* index variation is very sharp. This behavior is against the ideal expected performance of an engineering structure, illustrated in Figure 6a and Figure 23d and implies a rapid change of internal stiffness in the structure. Here another capability of U^* index can be pointed out. Comparing the results of stress and the U^* index analyses, shown in Figures 23a and 23b, indicates that conventional stress analysis is not giving detailed information on possible structural problems in rear part. However, U^* index analysis revealed that even the rear part is not perfectly carrying heavy side loads, and design can benefit from removing the rear bent flange to avoid sharp changes in stiffness values.

In summary, it can be concluded that although stress analysis is a valuable tool for locating areas in the structure that might fail, the combination of its results with results of U^* analysis is very important to cover areas that might not show alarming stress values while poor load transfer behavior puts them in danger. Moreover, to understand the reason for different stress values, U^* index has proved to be a very useful indicator that will enhance the engineers with the ability to interpret the stress distribution in structures.

5-2-3-2- Design evaluation based on the U^* index analysis

To show how the U^* index theory can provide useful information for design evaluation and structural modification, a loading condition close to the expected working load in the strut was applied to the model. The results are then described in details to provide the real picture of load transfer in the structure, and to show how U^* index can help designers by providing additional information to the results of stress analysis. As demonstrated in Figure 24a, a symmetrical set of

loads was imposed on the frontal bolt-hole shanks. Based on the stress analysis results shown on Figure 24b; it is clear that almost the same areas found in the previous simulation (the upper neck and the wire clamp hole), are tolerating highest values of von Mises stress. However, due to a lower magnitude of the imposed loads, none of them reaches the critical stress values for failure. Then U* index analysis was performed for the new loading condition. To carry out a comprehensive load transfer analysis, after finding the distribution of U$^*_1$ (load transfer index from the loading point) U$^*_2$ (load transfer index for the reaction forces) was also calculated for all points of the structure.

σ (Von mises Stress)

4.5E2 pa $\longleftrightarrow$ 2.06E7 pa

U*(Load Transfer Index)

0 $\longleftrightarrow$ 1
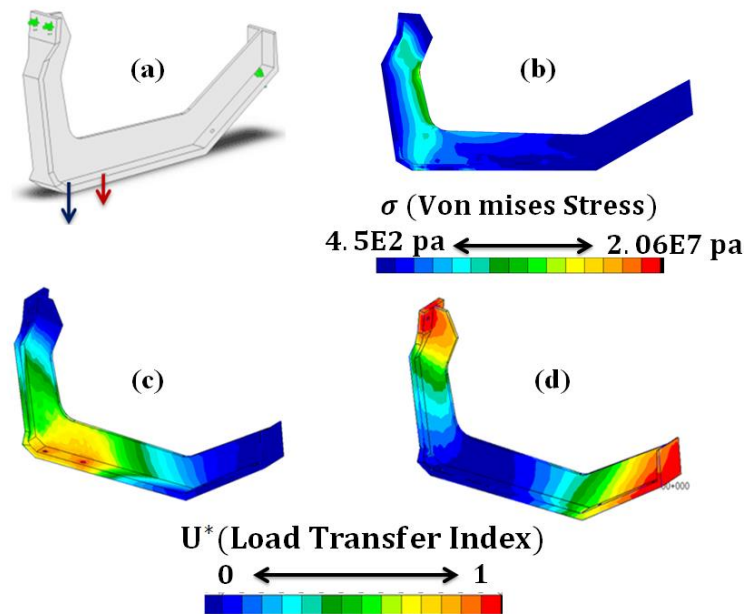
Figure 24) a: Computer model for the workload configuration, b: von-Mises stress distribution, c: Distribution of U$^*_1$ index for the applied load, d: Distribution of the U$^*_2$ index for reaction force

Figures 24c and 24d show the U$^*_1$ and U$^*_2$ distribution on the strut. The U* index value starts from one near the loading points and gradually decreases to 0 close to the constraints. Next, the detailed analysis on U* index is presented based on the results of Figures 24c and 24d.

Starting from the front part of the strut, in Figures 25a and 25b the U^* index is shown from loading point and the supporting point, respectively. Apparently, the bent flanges in lower and upper parts of the structure have led to some undesirable behavior in load transfer.

Path Length: Normalized length from loading point to the supporting point in each case.
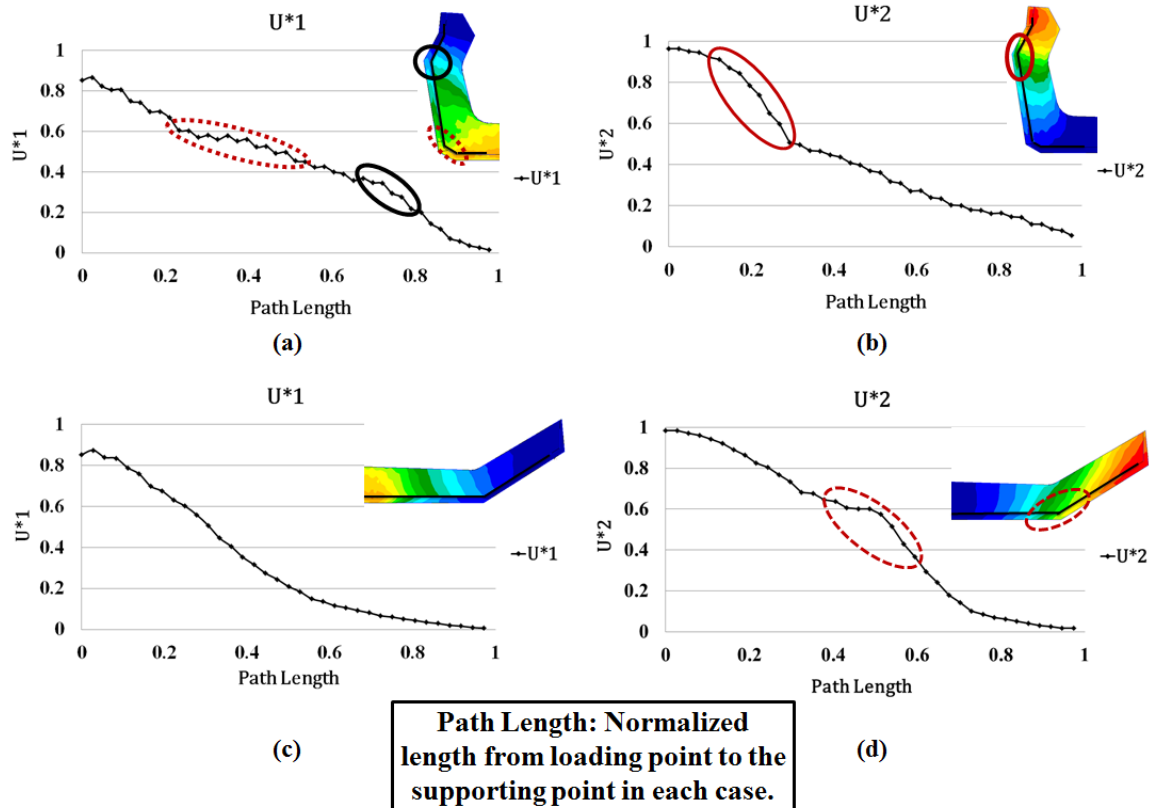
Figure 25) U^* variation along the: a- Front path from loading point, b- Front path from the support, c- Rear Path from loading point and d- Rear path from the support

Fluctuating values for U^* near the bent flange in lower part represents an undesirable stiffness profile in that area which should be considered as an alarming sign of potential problems. This area was shown to be one of the common places for the failure of the strut in the experiment. Moreover, it should be noticed that since the loading values are much lower than the experiment, the stress values are all lower than failure criterion. Consequently, based on stress results designers might consider that the structure is performing in a desirable manner, but U^* index

analysis shows (Figure 25b) a rapid decrease in U* index values in the upper bent flange which represents a rapid decay of stiffness in that area. Based on U* index variation a modified design of the top bent flange seems to be essential.

Next, the rear part has been taken into consideration. As Figures 25c and 25d show, the load transfer behavior of this segment is desirable and the stiffness decay rate is similar to the behavior of a linear spring. Nevertheless, there is a slightly odd decay in U* index near the bent flange, but it is not as severe as in the frontal part. Thus, U* index analysis shows that this structure is transferring vertically imposed loads properly to the supports in the rear part.

The last design parameter to consider is the consistency of load paths on the structure. The main load paths on the structure are displayed for both U$^*_1$ and U$^*_2$ in Figure 26a. It can be noted that rear part of the strut shows a perfect consistency of load paths, but the situation of load paths in the front part is not desirable. This conclusion is in agreement with the previous ones indicating questionable stiffness variation in the frontal segment.


(a) **(b)**
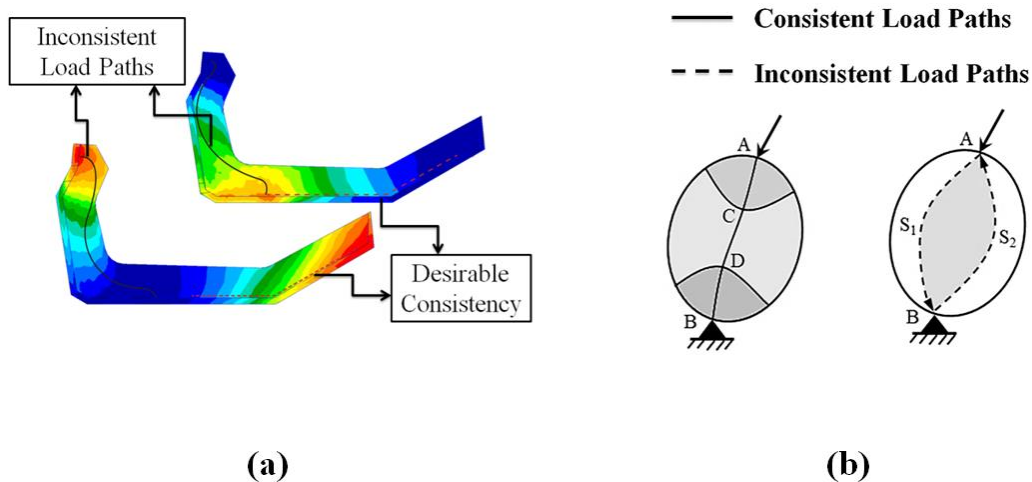
Figure 26) Consistency analysis of load paths a: Current Study b: Examples of consistent & inconsistent paths

Figure 26b shows an example of consistent and inconsistent load paths of a general sample structure for comparison with the results of the present study. Therefore, it can be concluded that consistency of load paths, drawn based on U^* index value, is a valid measure for evaluating load transfer behavior in different structures. This aspect of U^* index analysis helps to find certain parts of the structure that will or will not perform efficiently in a given loading scenario. As a result, designers can save time and expenses by focusing on improving areas with inconsistent load paths.

After separate evaluation of load transfer of the applied loading and reaction forces, now the overall picture of load transfer behavior can be presented using U^*_{sum}. The index of U^*_{sum} provides a complete picture of structural performance in carrying the applied loading and the reaction forces. Figure 27 demonstrates the distribution of U^*_{sum} in the structure. It should be noted that the colored fringe is mainly representing the significance of each part of the structure, in carrying the externally applied loads. As shown in Figure 27, the lower part of the front of the strut is showing undesirable load transfer.
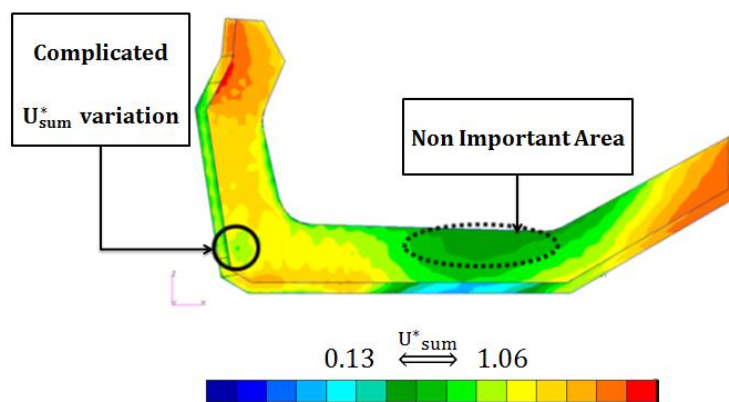

Figure 27) U^*_{sum} distribution in the strut

This fluctuating stiffness as shown in previous steps has led to failure. Also, in the middle of the strut, there is a relatively large area with minimal significance in load carrying. The reason is the low degree of connectivity between this area and the loading point; i.e. insignificant internal stiffness.

U^*_{sum} index can be considered as a very valuable tool for design modification on the structure. As shown in the above example on the strut, U^*_{sum} index is capable of identifying areas with non-desirable internal stiffness variations and more importantly, it can point out areas which do not have a significant role in load transfer. Since such parts of the structure have low internal stiffness, they can be removed in a weight reduction process on the structure without decreasing the overall stiffness. This capability of U^*_{sum} index can be applied in vehicle design process to achieve an optimum design with adequate stiffness along with low fuel consumption due to lower weight. It is worth to mention the stress analysis cannot predict areas that are suitable for material removal without affecting the overall stiffness of the structure. For example, the stress distribution shown on Figure 24b shows lowest stress values in the rear segments of the strut. However, as depicted in Figure 27, that area shows significant role in the load transfer process (main load path passes this area- Figure 26a), and it also has a very high internal stiffness. Thus, removing material from this section might not be desirable for the overall integrity of the structure and defectively alters the load path in the rear part.

Finally following the recently introduced concept of U^* index variance by Nambu et al. [32] distribution of different U^*_{sum} index values was investigated throughout the structure. Figure 28 illustrates the histogram of U^*_{sum} index distribution between nodes.
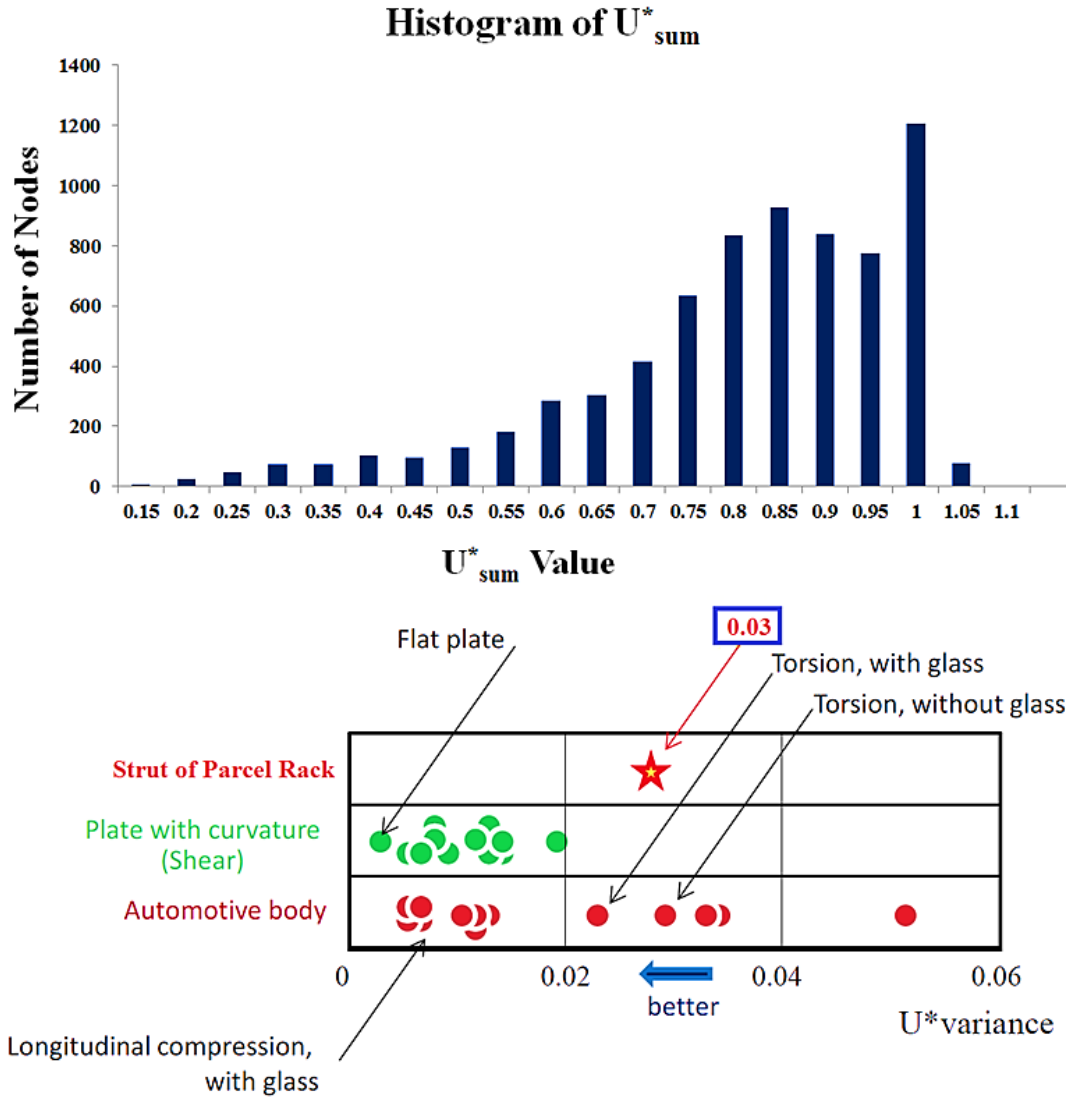
Figure 28) Statistical evaluation of load transfer in strut using U^*_{sum} histogram and comparison of U^*_{sum}

variation with statistical data [32]

The horizontal axis shows the U^*_{sum} index values, and the vertical axis represents the number of the nodes with the same U^*_{sum} index value. Calculation found that the mean value of this histogram is 0.77, and the variance of the U^*_{sum} of the system was 0.03. Comparing the variance magnitude to statistical data from research of Nambu et al. (2013) revealed that the U^* variance of the strut under the selected loading condition is relatively low and is in the range of some

other automotive body compartments. Consequently, despite some non-ideal distributions of U* index in the frontal part of the strut, this coach component has an acceptable design for the target loading condition but with room for improvement. This analysis proved that the U$^*_{sum}$ index variance is another important feature of the load transfer analysis. It demonstrates if most parts of a structure share the burden of carrying the applied in a uniform way. Such evaluation is certainly very useful for achieving a homogeneous design.

5-2-4- Conclusion

Through a comparison of conventional stress analysis, the experimental results and the load transfer index (U*), it has been shown that U* index is a useful parameter which can enhance designers with a thorough understanding of the structural response to external loading.

The main advantages of using this innovative concept can be listed in four categories. Firstly, U* index can provide additional information to the stress analysis, and such information can be used to justify the complex stress distributions in the structure. Secondly, U* index characterizes the structural performance in term of transferring the load, which is one of the primary functions of engineering structures. Such indications can locate the main load paths in the structure and can provide a guideline for structural design modifications. Thirdly, the U$^*_{sum}$ value provides an essential tool to identify the role of the different parts of the structure in the load carrying process. Therefore, this index can help designers to locate the appropriate points for adding stiffeners or removing extra and unnecessary material for weight reduction. Lastly, U$^*_{sum}$ variance quantifies the homogeneity of the structure, which can also be used for evaluating the structure efficiency in load transferring in comparison to other engineering structures.

5-3)   Load transfer analysis of the window pillar of the coach structure

In this section, the introduced U^* index based criteria for design evaluation were applied to determine the efficiency of the load transfer in a major load carrying component of a multiple passenger vehicle. The window pillar of such vehicle, shown in Figure 29, is selected for this analysis. These pillars carry the load applied to the vehicle structure between the roof and the lower superstructure.
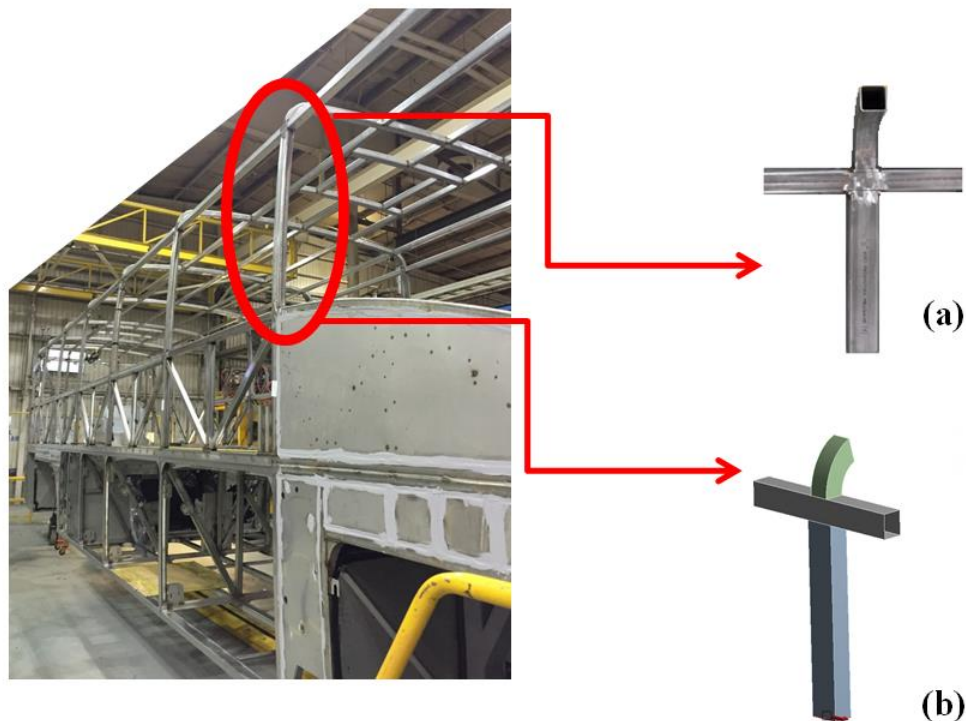
Figure 29) Window pillar structure of the coach: a) Testing specimen, b) Computer Model

It was necessary to select a proper loading condition for the window pillar before performing the computational load transfer analysis and also the experimental testing. As a result, in the first step, a full model of the vehicle[5] was used to obtain loading condition for the window frame

---

5 Provided by the manufacturer and modified for a better mesh by author

structure. Figure 30 shows this full model. MSC Nastran software package was used to perform a static analysis of the structure under different loading conditions.
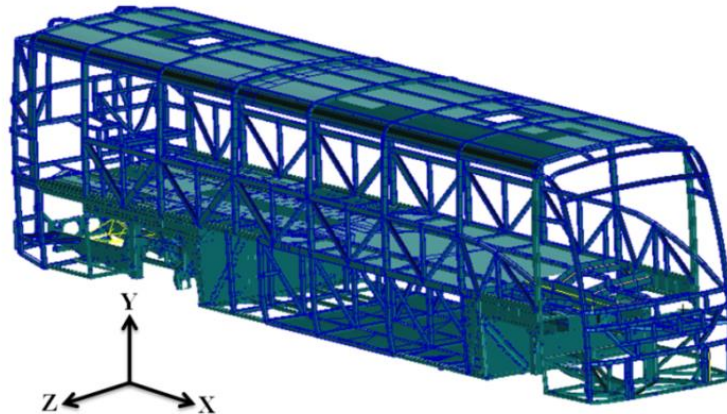
Figure 30) Full vehicle FE model used for static analysis for loading condition determination of the window pillar

Details of this model are not in the scope of this research; however, in summary, it can be stated that no constraints for the vehicle were considered, and inertia relief method was applied to the system instead. The model included 332,402 elements, out of which, just 1749 were beam elements that created the superstructure of the vehicle. The majority of the used elements were Quad Shells that formed the lower section of the vehicle along with the roof cover. The model was created using Aluminum and Steel material, based on the real coach materials. The MPC[6] feature was used to connect the shell and beam elements together. The correct mass distribution for the structure was achieved using 566 mass points; that represented almost 80% of the total 19.23 tons of structural mass.

---

6 Multi Point Constraints

The full vehicle model was analyzed using several loading conditions that were proposed by the manufacturer as the most crucial ones. Table 2 shows the considered loading conditions for the structure in the coordinate system of Figure 30.

Table 2) Full vehicle modeling - Different loading conditions

Loading Type	Acceleration (X dir.)	Acceleration (Y dir.)	Acceleration (Z dir.)	Conclusion
Vertical 1 G	0	-1 g	0	Least severe
Vertical and Lateral 0.4 G	0	-1 g	0.4 g	Medium Severity
Vertical and Braking 0.65 G	-0.65 g	-1 g	0	Most Severe

Then, based on the von Mises stress values obtained from these analyses, the most severe loading case was chosen for a detailed load transfer analysis on the selected component. The braking loading condition had the highest maximum von Mises stress in the model.
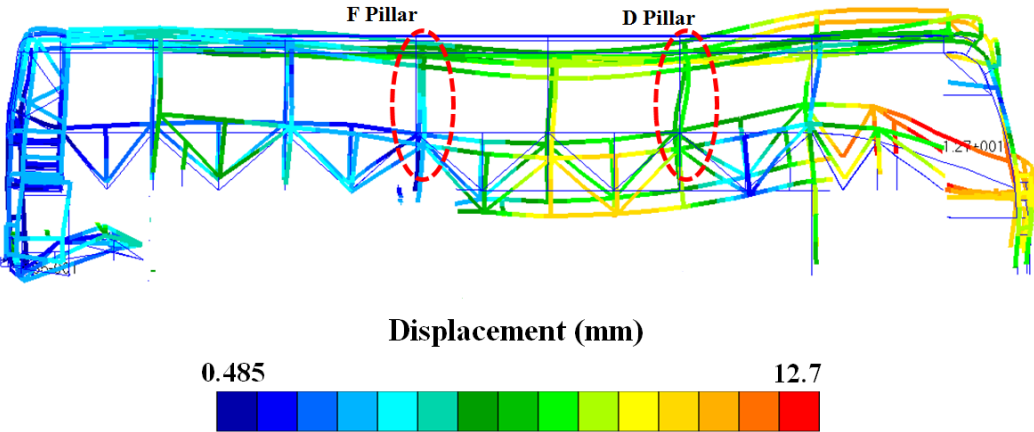

Figure 31) Displacement of beam elements in the vehicle model under vertical and braking loading

Figure 31 shows the displacement of the beams in the superstructure of the coach due to the most severe loading condition. It is clear that the pillar marked as "D-Pillar" is experiencing a major deformation mode compared to other pillars like the "F-Pillar." Figure 32 illustrated the von Mises stress in the vicinity of two of the window pillars.
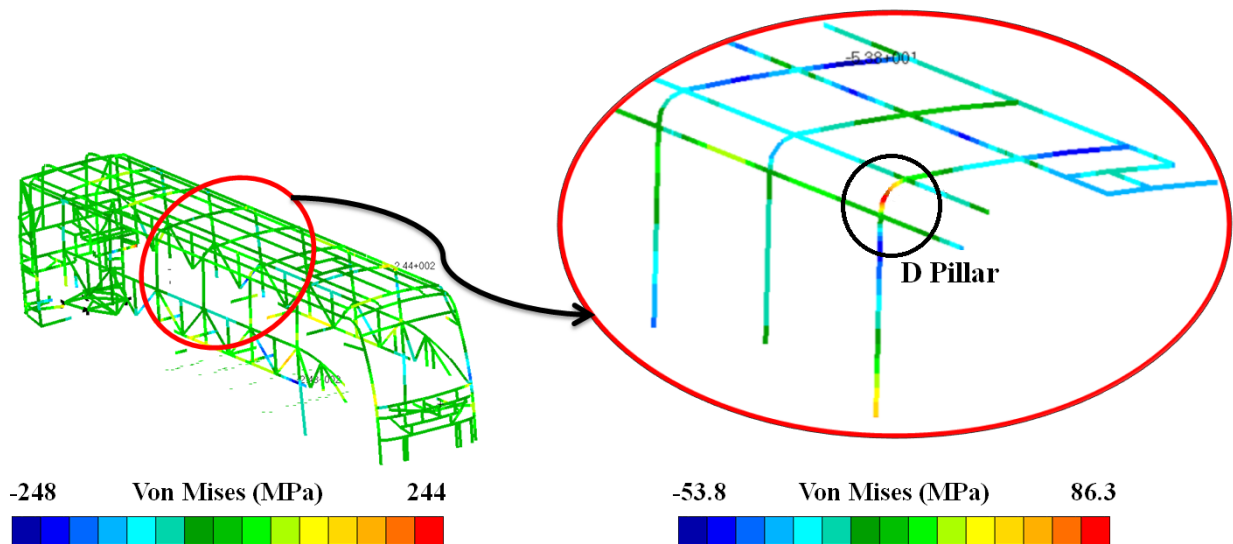
Figure 32) Stress distribution in structure and close the window pillar

Therefore, braking loading condition was chosen as the reference for the loading condition of the computer modeling and experimental testing of the window pillar.

5-3-1- Computer Modeling

The window frame consists of three main components, shown in Figure 33a: the upper arc-shaped part, the horizontal tube, and the vertical tube. These three parts are connected via two welded joints in the front and rear sides of the structure. The model provided by the manufacturer had oversimplified modeling for the window pillar, as it was modeled merely by beam elements. Although such simplification is justified for large vehicle model, in this study a detailed model of the pillar was created using MSC Patran/Nastran to provide a clear picture of

load transfer in this component. The model was created using 2508 CQUAD4 shell elements. Table 3 summarizes the necessary information for modeling the window pillar.

Table 3) Mechanical and geometrical properties of the window pillar

Material	Yield Strength (MPa)	Ultimate Strength (MPa)	Young's Modulus (GPa)	Poisson Ratio
SS 41003	346	513	200	0.3

For the modeling stage, initially, all of the applied loads on the window pillar were extracted from the full vehicle model. Then, those loads were imposed on the separate pillar model shown in Figure 33b. Conventional stress analysis was performed for this "Fully-Loaded" model for future reference.
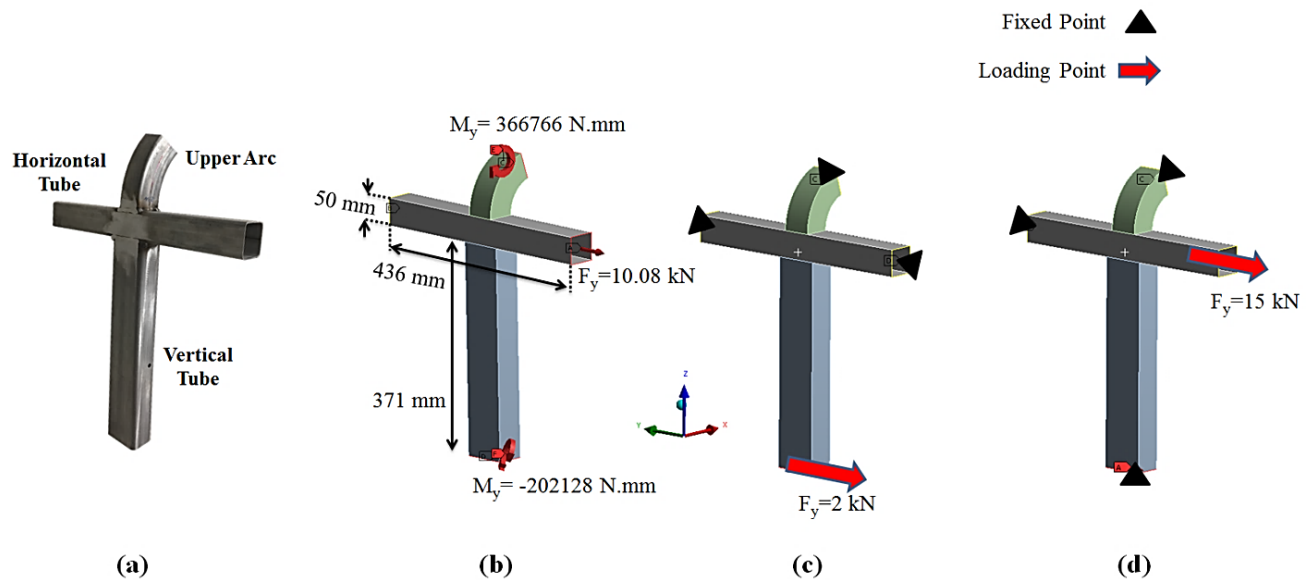

Figure 33) Window frame structure, a: Physical test specimen, b: Fully loaded model, c: Single loading at bottom (final model) and d: single loading at side

Due to the limitation of the experimental equipment, it was necessary to choose only one loading point for the model. Therefore, based on the highest magnitude of loading and the expected failure mode two options were selected as potential experimental loading conditions. Figure 33c and Figure 33d show these loading and boundary conditions. Based on the simulation results, the model of Figure 33c, with a loading magnitude of 2 kN was selected for further analysis. This model can provide similar failure mode to and results to the fully loaded model. This model was then used to conduct the structural analysis for the window pillar.

The von Mises stress variation along the connection between three parts of the window pillar was compared with the "Fully-Loaded" pillar (Figure 33b), to verify the selected single point loading condition (Figure 33c). The results are pretty similar and can justify the selection of the proposed loading condition. Figure 34 and Figure 35 show two samples of such comparisons between stress variations along the interfaces.
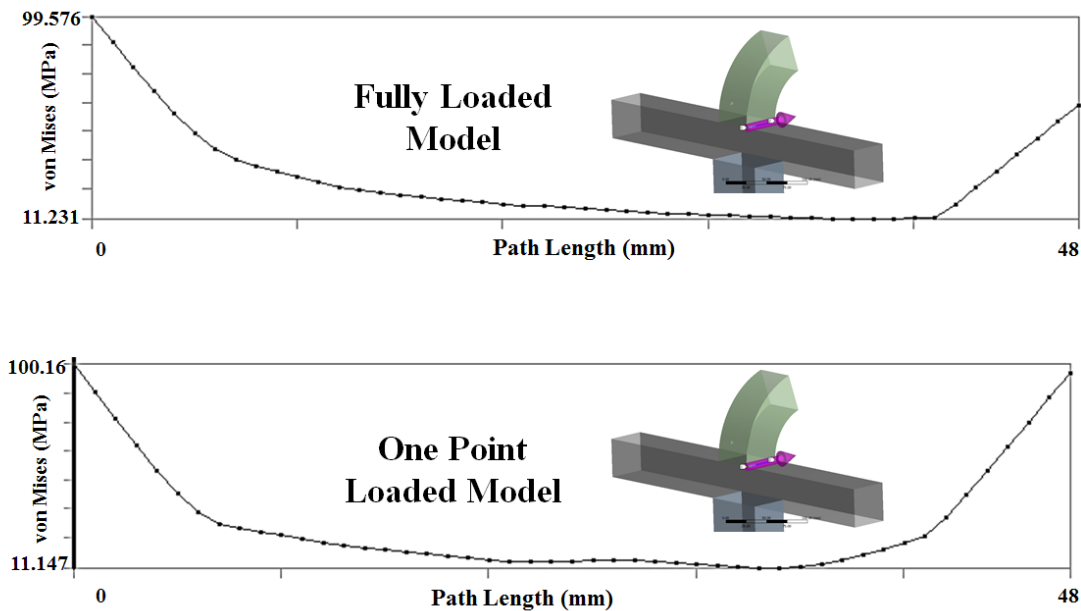
Figure 34) Sample stress variation along the upper-side connection path for experimental loading justification
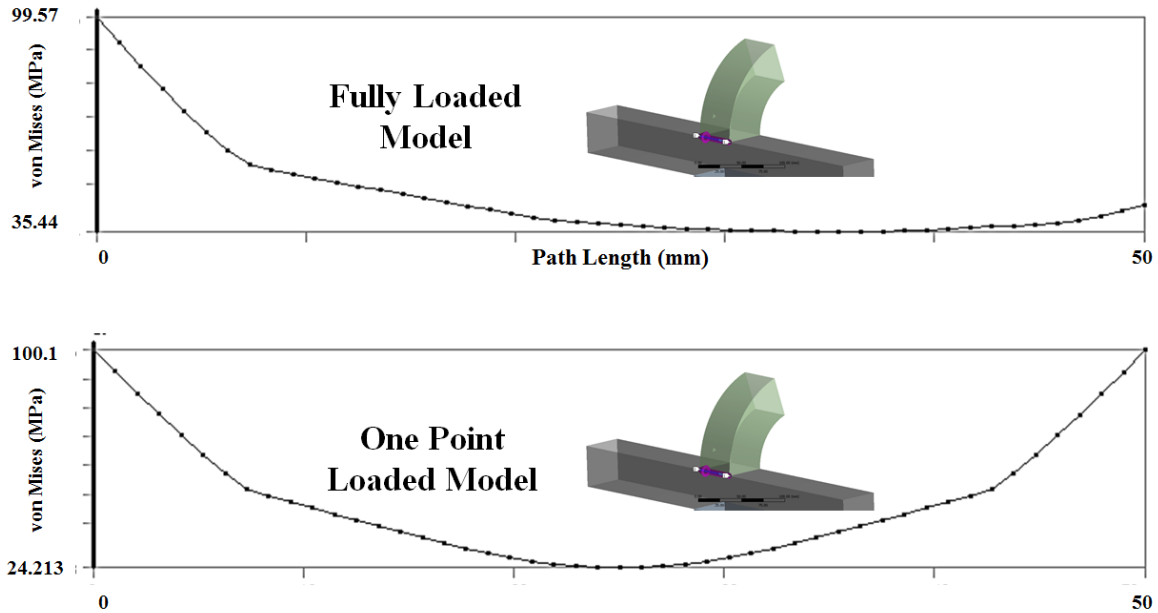
Figure 35) Sample stress variation along the lower-rear connection paths for experimental loading

justification

As shown in Figures 34 and 35, the von Mises stress variations along the selected paths follow the similar pattern for the selected model with one loading point and the fully loaded one. In contrary, the other loading condition candidate (Figure 33d) has inconsistent stress variations with the fully loaded model. Figure 36 is an example of such behavior. As a result, the proposed one point loading at the bottom of the pillar (Figure 33c) was an acceptable assumption for the analysis. The computer models were considered to have perfect bonding instead of the welds to evaluate the weak points that can occur even in an ideal perfect welding process. In this way, the load transfer analysis predicts the parts with questionable stiffness and can focus on design issues rather than the welding problems. Any design improvement on this model can make a sensible improvement to the actual structure, regardless of welding quality.
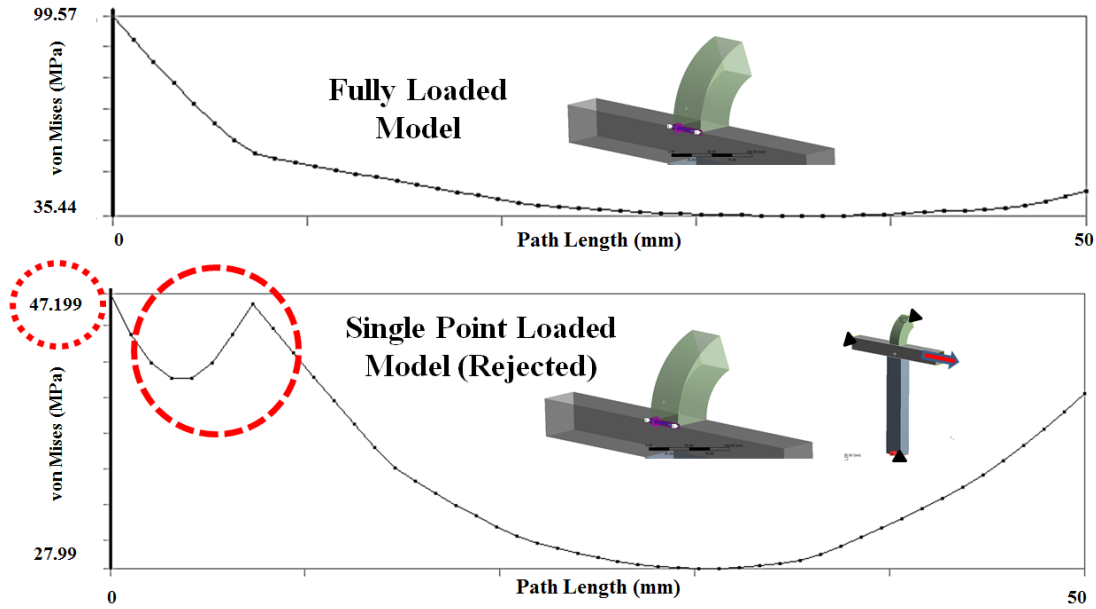
Figure 36) Inconsistent stress variation along the lower-rear connection path

5-3-2- Experimental testing

The experimental testing on the window pillar was performed to observe the behavior of this structure under the loading and boundary conditions used in the computational model. Figure 37 shows this experimental setup.
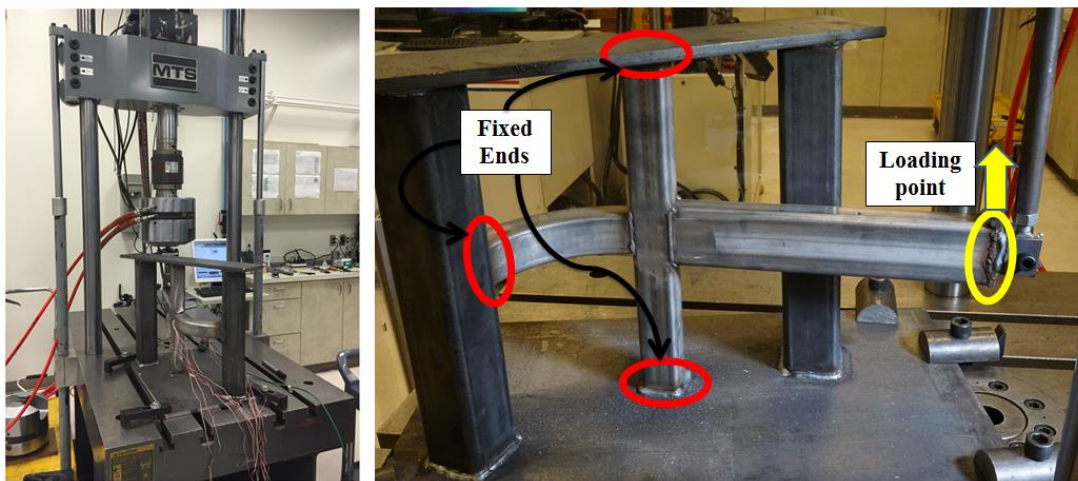
Figure 37) Experimental setup for the window pillar

The testing specimen is the same window pillar shown in Figure 33. It is made of steel (SS 41003) and is fixed on three marked locations of Figure 37 using a rigid fixture. It is important to notice that the welding of the fixture was made deliberately stronger than the connections between the different parts of the specimen itself. Thus, the failure can occur at the structure and not at the constraints. This way, the testing specimen has a closer behavior to the window pillar in the real vehicle.

The experiment initiates by applying a vertical tensile load at the marked loading location of Figure 37. Loading is imposed by an MTS loading at a rate of 10 mm per minute. The equivalent applied force and the displacements were measured, and the force-deflection curve for the experiment is derived. Comparison of the linear segment of force-displacements of the experiment and simulation can later verify the computer modeling process.

The measured data at this test was the peak load at the failure. Then, based on the objective of this experiment, failure locations were used to evaluate the accuracy of predictions that were made by the U^* index analysis. The results of U^* index simulation and the experiment are presented in the next section

5-3-3- Results and Discussion

In this section, the simulation results and the experimental results are presented. Firstly, the experimental results are shown and then the results from load transfer analysis with U^* index for the same loading and constraints condition of the physical test are presented. Therefore, they can be compared for further evaluation of structural behavior in load transfer process. Finally, a design improvement is suggested based on the U^* index results and its effect on structural behavior is evaluated by another set of load transfer analysis.

5-3-3-1- Experimental Results

By applying a quasi-static loading, the structure was pulled vertically from the marked location in Figure 37. The structure was behaving linearly up to 4.5 kN of the applied load and then the first signs of failure occurred. Therefore, the selected loading magnitude of 2kN for computational load transfer analysis with U^* index, which should be a linear analysis, is acceptable. The first failure was the buckling that happened in the tubes. Figure 38 shows the deformed structure. By further loading, the first cracks were initiated in the structure at around 10.1 (kN). The location of these cracks, marked in Figure 38, is at the corner of connection between horizontal and vertical tubes, i.e. the beginning of welded joint. In the next section, these results are compared with simulation results to prove the validity of modeling process.
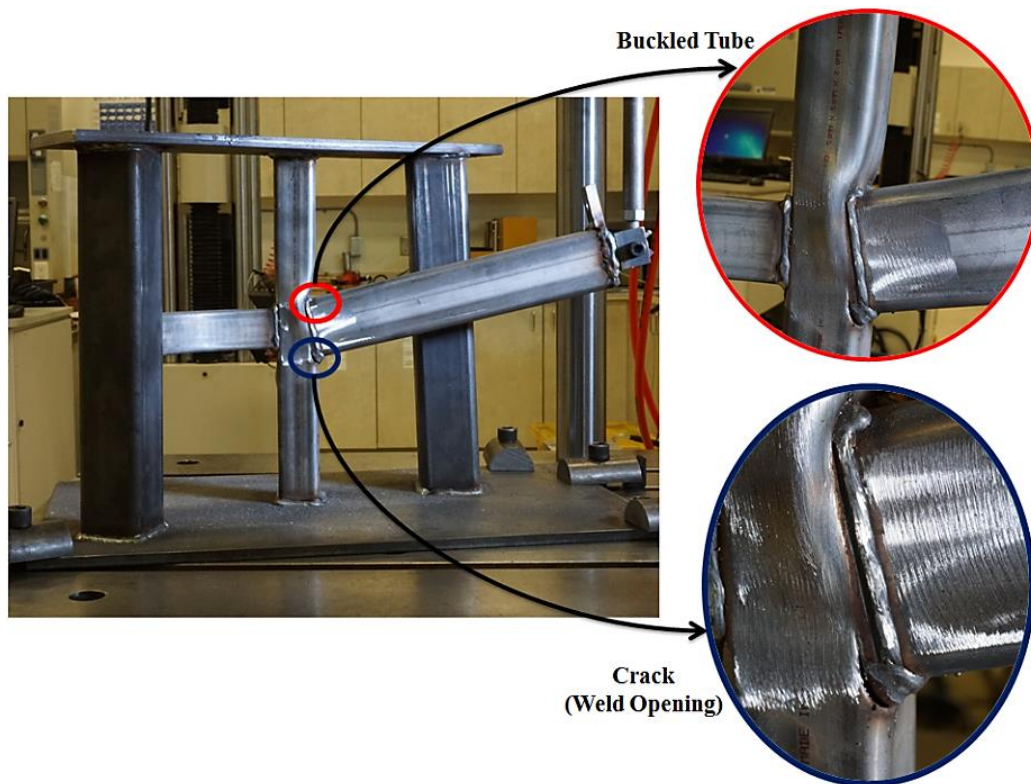

Figure 38) Deformed structure with marked buckled tube and the initial failure location (cracks)

5-3-3-2- Structural analysis results and discussion

A finite elements model was used for the computational analysis of the load transfer in the structure. The model was verified using the experimentally gathered data, and then the structural analysis was performed on the model, starting with a conventional stress analysis for comparing the failure locations with the experiment to validate the model. Then, a detailed load transfer analysis with U^* index was performed on the computer model to evaluate the load transfer and effectiveness of the existing design for providing a desirable load transfer.

   a. **Model Verification**

A computer simulation was conducted on the model by applying the same loading and boundary condition as for the experimental testing. The computer modeling was in the linear range while the experiment starts in a linear range and continues to higher loading and plastic deformation which is nonlinear. Therefore, the model validation can be done using the linear phase of the experiment. The force applied to the structure for a given displacement was extracted using the experimentally gathered data. Then, this load was applied to the computer model using remote force application. The resulting displacement was compared to the measured value of the experiment. The results are shown in Table 4 and can verify the accuracy of the predicted results by computer modeling. A displacement of 3.5052 mm in the linear region of the experiment was chosen, and the measured loading for that displacement, about 2.8 kN, was applied to the computer model. Then, the resulting displacement was measured from computer model which shows that the computer model is in good agreement with the experiment with only 9.8% of error. It can be concluded that the modeling process is accurate, and the simulation results are valid. In the next section, the load transfer analysis results are presented, and further discussion is made upon those results.

Table 4) Force- Displacement results for experiment and simulation

Applied displacement in the experiment	Measured force for the applied displacement	Applied force in the simulation	Measured displacement for the applied force
3.5052 (mm)	2838.72 (N)	2838.72 (N)	3.16 (mm)

b. Conventional stress analysis results

Considering the same loading and constraints that were used in the test and shown in Figure 33c, the simulations were done on the computer model. Figure 39 shows the stress distribution on the model. Since the applied loading (2 kN) is extracted from the full vehicle model under braking loading condition[7], it is far lower than the peak load at the failure in the experiment (≈10 kN). Consequently, the maximum stress value of the model is in the safe zone for Steel SS 41003 (around 150 MPa). However, the maximum stress is occurring at the same location as the initial cracks were happening; i.e. the tip of the welded joints in the actual structure. This result provides a general verification for the modeling procedure.
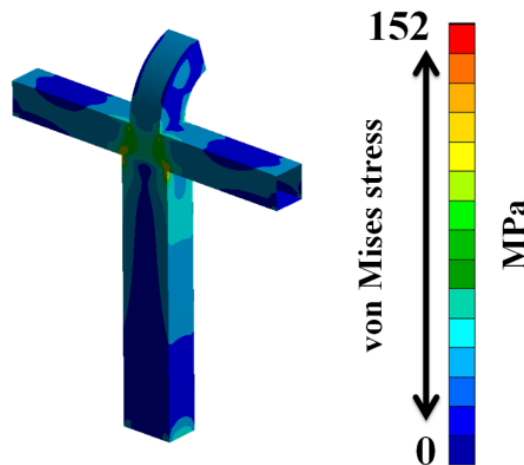
Figure 39) von Mises stress distribution on the structure

---

[7] Table 2 showed the justification for selectin this loading profile.

c. The U* index analysis results

The load transfer analysis was conducted for the extracted loading and constraint condition, and the U* index distribution in the structure is shown in Figure 40. The U^*_1 index distribution represents the pattern of the load transfer of the externally imposed load in the structure.
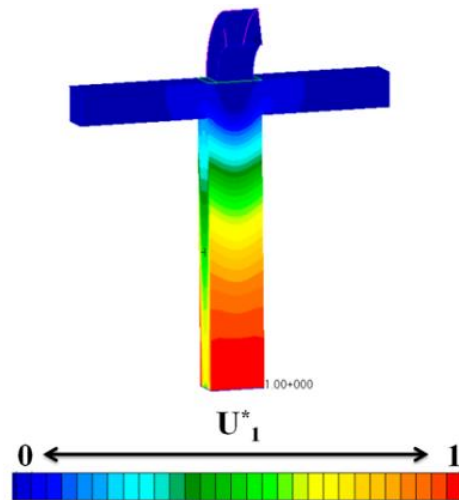
Figure 40) U^*_1 index distribution in the structure

The U^*_1 index in the structure starts from 1 at the loading area and goes down to zero as it gets closer to the supporting points. A detailed study of the U^*_1 variation and the resulting load path is shown in Figure 41. The main load path (dashed line on the structure in Figure 41) is plotted by connecting the points with highest U^*_1; starting from the loading point and ending at the supporting point following the algorithm provided by Takahashi and Sakurai [38].
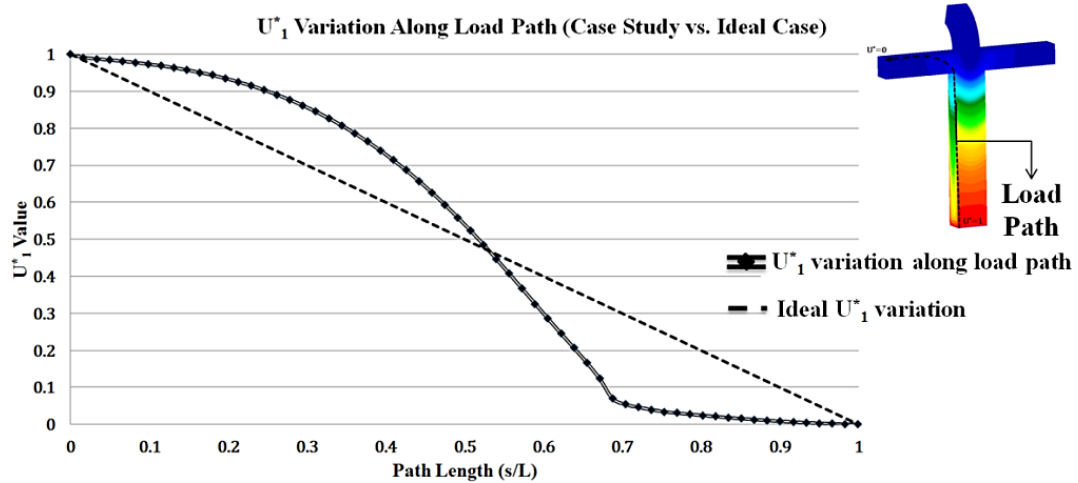
Figure 41) U^*_1 variation and main load along with the Uniformity Analysis

Uniformity analysis of the load path reveals that the structure shows acceptable behavior in transferring the applied loads in the vertical section but a sudden change in the decay rate if the U^*_1 happens just at the interface of the vertical and horizontal tubes. The connecting edges were probed in more details to investigate the U^*_1 variation at this interface. The result is shown in Figure 42.
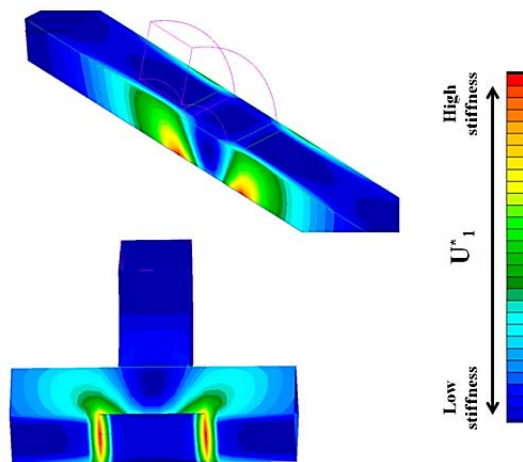
Figure 42) U^*_1 variation at the lower interface- Jump in the U^*_1 values along the lower surface of the interface

Clearly, there is a significant drop of U^* index, and thus internal stiffness, as load passes from the vertical tube to the horizontal one. Such sudden value jump in stiffness can lead to dangerous behavior of the structure and stress concentrations due to the sudden increase of strain. The experiment also showed that failure occurred at this location.

Since the area with concerning U^* index variation is closer to the supporting points, it will be more beneficial to evaluate the load transfer of the reaction forces imposed to structure from the supporting points. Figure 43 shows the U^*_2 distribution in structure. As it was expected, the U^*_2 value is equal to 1 at the supporting points and its value drops down till reaches zero at the loading point. One of the main load path of U^*_2, starting from the side supporting point is also shown in this figure.
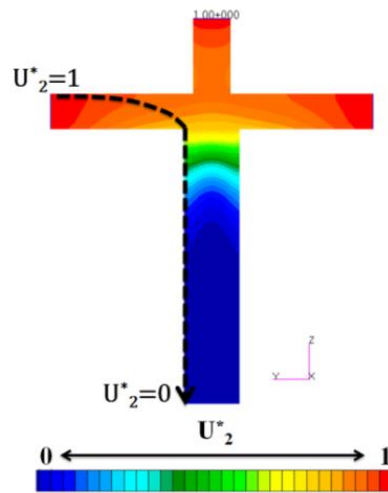
Figure 43) U^*_2 index distribution and the main load path of the side support reaction forces

The main load path for carrying the reaction forces was also plotted based on the values of U^*_2 index. Then, the uniformity analysis of U^* index along this main load path can highlight areas with more concerning load transfer issues. Figure 44 shows the U^*_2 variation along the depicted load path. The undesirable load transfer at the interface is marked in Figure 44.
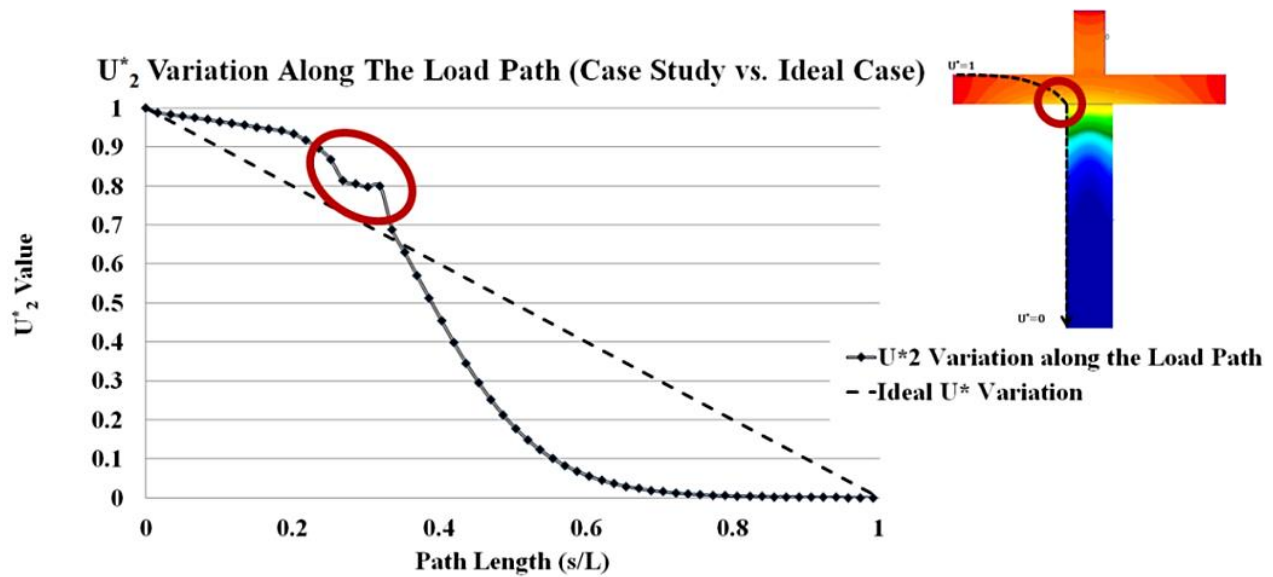
Figure 44) Uniformity analysis of U^*_2 variation along the load path.

Although the main load path is found to go through the vertical and horizontal tube, a part the reaction force is also being transferred to the upper arc-shaped section. Therefore, to have a global understanding of load transfer in this structure, it was necessary to study the U^* distribution and load paths in the upper arc too. Figure 45 shows the load path for the reaction force passing the upper arced shape part of the structure. The extreme changes in the U^*_2 values are visible on the side surface of the arc. Such rapid oscillations in the U^* values indicate undesirable stiffness variation in the structure that can lead to poor load transfer; or the in severe cases, might end up in failure.

The uniformity of U^*_2 index is studied to provide a quantitative evaluation of stiffness changes in the side surface of the arc. Clearly, as shown in Figure 45, the internal stiffness along the side surface experiences severe changes at the marked location which are the interfaces of the different tubes. These results suggest that the connection between the three components of the structure is not efficient for a proper load transfer.
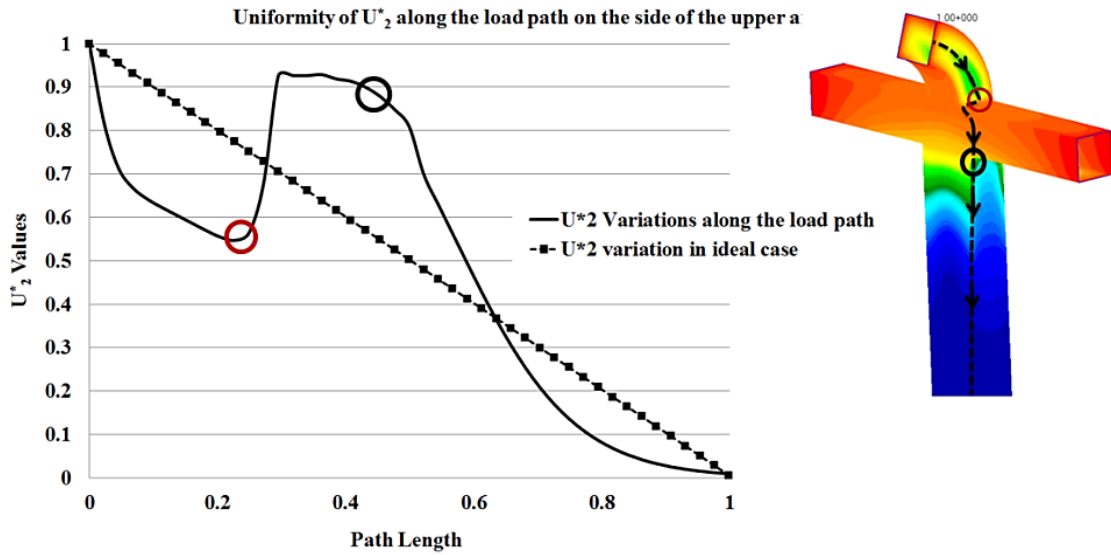
Figure 45) U^*_2 distribution, loads path and Uniformity analysis on the upper arc of the structure

Since both U^*_1 and U^*_2 analyses were performed on the structure, it was possible to evaluate the overall significance each part in the load transfer process using U^*_{sum} index. Figure 46 shows the U^*_{sum} index distribution in the structure.
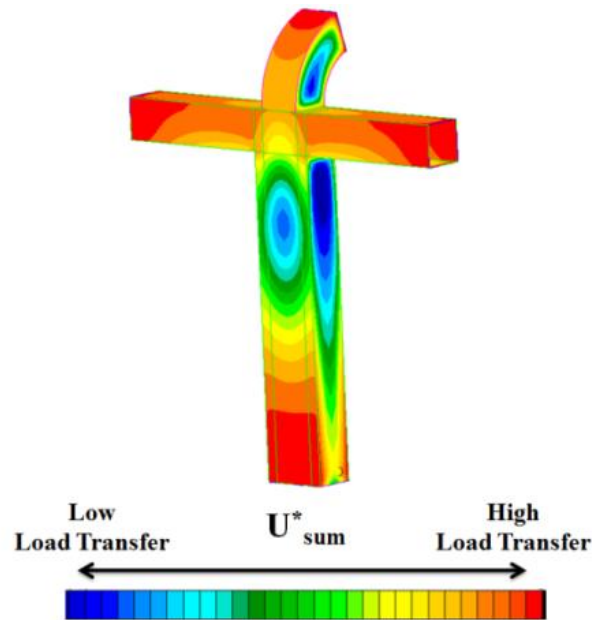
Figure 46) U^*_{sum} distribution in the structure.

As discussed in the description of the U^* index theory, the higher U^*_{sum} value represents a more significant role in the load transferring process and vice versa. A desirable load transfer needs a smooth transition of the U^*_{sum} values from high magnitudes to lower ones. Moreover, significant differences in the U^*_{sum} values of different location in the structure is a sign of unequal load transfer by those parts, which is considered an undesirable factor in design evaluation. To evaluate how close is the role of different parts of the structure in load transfer the histogram of U^*_{sum} indices can be used. Figure 47 shows the histogram along with the variance of U^*_{sum}. The mean value of U^*_{sum} of all points in the structure is 0.84, which demonstrates high rigidity of the structure and the U^*_{sum} variance is 0.011. Clearly, low values of U^*_{sum} variance indicates that the general distribution of stiffness in the structure is acceptable [32]; however, local problems found at the interfaces, as discussed in this section.
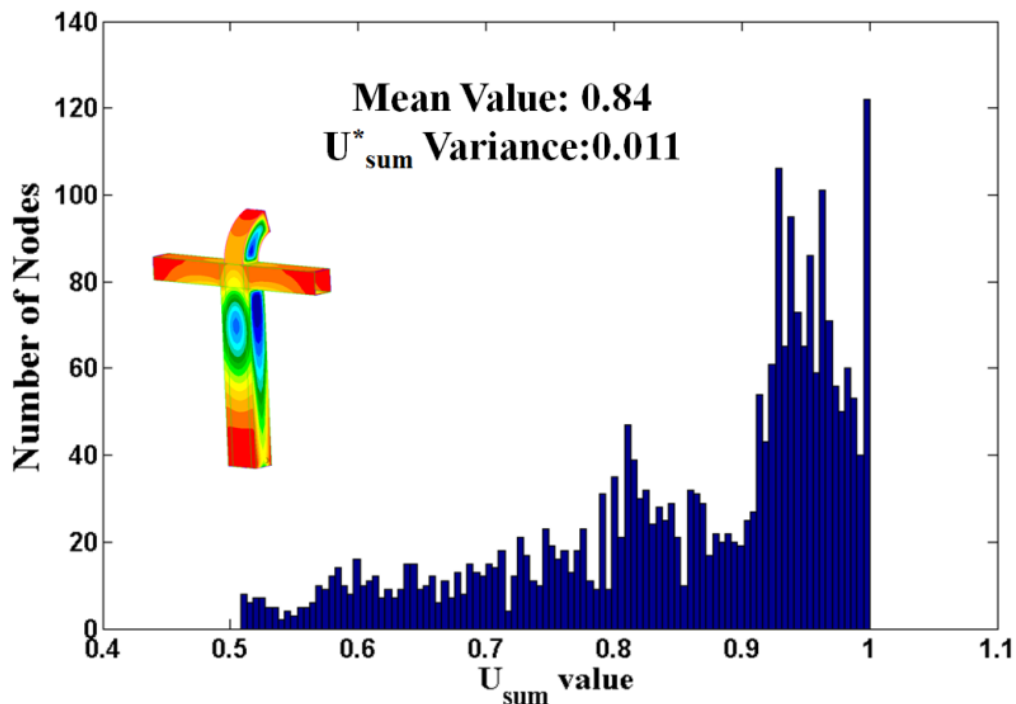
Figure 47) Histogram of the U^*_{sum} and the U^*_{sum} variance of the window pillar

To focus on weak points of the design and to compare the results with experiment, it can be more beneficial to concentrate on the interfaces of the connected tubes. Figure 48 summarizes that analysis.
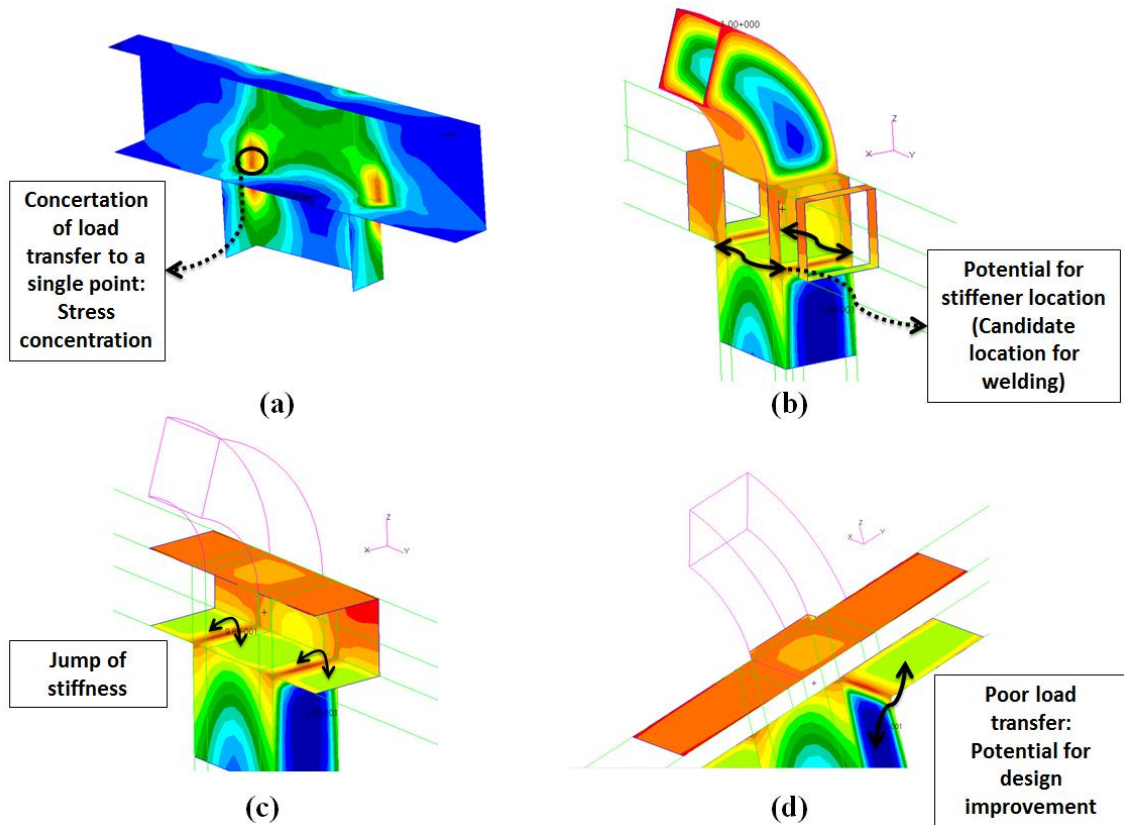
Figure 48) The distribution of a) von Mises stress, b, c and d) U^*_{sum} index in the in the inner and outer surfaces of the horizontal and vertical tube.

Figure 48a shows the stress distribution in the inner face of the horizontal tube through the cross section of the connecting interfaces. Figures 48b, 48c, and 48d are demonstrating the U^*_{sum} distribution in the same location from different views. Here capabilities of U^* index theory are used to describe the reason behind such complicated stress distribution and also to provide design modification suggestion that can improve the efficiency of load transfer. Figures 41 and 43 depicted the main load paths in the structure that suggest the major part of the applied loads

goes through the marked location in Figure 48a. Therefore, based on U^* index theory, the reason for the shown accumulated stress is the excessive load transfer from a single point.

Moreover, in the marked location of Figure 48b, there is a huge gap in the stiffness value. This jump of stiffness can lead to high stress and can be reduced by adding stiffeners in the marked location of Figure 48b and 48c.

Lastly, Figure 48d illustrates one of the best candidates for structural improvement. Clearly, based on experiment and simulation, it is necessary to lower the concentration of load transfer on the single point at the edge of the tube interfaces. Adding stiffeners to dictate a new load path can potentially improve the load transfer. However, it is essential to choose the best location to have efficient load transfer with minimum added weight.

The U^*_{sum} values shown in Figure 48d suggest that side surface of the vertical tube has a minimum contribution in load transfer, and thus connecting the stiffener to this surface will have minimum effect on improving load transfer. Instead, a thin and light triangular bulkhead can be added to transfer the load from frontal face of the vertical tube to the frontal face of the horizontal tube. This modification can efficiently improve the load transfer between the actual load carrying components without adding excessive material to random locations. Details of this design improvement and results are listed in the next section.

5-3-4- Design improvement based on U^* index results

As discussed above, the design improvement can be suggested based on the result shown in Figure 48d. Clearly, the side wall of the vertical tube carries a very limited amount of load. Therefore, to improve the load transfer, and reduce the load transfer from the tip of the welding, a bulkhead can be added just to the frontal surface of the tubes. Figure 49a shows a sample

modified structure. The modification has only been made to one side of the pillar to magnify its effectiveness in comparison with the other side. The result of stress analysis for the experimental peak load is shown in Figure 49b and proves that the modification, proposed based on the U* index theory, is indeed lowering the stress concentration on the side with the added bulkhead. Therefore, the modification can potentially increase the working load for this structure with only adding 0.95 % to the mass of the pillar.

(a)   **(b)**
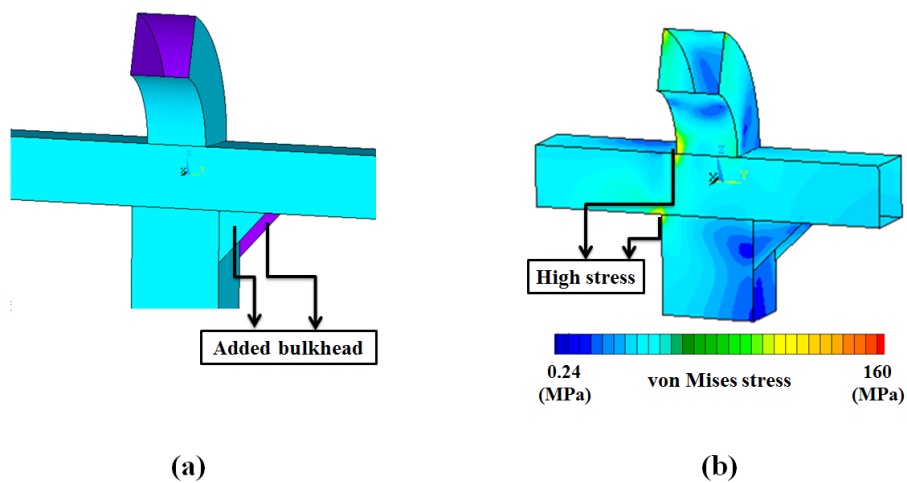
Figure 49) a: Modified structure with bulkhead on one side, b: von Mises stress distribution

Moreover, since this modification was suggested based on the load transfer analysis, it is necessary to show if the load transfer has also improved. Figure 50 shows the U* index distribution in the modified structure.
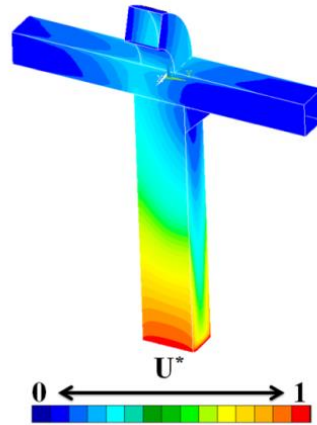
Figure 50) U* index distribution of the modified design

Figure 6b showed that in an ideal structure, the curvature of U* index should remain constant, zero, along the main load paths. However, as Figure 51 shows, the curvature of U* index variation along the left edge load path (original design) faces a rapid change at the intersection of the horizontal and vertical tube (dashed line of Figure 51). In contrary, the added bulkhead has made the load transfer much smoother on the right edge of the pillar, and the variations of curvature of U* index is not significant (marked line in Figure 51).

For a quantitative demonstration of the improvements in the load transfer, a continuity analysis was conducted on the modified structure. As proposed in [23], one of the design criteria that can quantify the efficiency of load transfer is studying the variations of curvature of U* index along the load paths.

Continuity Anlysis of U* Index Curvature
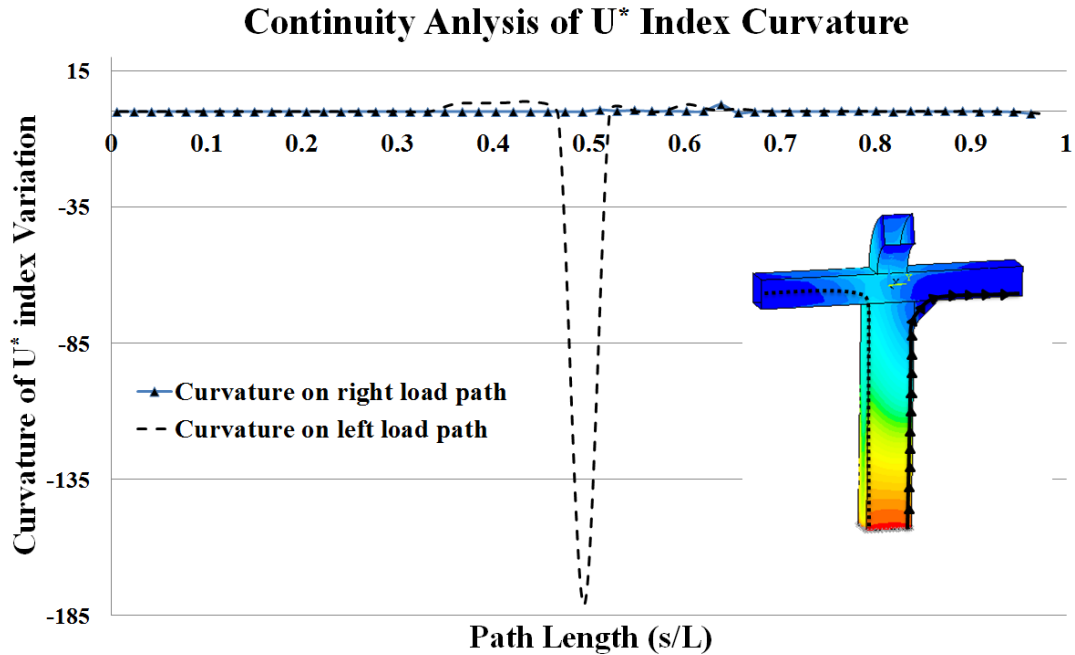
Figure 51) Continuity analysis of curvature of U* index along the left (original design) and right (proposed modification) edges of the pillar

This analysis clearly proves the improvement of load transfer behavior in the structure because of the proposed bulkhead. This example shows how U* index theory can improve the structural behavior of vehicle components by adding an insignificant amount of weight to the most efficient location, which is an important aspect of vehicle design.

5-3-5- Conclusion

In this study, a load carrying component of a multiple passengers vehicle was analyzed and using the U* index theory the internal stiffness of this structure was investigated under a severe type of loading condition. One of the significances of this study is the justification of the selected loading and boundary condition. A full vehicle model was analyzed under three significant loading conditions, to correlate the U* index theory to the actual needs of the manufacturer in the vehicle industry. Then, the most severe loading case was chosen for sub-modeling of the selected

component. The selected loading condition was used to define an experimental testing of the component which was later used to validate the simulation process.

Based on the U^* index theory, the load transfer behavior in the structure was evaluated, and locations with questionable stiffness were determined. Although U^* index theory is not supposed to be a failure criterion, a jump of U^* values in the adjacent parts suggest jumps in the internal stiffness that can be a considerable alarming sign for potential failure in the structure. Based on these results, a design modification was proposed, and a computer model was developed for the proposed amendment in the design.

The modified design had lower stress values in parts where the failure occurred in the original design and the experiment. Moreover, the U^* index analysis was performed on the modified model and using one of the design criteria proposed in the U^* index theory, the improvements in load transfer were shown in a sensible and quantified approach. The results indicate that U^* index theory can be used to evaluate structural behavior and propose design modifications that can improve load transfer, stiffness variation and overall behavior of the structure, with a negligible added weight, which is a critical factor in the vehicle industry.

5-4)   Load transfer on roof structure of the coach in the initial phase of impact

In the final case study of this dissertation, the U^* index theory is used to follow the load transfer on the roof of a baysection of a motor coach. The structure of a multiple passengers vehicle undergoes severe loadings during impacts, and there are several safety regulations for different vehicles in diverse types of accidents. On the other hand, manufacturers are encouraged to modify their design for producing lighter vehicles due to environmental obligations. Therefore, it

is necessary for engineers to use every possible tool to improve the structural behavior of vehicle during impacts without adding excessive material to the structure. Here, U^* index theory is considered to provide a new insight toward such design improvement.

5-4-1- ECE –R66 regulation for rollover impact

One of the well-known regulations for bus safety during rollovers is the ECE-R66 standard [39]. This agreement provides detailed requirements for different parts of the bus structure during rollover impact. As Figure 52 shows, for testing structural behavior based on ECE-R66, bus structure should be placed on a tilting platform with 800 mm distance from the ground. Then, by slowly rotating the platform, the structure starts to roll over with a zero velocity as it reaches the unstable point. Then, it will hit the ground as it does in a rollover accident.
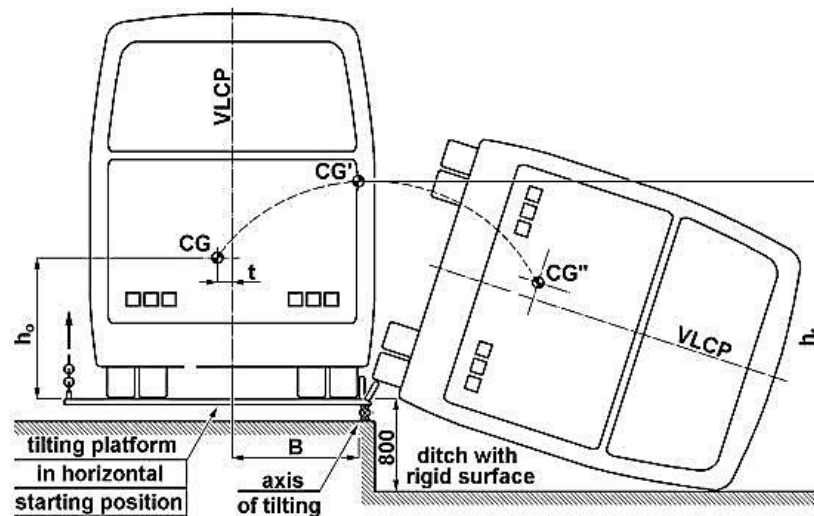

Figure 52) Test/Simulation setup for ECE-R66 rollover standard [39]

In one of the aspects of this regulation, engineers measure the overall deformation of the structure. It can be done on the full vehicle, or on a bay section of the model. Details of this regulation are not in the scope of this research but in general, a particular area inside the bus,

shall not be intruded by any part of the structure, for passenger safety issues. Moreover, ECE-R66 requires the emergency exit of the coach to remain closed during the rollover impact. However, the emergency exit hatch is made of plastic and in the case of motor coach that was investigated in this research, the hatch does not have any mechanical connection to the structure to transfer loads. Therefore, two major reasons can potentially lead to failure in ECE-R66 testing for the emergency exit:

1) Failure in the lock mechanism of the hatch due to excessive acceleration at impact, which is not in the scope of this research as it is not related to load transfer or structral analysis.

2) Excessive load transfer in the structural beams in the vicinity of the emergency exit, which can be studied using the U* index theory.

Therefore, lowering the deformation without adding too much weight can probably improve the chance of structure for passing standard requirements. The U* index theory is used in the next section to analyze the load transfer in the roof, in a bay section, in the very initial phase of roll over impact.

5-4-2- Load transfer analysis with U* index theory

Currently, the U* index theory is not a part of necessary simulations in assessing structural behavior according to ECE-RR 66. Nevertheless, to keep consistency with other methods of simulation, requirements of ECE- R66 is considered for the presented study. The baysection of the full vehicle was chosen for this analysis, as it is one of the acceptable models of simulation based on the regulation. The baysection is extracted from a full vehicle model, provided by the manufacturer, and includes major features of the structure, including the partial superstructure,

two kinds of window pillars, seat stands, and the emergency exit structure. Figure 53 shows the bay section structure modeled in Ansys APDL.
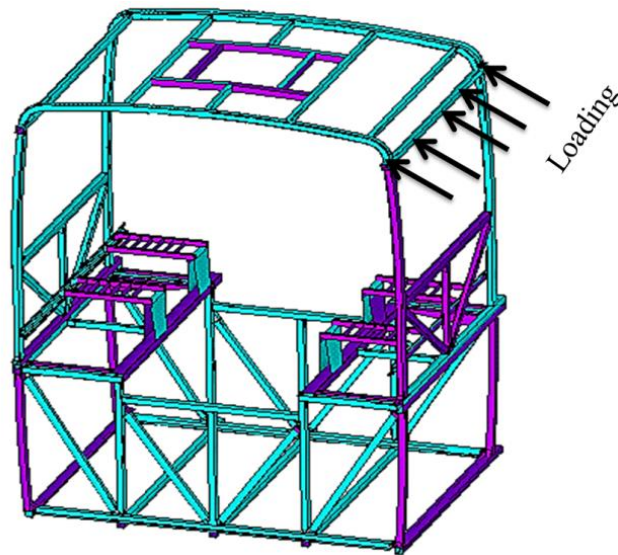
Figure 53) Bay section model

The structure was modeled using 17440 Shell181 elements and the material properties were selected based on the original full vehicle model[8]. For the loading and boundary condition selection, the ECE-R66 requirements were taken into consideration. As proposed in the regulation, the structure will rotate as it leaves the tilting table. Considering the initial 800 mm distance from the ground and the height of the superstructure, the loading condition at the initial impact moment can be estimated using Figure 54.

---

[8] Structural Steel.
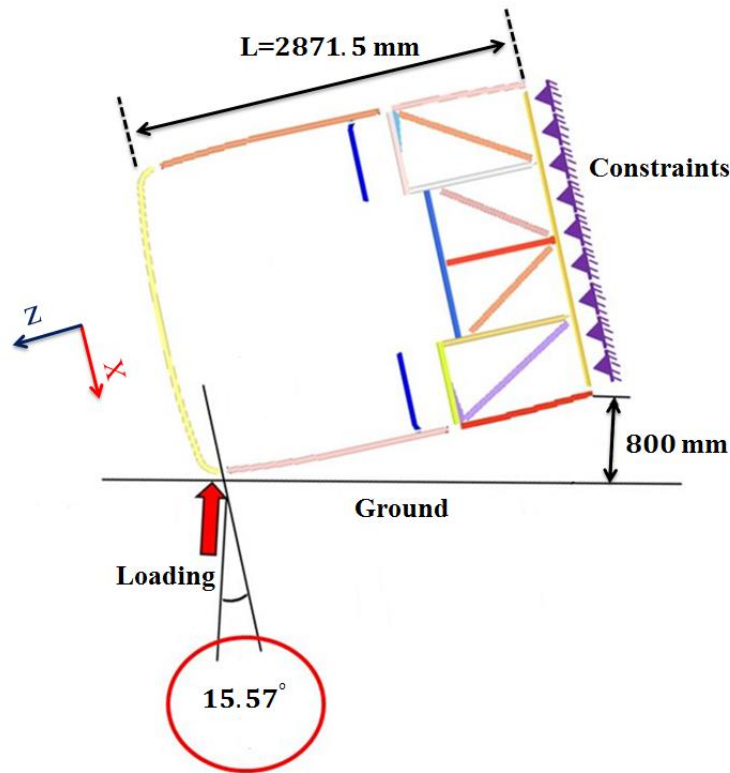
Figure 54) Loading and boundary condition of the rollover model for U* index analysis

As shown in the figure, as the structure hits the ground the beams on the roof make 15.57 degrees with the normal force direction. Therefore, the loading can be divided into two components, one in the x-direction and one in the z-direction, according to Figure 54. The magnitude of the load is not a matter of concern for U* analysis, as this index is based on a ratio and is insensitive to loading magnitude. Therefore, a 100 N load was selected as a sample loading which was divided into a -96.3 N in the x-direction and a -26.8 N in the z-direction. The structure does not have an actual fixed point in real experiment proposed in ECE-R 66, but as this analysis was performed for the very first moment of impact the lower section of the structure can be considered as the physical constraints of the system, i.e. the ending point of all load paths.

5-4-3- Preliminary Results

The U* index distribution in the bay section and its upper section are presented in Figure 55.

0	U* Index	1

(a)

0.72	U* Index	1

(b)
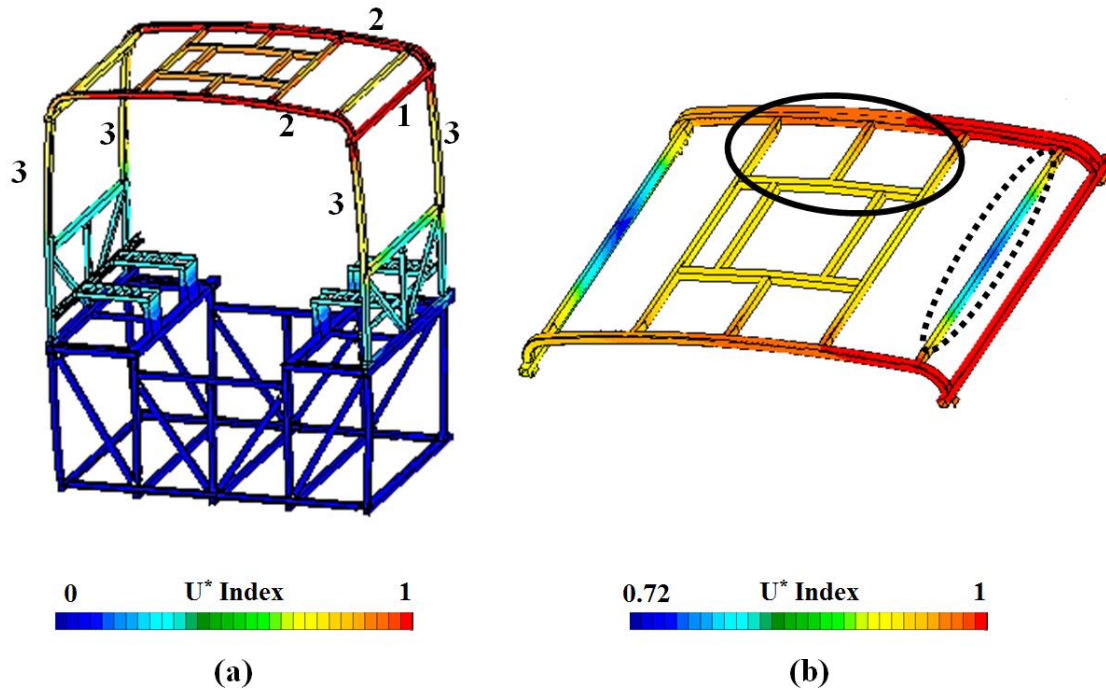
Figure 55) U* index distribution in a) the bay section and b) unmodified roof section

The results of the full baysection show that the applied load was transferred mainly from the outer horizontal beam (Beam #1) of the roof to the edge beams (Beams #2) and from there to the vertical pillars (Beams #3) and finally toward the constraints. Although it is the main load path, it is not the only one, and two potential ways can be observed in Figure 55b to improve the load transfer performance and improve the chances of the emergency exit to meet the requirements of ECE-R66.

1) The dashed marked beam of Figure 55b is showing 30%   lower U* index values compared to its surrounding beams. Therefore, the dashed marked beam is not

contributing enough in transferring the initially applied impact load due to lower internal stiffness, and it can benefit from some design modifications.

2) The marked area close to the emergency exit area is showing high stiffness. By conventional definition, high stiffness suggests lower displacement. However, as discussed earlier, there is no mechanical connection (e.g.: bolt, weld) between the shown beams on the roof and the plastic hatch of the emergency exit. Thus, roof deformation is probably not the main reason for potential failures. Therefore, high stiffness does not seem to be necessary. In contrary, transferring too much load toward the hatch location can provide potentials for extreme acceleration or stress concentrations that can lead to failure in other stages of the rollover impact. As a result, design modification in this area can also be helpful for achieving a better behavior in case of a rollover.

In the next section, three different design modification are presented based on the preliminary results of U* index analysis on the baysection.

5-4-4- Design Modification 1

Based on the outcome of the preliminary U* index analysis of the baysection, the first design modification was proposed for the roof structure. As it was addressed above, the bar, marked with a dashed line in Figure 55b, was not significantly contributing to the load transfer process. Therefore, to increase its role in the load transfer and to diverge some of the applied loads from the vicinity of the emergency exit, the fist design modification was proposed. Figure 56 shows the baysection with the modified roof. As it is highlighted in Figure 56b, two bars were added to create a potential new load path for removing the load carrying pressure from the emergency exit area. The arrows on Figure 56b are an illustrative representation of the expected new load paths which is the objective of the proposed design.

(a)   (b)
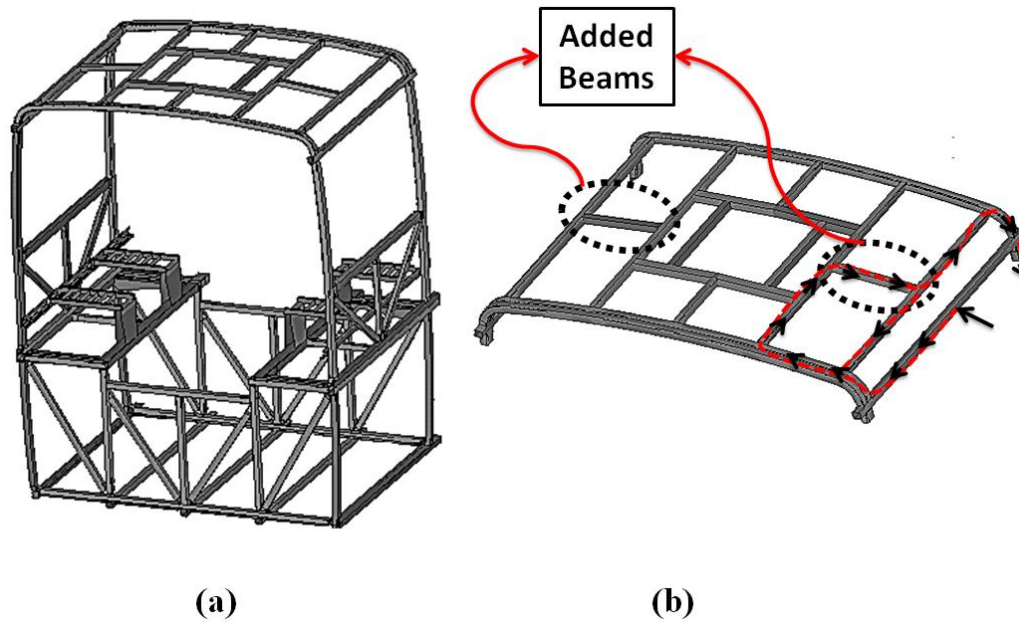
Figure 56) First design modification and one of the expected new load paths

To verify the efficiency of the proposed design load transfer analysis was performed on the new model. Figure 57 shows the U^* index distribution in the baysection and on the roof.

The results reveal that the first objective, which was increasing the significance of the marked beam of Figure 57b in load transfer process, has been achieved. However, there are some remaining concerns. Firstly, the U^* index values in the vicinity of the emergency exit area did not change considerably, and secondly, the modification was done by adding relatively big steel beams into the structure, which seems to be an expensive way to improve the design due to weight limitations. Finally, the maximum deformation is still very close to the previous model, though reduced a bit (From 10.51 mm in original model to 10.42 mm in the first modification). Therefore, a second design modification was proposed to improve the behavior of the roof structure, considering the result of first proposed alteration.
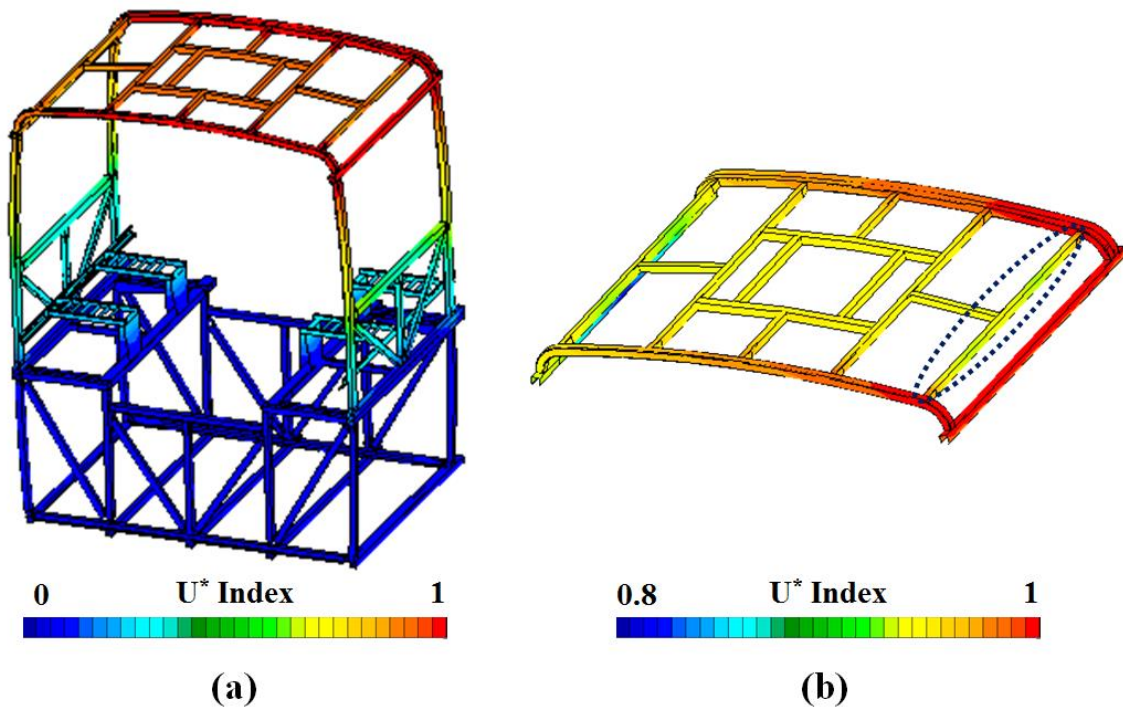
Figure 57) U* index distribution in a) the first modified model of the baysection and b) the roof structure

5-4-5- Design Modification 2

In the second proposed design, the added beams were moved from their initially proposed place to the new marked location of Figure 58a. This modification can potentially increase the role of the dashed beam of Figure 58b in the load transfer, with a minimum added weight. The results of the U^* index analysis are shown in the roof section in Figure 58b.

The results indicate that the marked beam of Figure 58b was this time actively participating in the load transfer, and the lower amount of material was used in comparison to the previous modification, which is a considerable improvement.
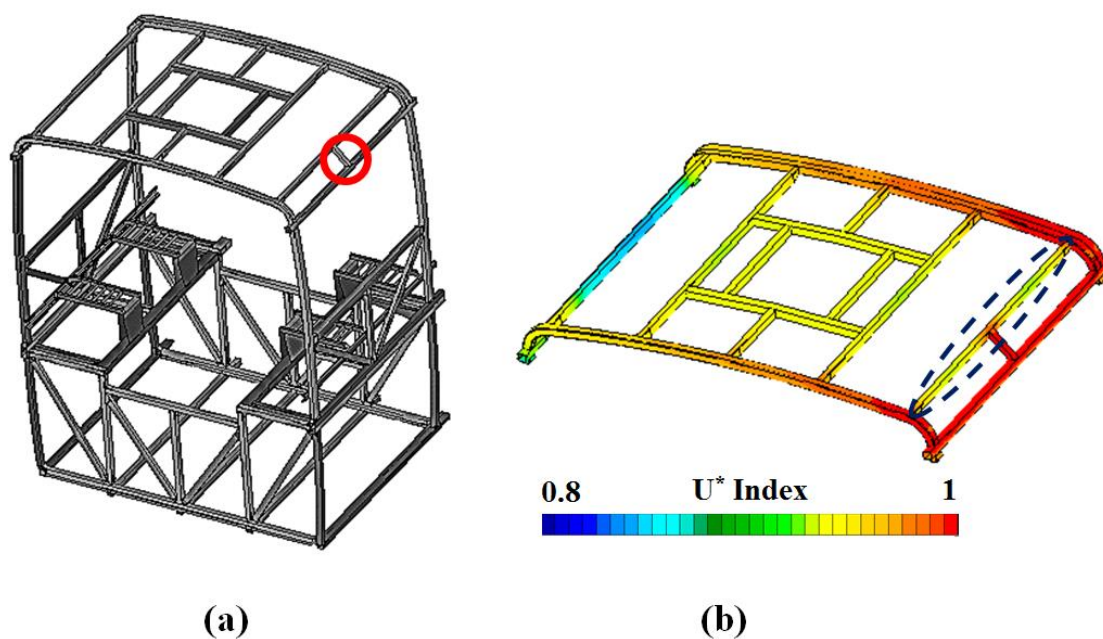
Figure 58) The second design modification a) Full baysection geometry, b) U* index distribution on the roof

However, maximum deformation has dropped only 0.02 mm from the first modification (10.40 mm in the new design compared to 10.51 mm of the original model). Moreover, the emergency exit area was still behaving almost identical to the initial design. Therefore a third modification was proposed that will be discussed in the following section.

5-4-6- Design Modification 3

The third design was suggested to reduce the amount of transferred load to the beams, surrounding the emergency exit. The marked beams in Figure 59a are not contributing the stiffness of the structure in case of bending of the vehicle, as there is a gap for placing the emergency exit. Therefore, they can potentially be removed from the structure without major

issues. Figure 59b shows the modified design, in which the potentially unnecessary beams were eliminated and two small beams were added just like previously proposed design.

The U* index theory was used for this model as well, and the results showed promising improvements. Not only the load transfer was improved as the small added beams increase the load carrying contribution of the marked beam of Figure 59a; but also, the overall weight of the structure was reduced by removing the unnecessary beams close to the emergency exit.
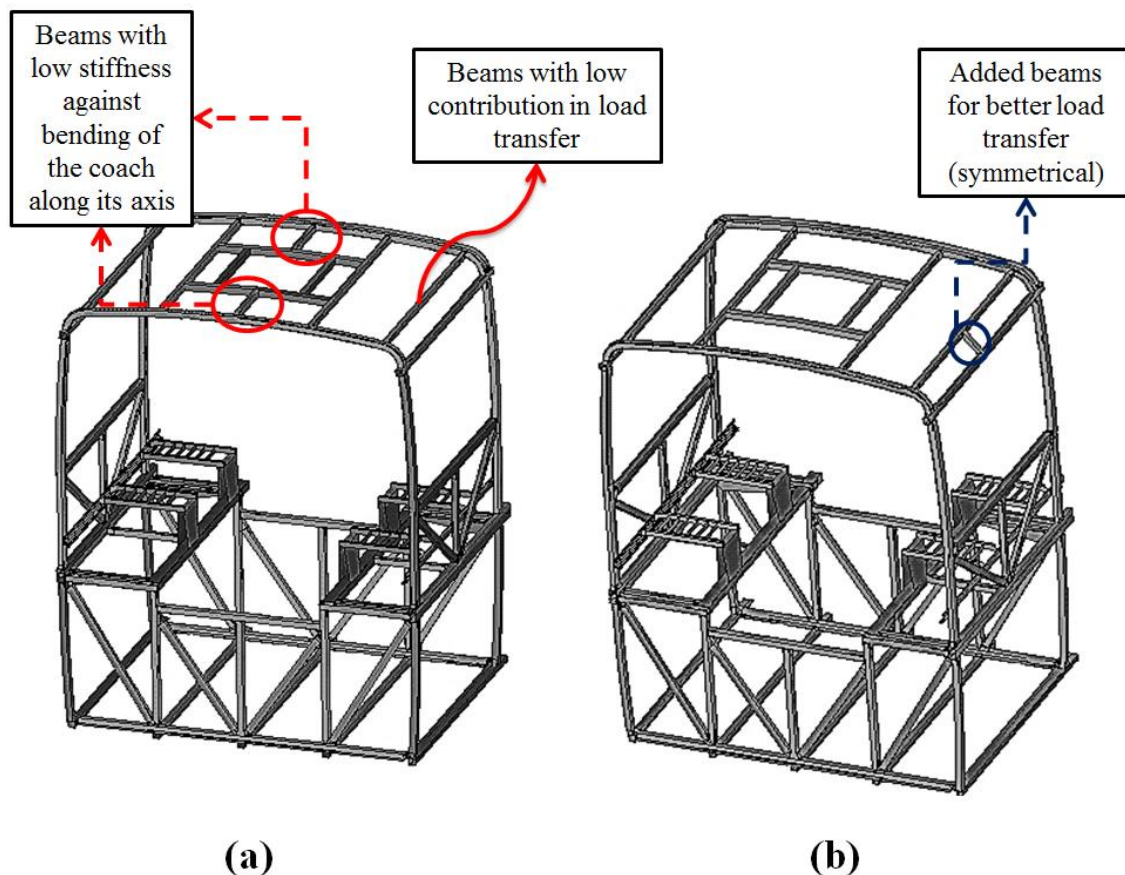
Figure 59) Baysection model a) original, b) last modification

Moreover, as Figure 60 shows, based on the U* index values, all main load paths diverge from the beams in the emergency exit neighborhood, and the design has potentially increased its chances for passing the ECE-R66 requirements for emergency exit.
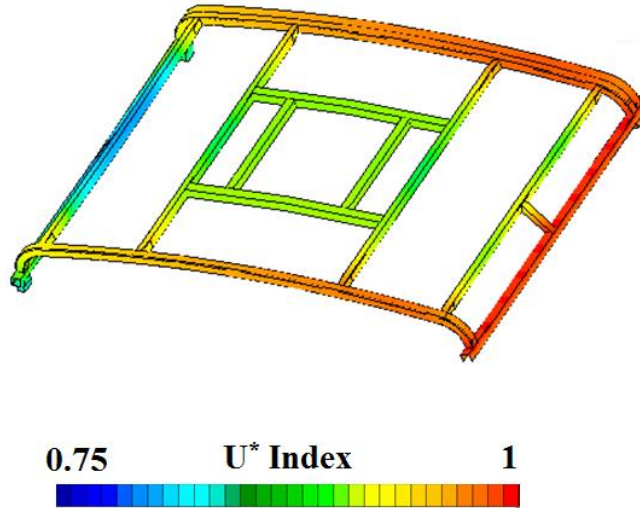
Figure 60) U* index distribution in roof structure of the last modification

In the next section, a summary of all modifications and results of each step is presented.

5-4-7- Summary of modifications

The load transfer analysis on the original structure revealed that one of the primary horizontal beams, close to the impact location is not contributing enough to the load transfer process at the initial impact. Moreover, the beams close to the emergency exit area were showing high U* index values, and thus some of the main load paths would pass through them, which is not a desirable situation considering requirements of ECE-R66. Therefore, three different modifications were proposed for the baysection design and the results of each of them is listed in Table 5.

Table 5) Summary of design modifications on the roof structure of the baysection

Design Number	Removed Parts	Added Parts	Max. Deformation	Pros	Cons
0 Original	N/A	N/A	10.51 (mm)	N/A	N/A
1	None	Figure 56b	10.42 (mm)	Better Load Transfer	Heavier, Almost same deformation, Load paths close to E.E.[9]
2	None	Figure 58a	10.40 (mm)	Better Load Transfer Lighter	Almost same deformation, Load paths close to E.E.
3	Figure59a	Figure 58a	10.23 (mm)	Better Load Transfer, Lighter, Less deformation, Less load transfer close to E.E.	Potential concerns due to beam eliminations

5-5- Summary and Conclusion

In this chapter of the dissertation, three different case studies were selected for load transfer analysis with U* index theory. All samples were chosen from a multiple passengers vehicle and

---

[9] Emergency Exit

based on technical problems proposed by industry, which is a significant matter as it proves the ability of U^* index theory for application in real life problems.

In the first sample, the strut of the parcel rack was modeled and analyzed under different loading conditions. The load transfer analysis results, which were also verified by experimental testing, provided the first rigorous and systematic comparison of U^* index theory with conventional stress analysis. As stress analysis is a well-matured theory, such comparison was essential, but missing in literature, for further development of the U^* index theory. Based on the analysis a complete design evaluation was performed on the strut, and its results were later used in another research project for a more efficient structural design.[10]

In the second analysis, the window pillar of the same vehicle was chosen for structural analysis. To perform a relevant research to needs of industry three possible loading conditions were proposed by the manufacturer of the vehicle and the worst case scenario was selected based on the full vehicle stress analysis. Then, using the U^* index theory, load transfer analysis was performed on the structure for the selected loading. Based on the results the reasons for the complicated stress distribution was explained, and the weak points in load transfer and internal stiffness variations were located, and best location for efficient design improvements was determined. Finally, a design improvement was suggested, and enhancements in stress distribution and load carrying capacity of the improved design were shown quantitatively.

Finally, the load transfer analysis with U^* index theory was used to evaluate the baysection of the studied vehicle. The significance of this study was the out of box thinking method that was used to deal with an established regulation for bus roll over, ECE-R66. This regulation defines certain

---

[10] Wang, Q., Pejhan, K., Wu, C. Q. and Telichev, I.: "Improvement of the weight efficiency of a vehicle component based on load transfer analysis using U^* index" Proceedings of the Institution of Mechanical Engineers, Part D: Journal of Automobile Engineering. In Preparation

requirements for different components of the bus, including the emergency exit kinematic behavior and overall deformation of the structure. Therefore, it seems, and of course is, necessary to perform dynamic analysis of the rollover impact and the kinematic analysis of the emergency exit for testing the structural behavior based on ECE-R66. However, it was shown for the first time in this study that a relatively simple static analysis with U^* index theory would provide a general awareness regarding the structure that can be used to propose modifications on the design before any expensive analysis on such huge models. Three different modifications were put forward for the structure, and the U^* index analysis showed step by step improvements that led to a lighter structure with lower deformation. Moreover, by detecting the load paths, it became possible to alter the design such that less amount of load would pass close to the emergency exit, which can potentially improve its behavior during the impact.

These three case studies firstly explored the capacities of the U^* index theory in comparison to matured current method of structural analysis. Secondly, the accuracy of the U^* index prediction was illustrated using experimental results and finally, it was demonstrated that U^* index theory opens new windows for design analysis, and improvements, even in cases where strict regulations, dynamic phenomena or large models can make any other method very time-consuming.

Chapter 6: Extension of U* index Theory to The Nonlinear Domain of Analysis

6-1) Introduction

Although as discussed in the literature review, the U* index has shown many useful features, it has always been limited to the linear elastic domain. This limitation is due to the definition of the U* index theory that is based on the linear elasticity equations. In the presented study, the main objective was to extend the U* index theory to the nonlinear domain for the first time. As the first step, the geometrical nonlinearity due to large deformations in the structure was set as the center of focus. It was shown in this study that a revision in the U* index theory can lead to a modified index (U$^*_{NL}$) which is capable of quantifying the internal stiffness of the structure under large deformation.

This new index was then used in some sample cases of structures in nonlinear domain. It was shown, using the proposed examples, the application of nonlinear analysis and U$^*_{NL}$ index would lead to more reliable load transfer analysis due to more accurate prediction of the internal stiffness of the structure. Accurate U$^*_{NL}$ index values become a necessity when structural integrity has the highest priority. In other words, inaccurate U* values for structures in the

nonlinear domain can lead to false decision makings. For example, in the case of design modification for making lighter structures, underestimated U* values can result in material removal from parts with a significant role in load transferring. Such decision endangers the integrity of the structure. Another example of cases in which high accuracy for U* values is crucial is location selection for stiffeners attachment. It is a common practice to attach stiffener's ends at locations with highest U*, so it is necessary to have a reliable U* index value for choosing the best place for stiffeners.

6-2)   Mathematical extension of U* index theory to nonlinear domain

The theory extension of the U* index is proposed by considering that the representative springs in Figure 4b can function in a nonlinear elastic domain. It is agreed upon that a good approximation for the reality of nonlinear springs is to assume that the Force-Displacement relation is in the form of a polynomial [40]. Therefore, instead of the simplified Hook's law for force displacement relationship, it can be written as:

$$F(x) = K_1 X + K_2 X^2 + K_3 X^3 + K_4 X^4 + \cdots + K_n X^n \tag{9}$$

Alternatively, in a closed form:

$$F(x) = \sum_{i=1}^{n} K_i X^i \tag{10}$$

In this equation, K_i (i=1,…,n) is the spring constant parameter for each term of the polynomial equation and X is the displacement. It is shown in [41] that accepted behavior for nonlinear spring can be presented by progressive (hardening) or degressive (softening) curves for force

displacement (Figure 61). As a result, the assumption of polynomial relationship is a fair consideration for spring behavior.
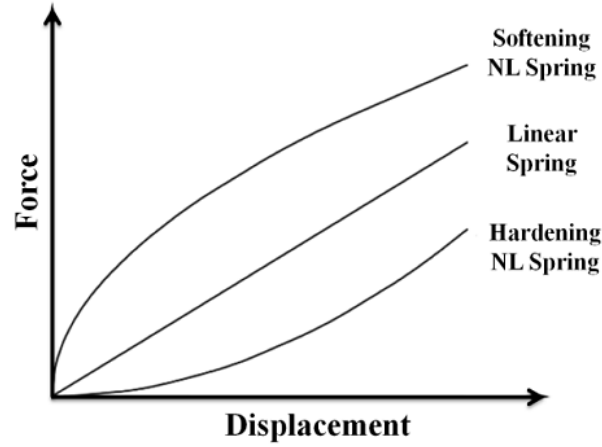
Figure 61) Force-Displacement curves for typical nonlinear springs [41]

Now the force- displacement equation of the system shown in Figure 4b can be re-written for springs without linear simplification:

$$
\begin{Bmatrix} P_A \\ P_B \\ P_C \end{Bmatrix} = \begin{pmatrix} k_{AA_1} & k_{AB_1} & k_{AC_1} \\ k_{AB_1} & k_{BB_1} & k_{BC_1} \\ k_{AC_1} & k_{BC_1} & k_{CC_1} \end{pmatrix} \begin{Bmatrix} d_A^1 \\ d_B^1 \\ d_C^1 \end{Bmatrix} + \begin{pmatrix} k_{AA_2} & k_{AB_2} & k_{AC_2} \\ k_{AB_2} & k_{BB_2} & k_{BC_2} \\ k_{AC_2} & k_{BC_2} & k_{CC_2} \end{pmatrix} \begin{Bmatrix} d_A^2 \\ d_B^2 \\ d_C^2 \end{Bmatrix} + \cdots
$$
$$
+ \begin{pmatrix} k_{AA_n} & k_{AB_n} & k_{AC_n} \\ k_{AB_n} & k_{BB_n} & k_{BC_n} \\ k_{AC_n} & k_{BC_n} & k_{CC_n} \end{pmatrix} \begin{Bmatrix} d_A^n \\ d_B^n \\ d_C^n \end{Bmatrix}
$$

(11)

where, P_i (i=A,B,C) is the force vector at each point, d_i (i=A,B,C) represents the displacement at the corresponding point and K_{ijm} (i,j=A,B,C & m=1,2,…,n), is the internal stiffness between the loading point i and the arbitrary point j for the mth term of the polynomial. The above equation can also be written in a closed form formulation:

$$\begin{Bmatrix} P_A \\ P_B \\ P_C \end{Bmatrix} = \Sigma_{i=1}^n \begin{pmatrix} k_{AA_i} & k_{AB_i} & k_{AC_i} \\ k_{AB_i} & k_{BB_i} & k_{BC_i} \\ k_{AC_i} & k_{BC_i} & k_{CC_i} \end{pmatrix} \begin{Bmatrix} d_A^i \\ d_B^i \\ d_C^i \end{Bmatrix} \tag{12}$$

Considering the constraint of the system (d_B=0):

$$F(x) = P_A = \Sigma_{i=1}^n ((k_{AA_i})d_A^i + (k_{AC_i})d_C^i) \tag{13}$$

For this nonlinear system (as in Figure 4b), the strain energy can be calculated using the formulation found for P_A:

$$U_{NL-Poly} = \int (\Sigma_{i=1}^n K_i x^i) dx = \frac{1}{2}(F(x).d_A - \Sigma_{i=1}^n ((\frac{i-1}{i+1}) K_n.d_A^i)) \tag{14}$$

where $U_{NL-Poly}$ stands for the stored strain energy in the nonlinear system with polynomial force-displacement equation. Inspired by the U* index definition by Takahashi's group, we propose an index, U^*_{NL}, for load transfer in structures that are governed by a polynomial nonlinear Force-Displacement equation:

$$U^*_{NL} = 1 - \frac{2U_{NL-Poly}}{2U'_{NL-poly}} \tag{15}$$

Here, $U'_{NL-poly}$ is the strain energy stored in the system, in case that point C is fixed, and d_A is applied to point A. The term $\Sigma_{i=1}^n ((\frac{i-1}{i+1}) K_n. d_A^i)$ of Equation 14 is a constant value for a given value of n (degree of polynomial). It will be straightforward to show that by substituting the Equation14 into Equation 15, the nonlinear load transfer index (U^*_{NL}) can be written as:

$$U^*_{NL} = (1 - \frac{2U_{NL-Poly}}{\Sigma_{i=1}^n (k_{AC_i}.d_C^i).d_A})^{-1} \tag{16}$$

Clearly, this index is proportional to the internal stiffness between the loading point and the arbitrary point C (k_{AC_i}) and thus can quantify the degree of connectivity in the structures that follow the proposed nonlinear polynomial equation (Equation 11). Consequently, it can be stated that the proposed extended U^*_{NL} index quantifies the internal stiffness and thus is an indicator of load transfer in structures in elastic nonlinear domain

6-3)   Case study – Application of U^* index theory in nonlinear domain

In this section, to evaluate the significance of applying U^*_{NL} in structures with large deformation (geometrical nonlinearity), two sample cases were selected, and the load transfer study was done for them with both U^* and U^*_{NL} indices. The comparison will show the effect of consideration of nonlinearity in load transfer analysis.

6-3-1- Load transfer analysis of cantilevered beam in large deformation

The first sample case is a simple cantilevered beam. The beam is modeled to be 1 m long with a 0.018 m^2 rectangular cross section. One end of the beam is fixed completely (cantilevered beam), and the other end is loaded vertically. To show that application of U^*_{NL} is justified, it is necessary to check the force- displacement curve. The proposed index is only valid if there is a polynomial relationship between force and displacement and as the Figure 62 shows, such relationship exists for the beam under large deformation.
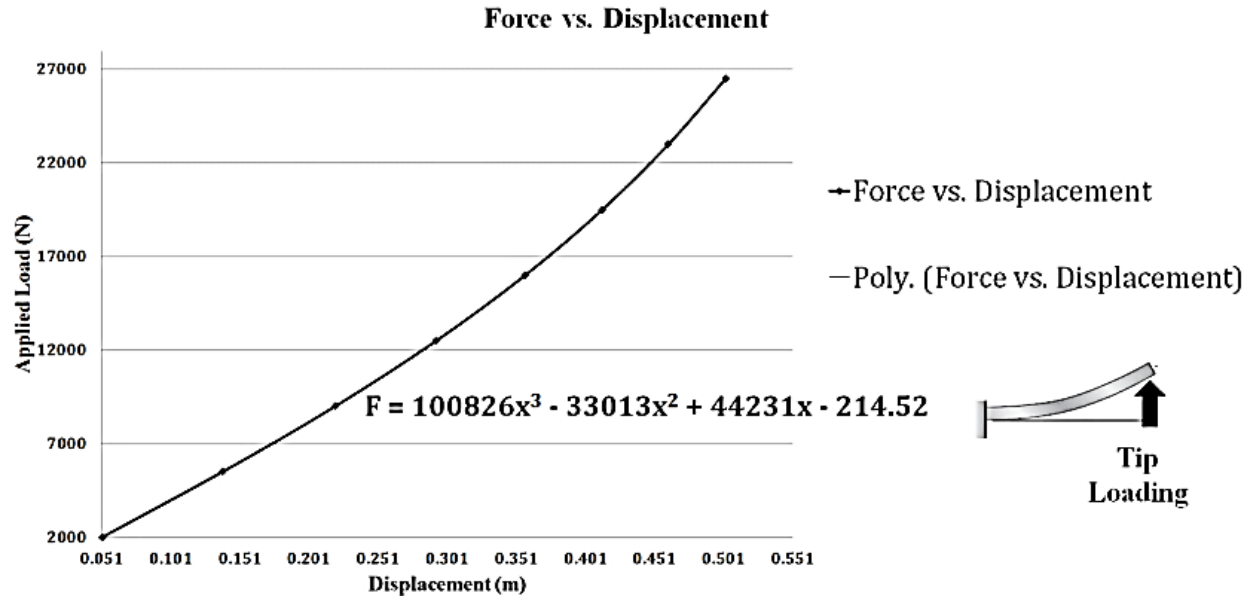
Figure 62) Force- Displacement Curve (Simulation data and polynomial fitted curve)

Clearly, the curve from actual data (created by MSC Nastran) is entirely consistent with a polynomial curve fitted to the nodal data in Matlab. As a result, the proposed index can be used to predict the load transfer behavior in the structure.

The necessary FEM data, including displacement and strain energies, were extracted using MSC-Nastran and the U^* and U^*_{NL} indices were calculated using an in-house developed a program using Matlab. In the first set of simulations, the large deformation condition was ignored to see how basic U^* index predicts load transfer for a simplified (linear) analysis. Then, the large deformation condition was assumed in the simulation and using a non-linear implicit analysis the load transfer analysis for the nonlinear case was executed.

6-3-2- Load transfer analysis of a thin plate under edge loading

In the second case study, a thin plate shown in Figure 63 is explored in both linear and nonlinear domains. The dimensions and loading and boundary condition for this model are all illustrated in Figure 63.
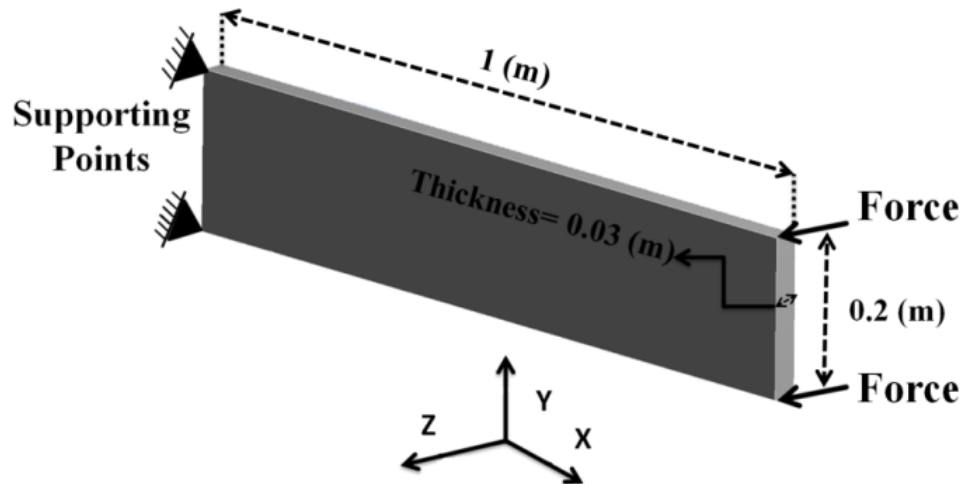
Figure 63) Structure and boundary conditions for the 2nd case study

Just like the previous case study, it is necessary to show that the force-displacement relationship can be assumed to be polynomial, i.e.: it should be justified that the U^*_{NL} applies to this problem. Figure 64 demonstrates the force vs. displacement curve at the loading point for both linear and nonlinear analyses. As it can be seen, the polynomial curve fitted on the extracted nonlinear data is exactly consistent with the force-displacement curve produced by the nonlinear simulation. Therefore, application for U^*_{NL} for load transfers analysis is feasible.

Force vs. Displacement

$$y = 112448x^4 - 218274x^3 + 157371x^2 - 47964x + 5378.1$$
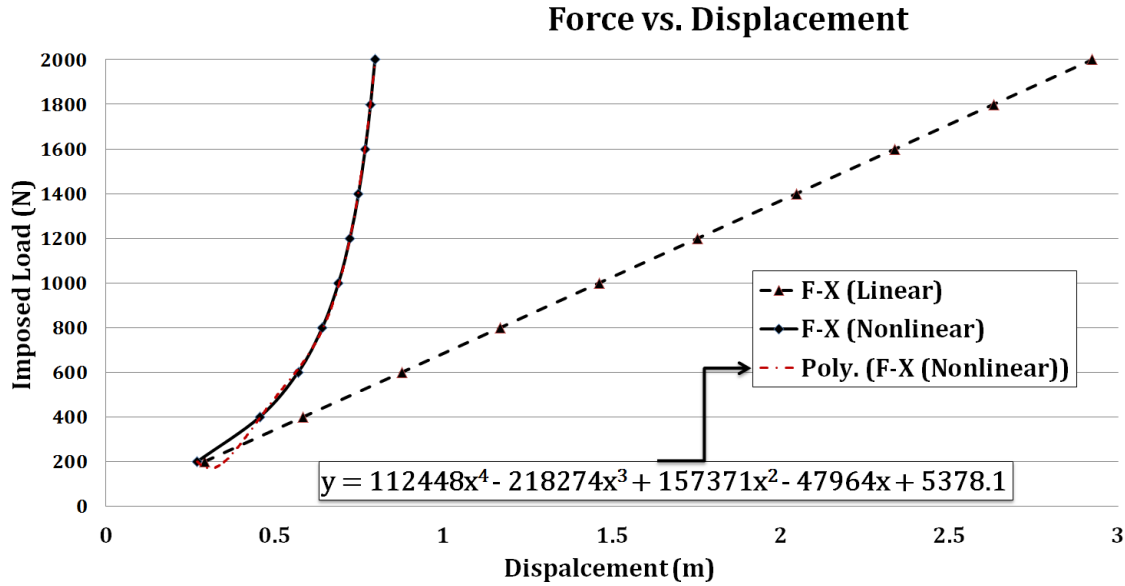
Figure 64) Force vs. Displacement curves for linear and nonlinear analyses and the polynomial fitting

6-3-3- Results and Discussion

In this section, the results of load transfer analysis of the proposed case studies are presented along with a discussion based on a comparison between the achieved results of U^* and U^*_{NL} indices.

6-3-3-1- Case Study 1: Results

In the first case study, the load transfer analysis was performed on the structure. By considering the large deformation of the beam, the U^*_{NL} index was calculated for all nodes of the beam. Figure 65 shows the U^*_{NL} index distribution on the beam.
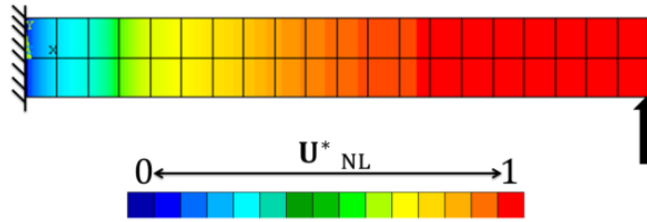
Figure 65) U^*_{NL} index distribution in the beam with large deformation

The U^*_{NL} value is equal to one at the loading point and goes down to zero at the supporting point. Then, to compare the effect of considering nonlinearity in the analysis the U^* values were calculated for the linear case, and the comparison of the results are shown in Figure 66. As it is shown in this figure, the U^*_{NL} can show higher values (up to 12% more) than the linear U^* index.
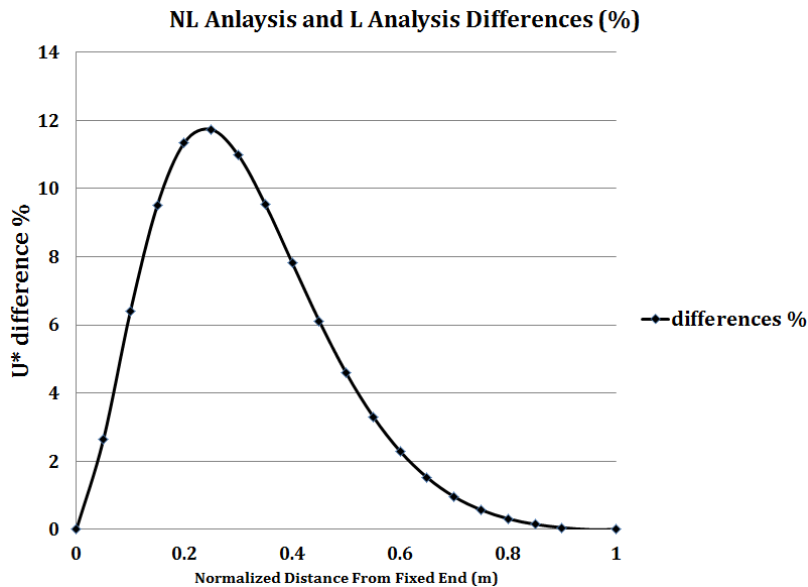
Figure 66) Percentage of difference between U^* and U^*_{NL} values in a cantilevered beam

6-3-3-2- Case study 2: Result

In the second case study, the same comparison is made between the U^* and U^*_{NL} values. In this structure, the variation of the U^* and U^*_{NL} values along the cross sections in the plate are

compared The results, shown in Figure 67 demonstrate the significance difference between the load transfer indices found in the linear and nonlinear analysis.
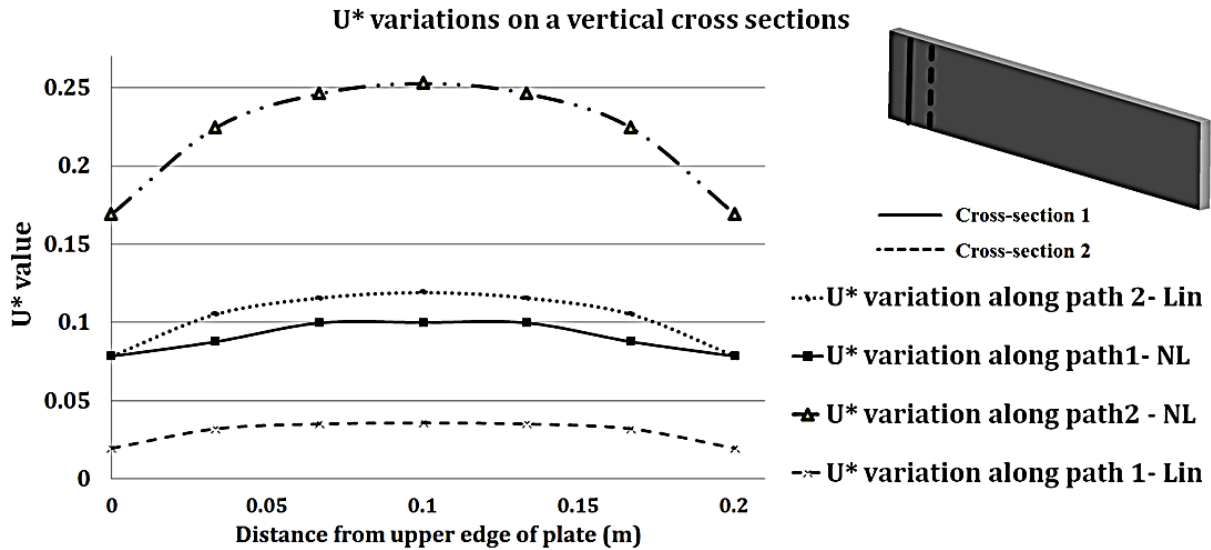
Figure 67) U^* and U^*_{NL} variations along two sample cross sections in the plate

The results show that the nonlinear analysis predicts much higher values for load transfer index (U^*_{NL}) while the basic U^* analysis underestimated the internal stiffness along these cross sections. The differences between the U^* values on five cross sections of the structure are shown in percentages in Figure 68 to get a more general picture of the effect of nonlinearity consideration on load transfer analysis.
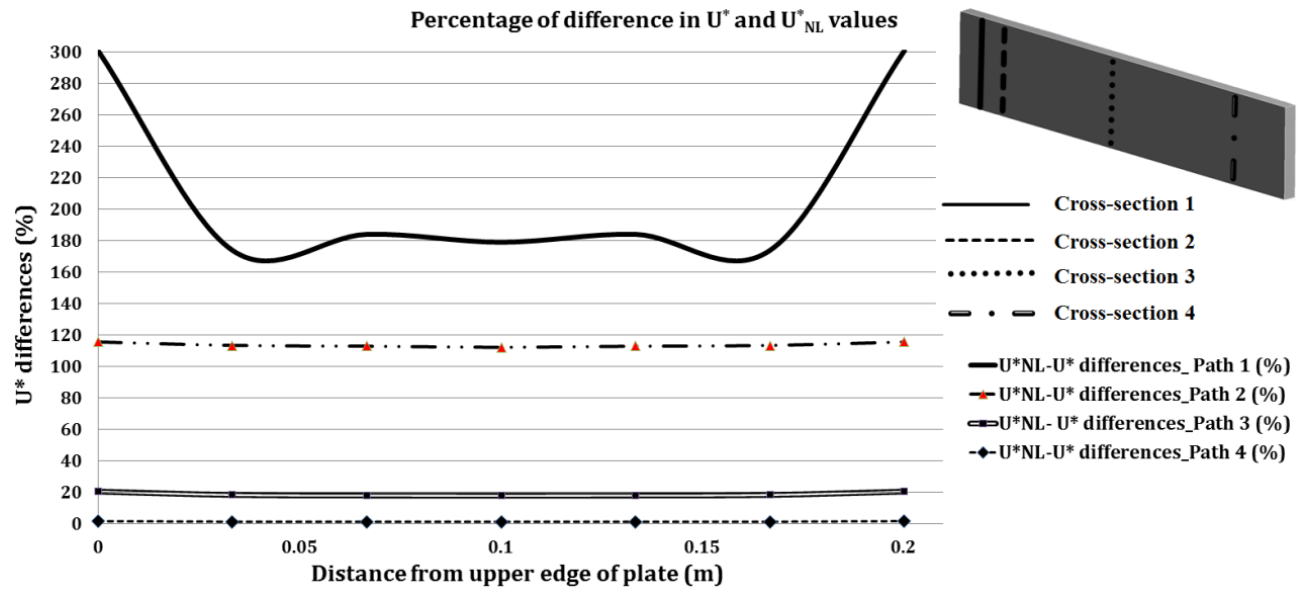
Figure 68) Difference of U^*_{NL} and U^* index values along different cross sections

The results indicate that the difference between predicted U^* value of linear analysis and U^*_{NL} value of nonlinear analysis varies from almost zero close to the loading location to more than 280 %, close to the constraints of the system. Based on the achieved results in these two case studies a discussion can be made that will follow in the next section.

6-3-3-3- Discussion on the results

In the first case study (the cantilevered beam), the U^* and U^*_{NL} variations along the beam were calculated. Due to simple geometry, the distribution of both indices seems to be close to each other, though, the U^*_{NL} values tend to be higher in most of the beam's length. This difference reached up to 12 percents, which is a significant amount of error in a simple structure like a beam.

A complete evaluation of the differences between the U^* values was performed in the second case study. It was demonstrated that considering the linear U^* index, despite the large

deformation (geometrical nonlinearity) can lead to underestimating the significance of different parts of the structure in load transferring; due to lower predicted U* values. Moreover, the load transfer behavior of a structure can be evaluated by following the trend of U* variation in the structure. Therefore, the linear and nonlinear analysis can lead to different conclusions from this perspective too. Comparing the U$^*_{NL}$ and U* variation along the cross-section shows that linear analysis predicts a lower rate of U* change; this can be considered as an over-optimistic evaluation of stiffness variations along the cross-section under the proposed loading. As a result, the results of the linear analysis are less reliable for cases, in which designers cannot make any compromise in the accuracy of their evaluations.

The results of following U* variations along a different cross section of the plate showed that there is a huge gap between the predictions of linear and nonlinear analysis close to the constraint points. Although the loading area did not show a significant difference between linear and nonlinear analyses, in a cross-section far away from both loading and supporting areas (cross section 3 in Figure 68), the U* index values are about 20% less than the predicted values for U$^*_{NL}$.

One sample problem that might occur by using the linear U* index is misjudgment for material removal; i.e. designer might calculate the U* value of a part of the structure up to 280% lower than its actual magnitude. Such a conclusion might urge the designer, to remove material from this part because of its apparently low significance in load carrying process; while the nonlinear analysis might change the designer's mind by showing much higher U$^*_{NL}$ value for the same part. As a result, in cases that integrity of the structure is much more important that its weight, the nonlinear analysis would be the reliable approach, and U$^*_{NL}$ is recommended. It should be noted that since U* index theory does not include a certain numerical criterion for evaluation

(unlike stress analysis), using the proposed index (U^*_{NL}) mainly depends on the precision required by the designer.

6-4)   Conclusions

This section of the presented study proposes the first extension of load transfer index (U^*) theory into the nonlinear domain analysis. By assuming nonlinear elastic equations for the basic concepts of the U^* index theory, it was shown that a modified index for the nonlinear problem (U^*_{NL}) could be calculated numerically, and it is proportional and can quantify, the internal stiffness of a structure under geometrical nonlinearities. Then, to show the significance of this extended index in engineering application, two well-known problems of cantilevered beam under vertical tip loading and thin plate under transverse loading were analyzed using the proposed index. The results show that linear (basic) U^* index tends to predict lower than real values for internal stiffness of the structure. These results can lead to underestimating the significance of certain parts of the structure in load carrying process. Such conclusion might end up to material removals that can endanger the integrity of the structure. Moreover, it was shown that the U^* changes in the structure can be different in linear and nonlinear analyses. As a result, a nonlinear analysis of load transfer with U^*_{NL} can provide a more reliable picture of the overall behavior of the structure in load carrying process and can provide designers with more accurate information for decision making.

The presented extension is the first step toward achieving a comprehensive indicator of load transfer. At this stage, the new index is limited to cases with geometrical nonlinearities, and the calculation process, which uses the implicit method of analysis, is time-consuming for more complicated structures. Also, it is necessary to point out that the presented approach for this

extension is based on considering nonlinear springs in defining the theoretical foundations. Therefore, the considered geometrical nonlinearity covers the softening or stiffening effects in the structure. In other words, there is potential for further development toward achieving a complete nonlinear index that can include other cases of nonlinearity; as rigid body motion of elements, material nonlinearity, plastic deformation, etc. Moreover, application of explicit methods for solving the nonlinear problem can guarantee the convergence of the solution, though it would increase the calculation time significantly.

Nevertheless, this extension opens up a new door for more development on the U* index theory. Future extensions can look for material nonlinearity, using multi-linear material models, or can tackle computational issues by providing an explicit analysis method which would remove the converging problems of current methods of analysis.

Chapter 7: Summary and Conclusion

7-1) Summary

In this chapter, a summary of all completed tasks in the dissertation is presented. As shown in chapters one to seven, load transfer analysis is a new emerging aspect of structural analysis that can provide a general awareness regarding the structural performance. The U^* index theory for load transfer analysis provides a global view of the structure that in combination with a local analysis, like stress analysis can provide precious information about performance and efficiency of design in mechanical structures.

In the presented study, after introducing the U^* index theory and reviewing its theoretical background, the first experimental validation of the theory was presented. Since U^* index theory is a relatively new paradigm in structural analysis, presenting an experimental validation was a major necessity toward developing this theory to a fully matured one.

The experimental validation provides a reliable benchmark for application of the U^* index theory in future industrial and academic problems. The presented test setup also clarified the concept of internal stiffness and its effect in load transfer in comparison to the conventional stiffness definition.

After providing the very first experimental validation of the U^* index theory, it was applied to three real life industrial problems. All the selected case studies were chosen from a heavy vehicle which provides significant distinction from the existing research in the literature, which was mainly focused on the lower section of a passenger car. Moreover, in each sample case study, one of the capacities of U^* index theory was tested, and its effectiveness was presented.

It is also important to point out that experimental testing was considered for two of the case studies to show the accuracy of the analysis results made by U^* index theory and to depict the unique capacities of this theory.

The outcome of the sample studies presented in this dissertation can be summarized as:

- Verification of U^* index theory prediction with experimental results,

- Systematic comparison of the U^* index theory with conventional analysis,

- Load path evaluation in major load carrying components of a multiple passengers vehicle,

- Explanation of complicated stress distribution in mechanical structures using U^* index distribution,

- Design improvement using theU^* index analysis results,

- Application of the U^* index theory for performance behavior of the structure, considering standard safety regulations.

Finally, as the U^* index theory is relatively new in the field of structural analysis, compared to other methods like stress analysis, it was, and still is necessary to extend this theory to different aspects to achieve a more mature theory. Therefore, in this study, the very first step toward achieving a nonlinear U^* index theory was taken. As shown in Chapter 6, a mathematical

extension was proposed to the nonlinear domain of analysis by considering the nonlinear elastic relationship between force and displacement for the illustrative springs. This force-displacement relationship has to be in a polynomial format but can be nonlinear of any degree. From a mechanical point of view, such extension can be applied to structures that undergo geometrical nonlinearities, like a beam with a large deflection. By providing the new U^*_{NL} index for such types of nonlinear problems, it was proved that internal stiffness is proportional to the new U^*_{NL} index. Then, this index was applied to two sample case studies in which it was demonstrated that the proposed U^*_{NL} index would predict the load transfer index with much more accuracy compared to a simplified linear U^* index. In conclusion, the proposed U^*_{NL} index is proved to be a useful tool for load transfer analysis in cases that designers need higher levels of accuracy in performing structural analysis.

7-2) Conclusion

The presented research can be considered as a major step in the ongoing process of U^* index theory development. Throughout this dissertation, a full and systematic comparison was made between the load transfer and conventional stress analyses. This comparison showed the exceptional capacities of U^* index theory and proved the necessity of consideration of load transfer evaluation in structural analysis studies. One of the significant outcomes of this research was the first experimental validation of U^* index theory that was missing in literature and makes this a referral point for future studies. Design evaluation and improvement using U^* index theory that was performed for the selected industrial cases is a clear example of the new load transfer-oriented approach for designers. As another necessary step toward a well-developed method, U^* index theory was extended to the nonlinear domain of analysis. Although the new index requires

expensive calculation due to complexities of nonlinear analysis, it is viewed as an important step forward as it has opened a new field of study on U^* index domain.

7-3)   Suggestion for future work

The U^* index theory can now be used in any academic or industrial problem focusing on the structural performance as it has been validated, tested in industrial applications and extended to nonlinearity in the presented dissertation. However, there are of course more ways to develop and apply the U^* index theory. Some of the main studies that are necessary and in case are undergoing in this field can be categorized as:

1) Extension of the U^* index theory to composite materials (Undergoing Research[11]).

2) Extension of the U^* index theory to nonlinear materials.

3) Extension of the U^* index theory to fully dynamics criterion.

---

[11] Wang. Q, Pejhan. K, Wu. C. Q., and Telichev. I., "Load Transfer Index for Composite Materials", ASME 2015 International Mechanical Engineering Congress and Exposition. American Society of Mechanical Engineers, November 2015

References

[1] "Clean Vehicles," Union of Concerned Scienetists, 31 1 2014. [Online]. Available: http://www.ucsusa.org/clean_vehicles/why-clean-cars/global-warming/. [Accessed 10 03 2014].

[2] A. Fazeli, A. Khajepour and C. Devaud, "A novel compression strategy for air hybrid engines," Applied Energy, vol. 88, no. 9, pp. 2955-2966, 2011.

[3] A. Fazeli, M. Zeinali and A. Khajepour, "Application of addaptive sliding mode control for regenerative braking torque control," in Transactions on Mechatronics, IEEE/ASME, 2012.

[4] A. C. a. R. Broda, "Impact of Vehicle Weight Reduction on Fuel Economy for Various Vehicle Architectures," Ricardo Inc., Detroit, 2008.

[5] C. W. Lynette, A. P. Bnadivadekar, K. M. Bodek, E. P. Kasseris and J. B. Heywood, "The trade-off between automobile acceleration performance, weight, and fuel consumption," SAE International Journal of Fuels and Lubricants , vol. 1, no. 1, pp. 771-777, 2009.

[6] C. W. Lynette, "Materials flow analysis and dynamic life-cycle assessment of lightweight automotive materials in the US passenger vehicle fleet," in IEEE International Symposium on Sustainable Systems and Technology, 2009.

[7] Uniform Technical Prescriptions Concerning the Approval of Large Passenger Vehicles with Regard to the Strength of their Superstructure, United Nations, 2010.

[8] Federal Motor Vehicle Safety Standards- Standard No. 220, U.S. Department of Transportation- Federal Motor Carrier Safety Administration, 2013.

[9] T. J. R. Hughes, The Finitel Element Method: Linear Static and Dynamics Finitle Element Analysis, Dover Publication, 2012.

[10] M. Petyt, Introduction to Finite Element Vibration Analysis, Cambridge University Press, 1990.

[11] H. Huo, A. Bobet, G. Fernandez and J. Ramirez, "Load transfer mechanisms between underground structure and surrounding ground: evaluation of the failure of the Daikai Station," Journal of Geotechnical and Geoenvironmental Engineering, vol. 131, no. 12, pp. 1522-1533, 2005.

[12] G. Doudak, G. McClure and I. Smith, "Experimental evaluation of load paths in light-frame wood structure," Journal of Structural Engineering, vol. 138, no. 2, pp. 258-265, 2012.

[13] D. W. Kelly and M. Elsley, "A Procedure for Determining Load Paths in Elastic Continua," Engineering Computations, vol. 12, no. 5, pp. 415-424, 1995.

[14] D. W. Kelly and M. W. Tosh, "Interpreting Load Paths and Stress Trajectories in Elasticity," Engineering Computations, vol. 17, no. 2, pp. 117-135, 2000.

[15] P.R. Chaperon, M. Heller, R. Jones, S. Pitt, and F. Rose, "Load flow visualisation in structural optimisation," in Australian Conference on Structural Optimisation, Sydney, 1998.

[16] D. W. Kelly, P. Hsu and M. Asudullah, "Load Paths and Load Flow in Finite Element Analysis," Engineering Computations, vol. 18, no. 1/2, pp. 303-313, 2001.

[17] D. W. Kelly, A. A. Reidsema and M. C. Lee, "An Algorithm for Defining Load Paths and A Load Bearing Topology in Finite Element Analysis," Engineering Computations, International Journal of Computer Aided Engineering and Software, vol. 28, no. 2, pp. 196-214, 2011.

[18] M. I. Chung, "Investigation of Load Path in Impact Respons of a Helicopter Fuselage Frame," The University of New South Wales, 2011.

[19] R. Li, D. Kelly, A. Crosky, H. Schoen and L. Smollich "Improving the efficiency of fiber steered composite joints using load path trajectories," Journal of Composte Materials, vol. 40, no. 18, pp. 1645-1658, 2006.

[20] R. Li, D. Kelly, A. Crosky "Strength improvement by fibre steering around a pin loaded hole," Composite Structures, vol. 57, no. 1, pp. 377-383, 2002.

[21] M. Shinobu, D. Okamoto, S. Ito , H. Kawakami and K. Takahashi, "Transferred Load and Its Course in Passenger Car Bodies," JSAE Review, vol. 16, no. 2, pp. 145-150, 1995.

[22] K. Takahashi, "Relative Rigidity of structures and Saint Venant's Principle," The Japan Society of Mechanical Engineers, vol. 52, no. 68, pp. 2615-2621, 1986.

[23] H. Hoshino, T. Sakurai and K. Takahashi, "Vibration Reduction in The Cabin of Heavy-Duty Truck Using The Theory of Load Transfer Paths," JSAE Review, vol. 24, no. 2, pp. 165-171, 2003.

[24] T. Sakurai, K. Takahashi, H. Kawakami and M. Abe, "Reduction of Calculation Time for Load Path U^{*}Anlysis of Structures," Journal of Solid Mechanics ad Material Engineering, vol. 11, no. 11, pp. 1322-1330, 2007.

[25] T. Sakurai, M. Tada, H. Ishii, T. Nohara, H. Hoshino and K. Takahashi, "Load Path U[*] Analysis of Structures under Multiple Loading Conditions," The Japan Society of Mechanical Engineers, 2007.

[26] E. Wang, X. Zhang and K. Takahashi, "Load Path U[*] analysis of a square pipe under collision," in Society of Automotive Engineers of Japan Annual Congress, Yokohama, 2007.

[27] Y. Okano, T, Matsunaga, S. Maruyama, M. Hanazati, K. Takahashi "Load Path Analysis of Vehicle Body Strucutres under Eigenmode Deformation of Bending Vibration," International Society of Automotive Engineering , 2009.

[28] E. Wang, T. Nohara, H. Ishii, H. Hoshino and K. Takahashi, "Load Transfer Analysis Using U[*] and U[**] for Truck Cab Structures in Initial Phase of Frontal Collision," Advanced Materials Research, vol. 156, pp. 1129-1140, 2011.

[29] H. Koboyashi, T. Naito and Y. Urushiyama, "Study on Similarity of Load Path Distribution in Body Structure," Honda R&D Technical Review, vol. 23, no. 1, pp. 80-89, 2011.

[30] T. Naito, H. Koboyashi, Y. Urushiyama and K. Takahashi, "Introduction of the New Concept of U[*]sum for Evaluation of Weight- Efficient Structure," SAE International Journal of Passenger Cars- Electronic and Electrical Systems, vol. 4, no. 1, pp. 30-41, 2011.

[31] T. Naito, H. Koboyashi and Y. Urushiyama, "Application of Load Path Index U[*] for Evaluation of Sheet Steel Joint with Spot Welds," SAE Technical Paper, 2012.

[32] Y. Nambu, T. Mizuno, K. Takahashi, M. Omiya, Y. Urushiyama, M. Naito, K. Koboyashi, T. Maki and T. Sakurai, "Relation Between Statistical Load Transfer Ustar Index and Vehicle Body Stiffness," in JSAE Annual Congress, Nagoya, 2013.

[33] K. Takahashi, M. Omiya, T. Iso, Y. Zaiki, T. Sakurai, T. Maki, Y. Urushiyama and T. Naito., "Load Transfer Ustar (U[*]) Calculation in Structures under Dynamic Loading (In japanese)," Nihon Kikai Gakkai Ronbunshu, A Hen/Transactions of the Japan Society of Mechanical Engineers, vol. 79, no. 807, pp. 1657-1668, 2013.

[34] M. O. K. T. Satochi Akima, "Load Transfer of Passenger Car Compartment for Improvement of Structural Performance in Side Impact," Gothenburg, 2015.

[35] K. Pejhan, C. Q. Wu and I. Telichev, "Comparison of load transfer index (U[*]) with conventional stress analysis in vehicle structure design evaluation," International Journal of Vehicle Design, vol. 68, no. 4, pp. 285-303, 2015.

[36] T. H. Pian and P. Tong, "Basis of finite element methods foe solid continua," International Journal of Numerical Methods in Engineerings, vol. 1, no. 1, pp. 3-28, 1969.

[37] Bertec, " Intrumented Treadmills," BERTEC Corporation, [Online]. Available: http://bertec.com/products/instrumented-treadmills/. [Accessed 17 February 2015].

[38] K. Takahashi and T. Sakurai, "Expression of Load Transfer Paths in Structures," Transactions of Japan Society of Mechanical Engineers Series A, vol. 71, no. 708, pp. 1097-1102, 2005.

[39] "www.unece.org," 22 February 2006. [Online]. Available: http://www.unece.org/fileadmin/DAM/trans/main/wp29/wp29regs/r066r1e.pdf. [Accessed 08 August 2016].

[40] R. H. Enns, It's a nonlinear world,, Springer, 2011.

[41] H. Z. Arefin Ahmed, "Spring Synthesis for Nonlinear Force- Displacement Function," International Journal of Engineering Research and Technology, vol. 3, no. 3, pp. 168-173, 2014.

[42] J. E. Mark, Physical Properties of Polymer Handbook, New York: Springer, 2007.

Appendix A: Stress trajectory method for load path analysis

The stress trajectory method was the first established method for load path detection in mechanical engineering. Although it has its shortcomings as covered in the literature review, it had its applications too, and it can be beneficial to review this theory and the proposed algorithm based on this theory for load path detection. Therefore in this section, a general overview based on [16] and [17] is presented to summarize the stress trajectory method for load path detection.

This theory defines load path as a path along which a constant force is being transferred. In structural mechanics, unlike fluid flows, there is no continuity for the applied force. However, continuity applies to components of the force in an arbitrary set of orthogonal directions because of the requirements of equilibrium. Therefore for the structure shown in Figure A1, equilibrium suggests that $F_a = F_b$.
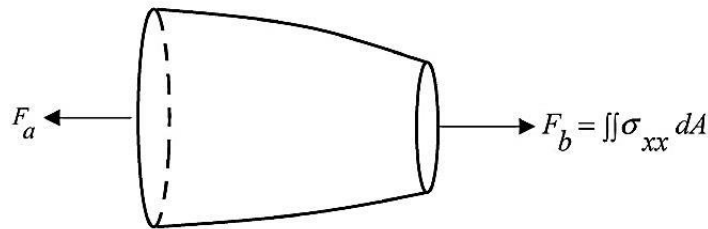

Figure A1) Sample structure and horizontal component of applied load [16]© Emerald Group Publishing

If Figure A2 is a segment with unit area of the side wall of the structure shown in Figure A1, then the normal vector of this surface can be defined as $\hat{n}$:

$$\vec{n} = \begin{bmatrix} n_x \\ n_y \\ n_z \end{bmatrix} \; (n_x^2 + n_y^2 + n_z^2 = 1) \tag{1-A}$$

Then, using the normal vector and the components of the total stress, it will be straightforward to find the force components applied on the surface of the side wall shown in Figure A2 as shown in Equation (2-A).
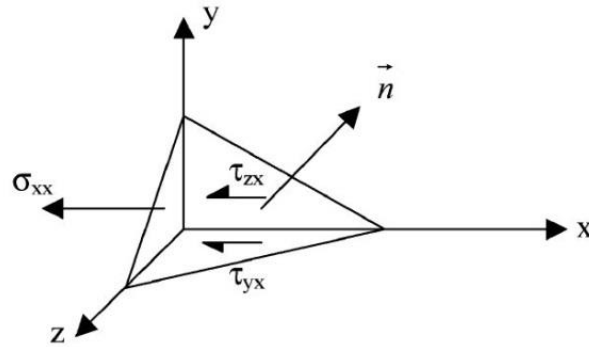

Figure A2) A unit area of surface of the side wall along with the normal vector, and horizontal components of the total stress [16]© Emerald Group Publishing

$$T_x^n = \vec{\sigma}_x \cdot \hat{n} \, , T_y^n = \vec{\sigma}_y \cdot \hat{n} \, \& \, T_z^n = \vec{\sigma}_z \cdot \hat{n} \qquad \text{(2-A)}$$

where the total stress vectors are made of three components (e.g. $\vec{\sigma}_x = \sigma_{xx}\vec{i} + \tau_{yx}\vec{j} + \tau_{zx}\vec{k}$). Therefore components of the total stress vector for an area A can be rewritten as:

$$\vec{T}_x = \sigma_{xx}An_x + \tau_{yx}An_y + \tau_{zx}An_z \qquad \text{(3-A-1)}$$

$$\vec{T}_y = \tau_{xy}An_x + \sigma_{yy}An_y + \tau_{zy}An_z \qquad \text{(3-A-2)}$$

$$\vec{T}_z = \tau_{xz}An_x + \tau_{yz}An_y + \sigma_{zz}An_z \qquad \text{(3-A-3)}$$

As equilibrium of force components suggests, there should be no contribution in the force components (e.g. X-direction) from the side wall. Therefore, for x-direction:

$$\vec{T}_x = \sigma_{xx}An_x + \tau_{yx}An_y + \tau_{zx}An_z = 0 \qquad \text{(4-A)}$$

This equation can be re-written as:

$$[\sigma_{xx} \quad \tau_{yx} \quad \tau_{zx}]\begin{bmatrix} n_x \\ n_y \\ n_z \end{bmatrix} = 0 \qquad (5\text{-A})$$

The above equation is the mathematical condition for two vectors to be orthogonal. Since the vector $\hat{n}$ is the normal vector of the surface of the load path, the stress vector is a tangent vector of the load path. The tangent vector of the load path is therefore defined by a component of the total stress vector [16].

An example of the application of this theory was presented in [16]. The aircraft wing spoiler shown in Figure A3-a was elected as the case study. The structure is supported by three hinges on the front spar. These hinges cannot carry any moment however they resist chord-wise and normal forces. An actuator is placed behind the central hinge to carry the moments. Kelly et al. predicted the deformed shape of this wing spoiler as shown in Figure A3-b using MSC-Nastran.


(a)   (b)
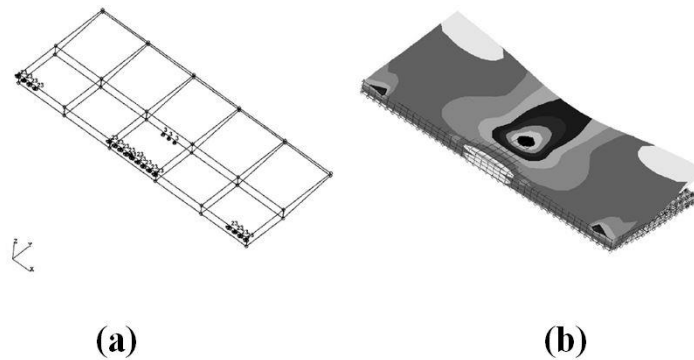
Figure A3) a: Wing Spoiler & constraints, b: Deformed shape & minimum principal stress contours [16]©
Emerald Group Publishing.

Figure A4 shows the load flow and load paths detected by the stress trajectory method for two arbitrary orthogonal directions; span-wise in Figure A4-a, and chord-wise in Figure A4-b.
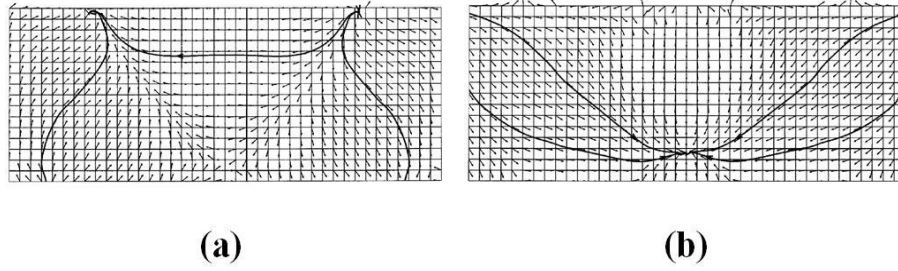
Figure A4) a: Span-wide load paths, b: Chord-wide load paths [16]© Emerald Group Publishing.

Although considering the location and nature of the hinges, the predicted load paths are in agreement with the physics of the problem; it is still not very clear how one should depict the actual paths. Therefore a review on the algorithm proposed in [17] can be more clarifying.

It was shown above that load paths can be defined by plotting contours aligned with total stress ''pointing'' vectors given by the columns of the stress matrix [17]. These pointing vectors can be defined as:

$$\vec{V}_x = \sigma_{xx} i + \tau_{yx} j + \tau_{zx} k \qquad \text{(6-A-1)}$$

$$\vec{V}_y = \tau_{xy} i + \sigma_{yy} j + \tau_{zy} k \qquad \text{(6-A-2)}$$

$$\vec{V}_z = \tau_{xz} i + \tau_{yz} j + \sigma_{zz} k \qquad \text{(6-A-3)}$$

So, to find the load path the in the first step the pointing vectors $\vec{V}_x$, $\vec{V}_y$ and $\vec{V}_z$ should be formed and normalized ($|V_i| = 1$) based on the calculated stress components. Then a fourth-order Runge-Kutta scheme can then be used to find the vector field for load path detection. If point p_i is the first point on the load path (e.g. the loading point) and the second point on the path is p_{i+1}, the following equations can calculate the exact location of p_{i+1}.

$$dp_1 = V|_{p_i} \Delta s \qquad \text{(7-A-1)}$$

$$dp_2 = V|_{p_{i+\frac{1}{2}dp_1}} \Delta s \tag{7-A-2}$$

$$dp_3 = V|_{p_{i+\frac{1}{2}dp_2}} \Delta s \tag{7-A-3}$$

$$dp_4 = V|_{p_{i+\frac{1}{2}dp_3}} \Delta s \tag{7-A-4}$$

$$p_{i+1} = p_i + \frac{1}{6}(dp_1 + 2dp_2 + 2dp_3 + dp_4) \tag{7-A-5}$$

where p_{i+1} is the next point in the load path, $V|_p$ is the value of the vector field V, evaluated at point p and Δs is a scalar spatial discretization that represents a small increment along the load path [17]. Figure 5A shows a schematic load path created using the presented algorithm [17].
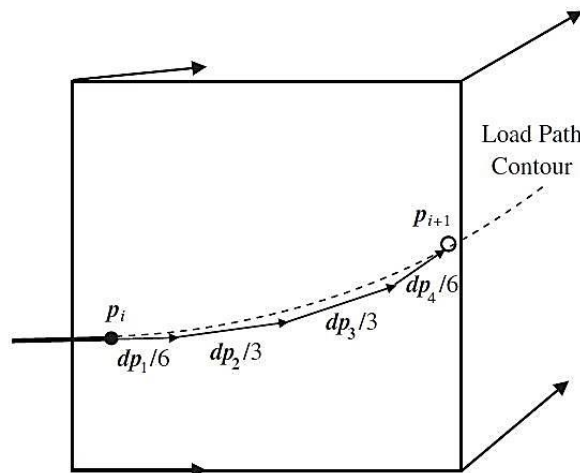

Figure A5) Nodal pointing vectors and Runge-Kutta vectors for path creation [17]© Emerald Group Publishing.

Appendix B: Correlation of U* index and K$_{AC}$

The U* index theory represents the structure with (at least) three linear illustrative spring. The third chapter of this dissertation covered the fundamentals of the U* index theory in details. However, one would still wonder about the core claim of the theory that was built upon Equation 6. This equation is presented here again as Equation B-1.

$$U^* = 1 - \frac{U}{U'} = \left(1 - \frac{2U}{(K_{AC}d_c).d_A}\right)^{-1} = (1 - \frac{(K_{AC}.d_c)d_A + (K_{AA}.d_A)d_A}{(K_{AC}.d_c)d_A})^{-1}$$ (B-1)

Throughout literature, it has been mentioned that higher U* index at any point in the structure represents a greater degree of connectivity between that point and the loading point, i.e. higher K$_{AC}$. However, it is not straightforward to show the proportional dependence between U* index and K$_{AC}$ from Equation B-1.

It is necessary to study the relationship of U* index value with the location of the arbitrary point C in the structure, before discussing the dependence of U* index to K$_{AC}$. Figure B1 shows the illustrative representation of the system with linear springs which was discussed in Chapter 3.
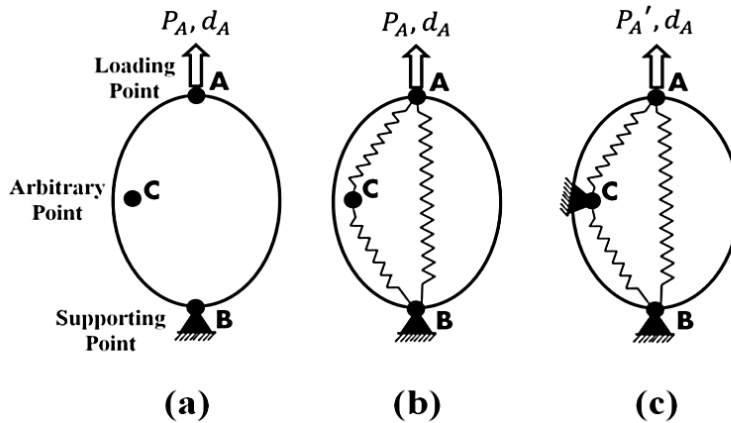
Figure B1) Illustrative representation of the actual structure (a) using linear springs (b) and with modified

constraints for U* calculation (c).

The strain energy of the system, shown in Figure B1-b, is the term U in Equation B-1, and the strain energy of the modified system (Figure B1-c) is the term U'. Point C, in Figure B1-c, can be any point in the structure and if converges to point B, which is the actual constraint in the system, structures shown in Figure B1-b and B1-c will be identical. In other words:

$$C \implies B: U = U' \implies U^* = 0 \qquad \text{(B-2)}$$

Following the similar approach, it can be shown that as point C coincides with the loading point (A), U* index value converges to 1.

$$C \implies A: \implies U^* = 1 \qquad \text{(B-3)}$$

In conclusion, U* index value goes up as point C gets closer to the loading point, and its magnitude goes down as point C goes toward the supporting point (B).

Moving on to the correlation of U* index and K$_{AC}$, the structure shown in Figure B1-a can be any mechanical structure, including a spring. By assuming the structure to be a linear spring, U* index calculation stands based on the same procedure, which is representing the system with three illustrative springs. Figure B2 shows the real structure and its illustrative representation.

The original system, shown in Figure B2-a, has a certain stiffness (e.g. 100 N/m). The spring represetation of Figure B2-b should have the same overall stiffness. Therefore in this case:

$$K = k_{AB} + (\frac{1}{k_{AC}} + \frac{1}{k_{CB}})^{-1} = 100 \qquad \text{(B-4)}$$

while K is the actual stiffness of the structure, and k_{ij} (i,j = A, B and C) is the internal stiffness between points i and j.


(a)

(b)
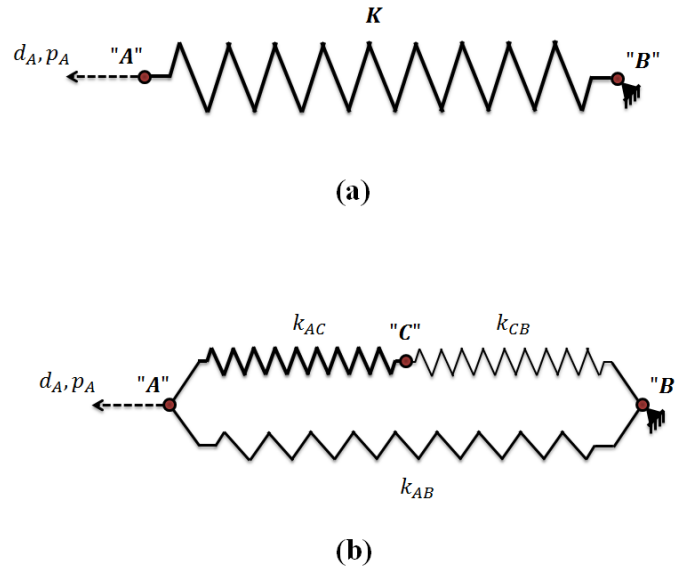
Figure B2) Selected engineering structure for studying the dependence of U* index to K_{AC}: (a) original structure, (b) illustrative representation of the structure.

In the model shown in Figure B2-b, loading point (A), and primary constraint (B) are now moving. Thus, k_{AB} will have a constant value. Assuming $k_{AB} = 50 \ N/m$, then:

$$(\frac{1}{k_{AC}} + \frac{1}{k_{CB}})^{-1} = 50 \tag{B-5}$$

To calculate U* index for the whole structure, point C shall move around the system. However, if point C coincides with the constraint (point B), then the spring with the stiffness of K_{CB} will vanish and based on the assumed values in previous equations, K_{AC} will have a magnitude of 50 N/m. Now, by moving the point C away from the support (Point B), K_{CB} will reappear in the system and calculations. Moreover, as K_{AC} and K_{CB} are in series, they have individual values, larger than their equivalent stiffness (in this case, 50).

In summary, as K_{CB} appears in the structure, it will have non-zero values. Therefore, both K_{AC} and K_{CB} will have magnitudes larger than 50N/m. In other words, as point C moves from the supporting point (B) toward the loading point (A) K_{AC} value increases.

On the other hand, it was shown in Equations B-2 and B-3 that U^* index values increase from zero to one, as point C moves from support to the loading point. So it can be concluded that both U^* index and K_{AC} value increase as the arbitrary point C goes toward the loading point and vice versa; i.e.: $U^* \propto K_{AC}$.

Appendix C: U* index response to loading variation

In chapter 4 of this dissertation, the first experimental validation of U* index theory was presented. For that test, a certain loading condition was selected, and the predicted load path of the U* index theory was proven to be accurate by comparing it to the actual load path determined in the experiment. Therefore, it is now shown that internal stiffness is the governing factor for load transfer paths. However, the internal stiffness of any point in the structure is function of geometry (location of that point in the structure) and loading condition. Consequently, to provide a thorough experimental study on U* index theory, it was necessary to evaluate the response of the U* index theory to loading variation too. Thus, the setup for the presented experiment of Chapter 4 was modified so a new loading condition can be tested and the response of the U* index theory to this modification can be evaluated.

Figure C1 shows the new loading condition. In contrary to the original test setup (Chapter 4) the loading bars were placed in the middle of the table-shaped testing specimen.
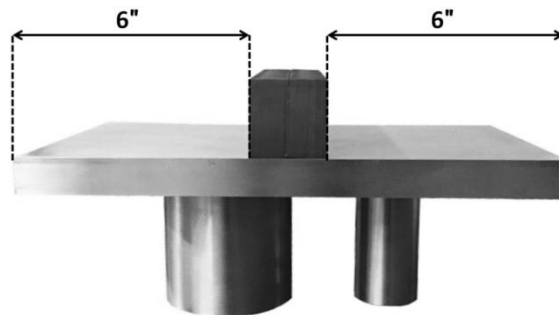

Figure C1) Loading condition on the testing specimen for the modifies test setup

As in the original validation experiment, the gathered data in both stages of this experiment was the vertical component of the force applied to the force plates. Firstly, the results were showing the portion of the body weight that was carried by each shaft. Then, the measurement was done

just for the additional external load that was applied to the able-shaped structure by placing the steel loading bars on it. These data represented the ending point of the two load paths going through the shafts. Data gathering was performed using the 16- bit digital data accusation system of the force plates. The gathered information was then amplified using the external amplifier of the DAQ system and was recorded on a Core i7, 3 GHz computer for further processing. Figure C2 shows the result of this experiment.
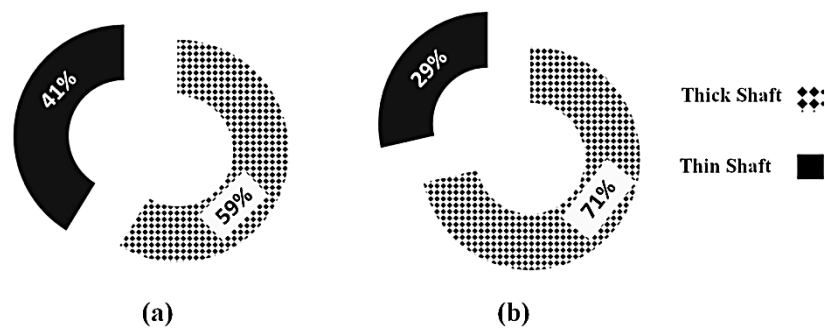

Figure C2) Load carrying significance of shafts under (a) No external loading, (b) External loading in the middle

The first stage of the experiment was the exact replicate of the presented results in Chapter 4. 59% of the body weight was carried by the thicker shaft. Then, all the readings on the measurement devices were set to zero, and the external load was applied to the system by placing the loading bars in the middle of the table-shaped structure. This time, the thick shaft carried almost all of the external load (71%) which is in contrary to the results of the loading condition of the experiment in Chapter 4, in which only 42% of the external load was carried by the thick shaft.

These results show that internal stiffness varies with loading condition, as well as the geometry variations. Now it was necessary to validate that U* index theory was capable of following these

changes or not. Therefore, the analytical load transfer analysis with U^* index theory was performed on the modified computer model. The results are presented in Figure C3 and show that as the loading condition changed in the model, the degree of connectivity of every point in the structure and the loading points has changed. This time, the thicker shafts shows higher U^* index values (Fig. C3-b), which corresponds to a more significant load transferring role for this shaft under this loading condition. These results are in complete agreement with the experimentally determined load paths. Therefore, this new experiment and simulation revalidated the U^* index theory and also proved its capacity to follow the changes in the internal stiffness due to loading variations.
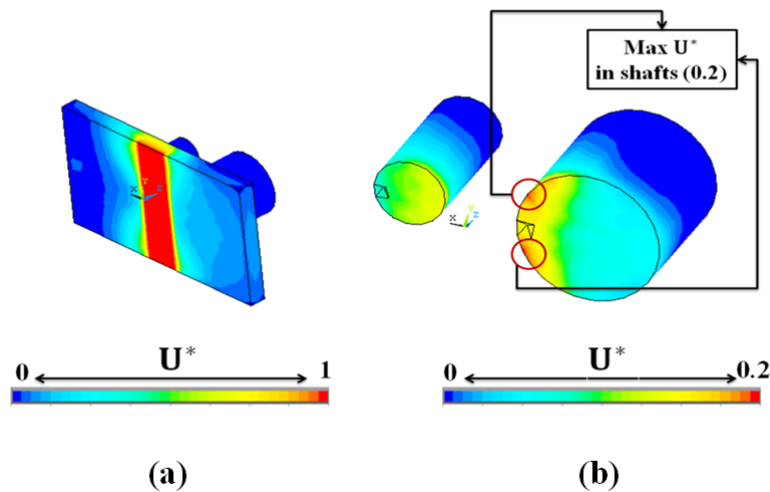

Figure C3) U^* index distribution; (a): In the complete structure, (b) In the supporting shafts

In conclusion, it can be stated that based on the presented analysis in this appendix and also in Chapter 4, internal stiffness is the true governing parameter in load transfer in engineering structure and U^* index theory is now a reliable tool to study the internal stiffness in the structure.

BIOGRAPHICAL SKETCH

Khashayar Pejhan was born in 1986 in Tehran, Iran. He obtained his Bachelor of Science and degree in Mechanical Engineering from Iran University of Science and Technology in September 2009, and he got his Master of Science degree in Automotive Engineering from the same university in April 2012. In the fall of 2012, he was enrolled in the Ph.D. program at University of Manitoba. Since 2012 for over four years he was working as a graduate research assistant at the Mechanical Engineering Department of University of Manitoba supervised by Dr. Christine Wu and Dr. Igor Telichev. Khashayar was involved in different research projects sponsored by NSERC and Motor Coach Industries. Most of his work was about structural analysis of the motor coach structure. He was also involved in helping with teaching undergraduate courses: Kinematics and Dynamics, Mechanics of Materials and Aerodynamics.

Refereed journal publications:

- **Pejhan, K**., Wang, Q., Wu, C.Q. and Telichev, I., "Experimental Validation of the U^* Index Theory for Load Transfer Analysis", 2016, International Journal of Heavy Vehicle Systems, In Press.

- **Pejhan, K.**, Wu, C.Q. and Telichev, I., "Comparison of load transfer index (U^*) with conventional stress analysis in vehicle structure design evaluation", 2015, International Journal of Vehicle Design, vol. 68, no. 4, pp: 285-303

- Wang, Q., **Pejhan, K.,** Wu, C.Q., and Telichev, I., "Extensions of the U^* theory for applications on orthotropic composites and nonlinear elastic materials." International Journal of Mechanics and Materials in Design: 1-12.

- **Pejhan, K**., Kuznetcov, A., Wang, Q., Wu, C.Q. and Telichev, I., "Design Assessment of a Multiple Passenger Vehicle Component Using Load Transfer index (U*) Method" International Journal of Mechanics and Materials in Design, Under Review.

- Wang, Q., **Pejhan, K.,** Wu, C.Q., and Telichev, I., "Improvement of the weight efficiency of a vehicle component based on load transfer analysis using U* index" Proceedings of the Institution of Mechanical Engineers, Part D: Journal of Automobile Engineering. Under Review

Reviewed proceedings and symposia articles:

- **Pejhan, K**., Wu, C.Q. and Telichev, I., "Application of Load Transfer Index (U*) in Structural Analysis in Comparison With Conventional Stress Analysis", ASME 2014, International Mechanical Engineering Congress and Exposition. Volume 9: Mechanics of Solids, Structures, and Fluids. Montreal, Canada. November 14-20, 2014.

- **Pejhan, K.**, Wang, Q., and Telichev, I., "Extension of U* Index Theory to Nonlinear Case of Load Transfer Analysis." ASME 2015 International Mechanical Engineering Congress and Exposition. American Society of Mechanical Engineers, 2015

- **Pejhan, K.**, Wang, Q., and Telichev, I., "Experimental Study of U* Index Response to Structural and Loading Variations." ASME 2015 International Mechanical Engineering Congress and Exposition. American Society of Mechanical Engineers, 2015.

- Wang, Q., **Pejhan, K.**, Wu, C. Q., and Telichev, I. "Load Transfer Index for Composite Materials." In ASME 2015 International Mechanical Engineering Congress and Exposition, pp. V009T12A009-V009T12A009. American Society of Mechanical Engineers, 2015.